AFFIDAVIT

I declare that I have authored this thesis independently, that I have not used other than the declared sources/resources, and that I have explicitly indicated all material which has been quoted either literally or by content from the sources used. The text document uploaded to TUGRAZonline is identical to the present doctoral thesis.

_____   _____
Date   Signature

Acknowledgments

First, I want to thank my supervisor Dr. Otto Glatter for his relentless support during the duration of this thesis and beyond. All advancements that I could achieve in this field and for myself would not have been possible without his guidance and insight. He enabled me to gather important experiences and meet all kind of interesting people here and abroad. Merci beaucoup Otto!

Second, I want to thank Dr. Gregor Trimmel for welcoming me in his group although our fields only overlap on the edges. His input and ideas for the synthesis procedures was invaluable.

Third, I want to thank Dr. Stefan Salentinig for bringing his project to me and his input throughout the process.

Furthermore I want to thank my old and new colleagues like Dr. Angela Chemelli, who always had an open ear for my scientific problems and more than once a constructive input or Dr. Manfred Kriechbaum who kept the ship (the SAXSess) up and running and provided me with all necessary tips and tricks to improve my 'scattering skills'. I especially want to thank my office colleague Dr. Manuel Hollauf for his help and input in doing the synthesis and the subsequent NMR characterization.

Also a big thank you to my family and friends who always had an open ear for my problems and troubles and always helped me through with a good advice or one, too many beers.

Finally I want to thank my girlfriend, Ulli for supporting me throughout this time. After a long day I could always look forward to come home to you and rest in your arms. I could not have done it without your support!

Table of Contents

Abstract

English version

This thesis examines the properties and application possibilities of internally self-assembled somes (ISAsomes) which are emulsions that contain a liquid crystal structure confined within stabilized droplets. Until now ISAsomes are usually oil in water (O/W) emulsions which are used for the incorporation of hydrophilic, lipophilic and amphiphilic functional molecules. This allows numerous applications as carrier systems or as controlled release systems. The main goal of this thesis was to formulate a water in oil (W/O) emulsion instead of a O/W emulsion. This goal was achieved and culminated in a publication in *Langmuir*. This publication covers three main objectives. (1) Finding a hydrophilic liquid crystal that would form a hexagonal phase with a certain amount of tetradecane and more importantly will not be destroyed in presence of excess tetradecane. (2) Finding a stabilizer that would allow the dispersion of said hydrophilic liquid crystal and provide emulsion stability. (3) Characterization of the resulting emulsion and investigation of its stability. All of the objectives were met and a hydrophilic hexagonal liquid crystal could be created with commercially available short chain polyethylene glycol alkyl ethers (so-called Brij) and a high molecular weight tri-block copolymer (Pluronic L64). This hexagonal liquid crystal then was successfully dispersed in excess tetradecane and stabilized by low hydrophilic-lipophilic balance triblock copolymers (synthesized in our laboratory or commercially available ones) as well as commercially available hydrophobized silica nanoparticles.

Furthermore a project was carried out within the scope of this thesis to modify W/O ISAsomes in a way to achieve phase transfers via a trigger. In that case the formation of carbamate when an amine reacts with CO_2 was chosen. The amine used for the formation of the liquid crystal structure would change the head group area drastically when the reaction with CO_2 to a carbamate takes place. This would change the curvature and possibly induce a phase transformation. Oleylamine (OLA), 2-Dimethylaminoethanol (DMAE) and 2-(Dibutylamino)ethanol (DBAE) were tested for their suitability as functional molecules for the reaction. Oleylamine showed a too low reactivity. Furthermore the low concentrations of amines that were used to form a liquid

crystal structure were not sufficient to show the desired phase transformation. However DMAE and DBAE are much more reactive than oleylamine. Although no phase transfer could be observed a clear shift of the q-value in the SAXS curve and a reordering of the liquid crystal phase were found when the samples were bubbled with CO_2. This project could not be finished entirely and possesses great potential for a publication in the future.

Concluding two publications that were carried out in preparation for the main project during my PhD are attached. The first publication led to a better understanding of the behavior of the lipids within the ISAsomes by examination of the transfer characteristics between two liquid crystal phases. Furthermore the transfer rate could be controlled by embedding the emulsion in a hydrogel. The second publication elucidates the formation of particle stabilized emulsions (so-called Pickering emulsions) with intact liquid crystals. To achieve this, silica nanoparticles were successfully hydrophobized with oleic acid.

Deutsche Version

Diese Doktorarbeit untersucht die Eigenschaften und möglichen Anwendungen von so genannten ISAsomes (kurz für: Internally Self-Assembled somes). Dabei handelt es sich um Emulsionen die eine flüssig-kristalline Phase enthalten. Bis jetzt wurden solche Emulsionen als Öl in Wasser (O/W) Emulsionen hergestellt. In die darin enthaltene flüssig-kristalline Phase können hydrophile, lipophile und amphiphile Moleküle eingelagert werden. Dies erlaubt zahlreiche Anwendungen als carrier - Systeme und als System zum kontrollierten Freisetzen von Substanzen. Das Hauptziel dieser Dissertation war die Entwicklung von einer Wasser in Öl (W/O) Emulsion anstatt einer O/W Emulsion. Dieses Ziel wurde erreicht und die Ergebnisse wurden gesammelt als wissenschaftlicher Artikel in *Langmuir* veröffentlicht. Diese Publikation beinhaltet im Wesentlichen drei Hauptziele. (1) Die Suche nach einem hydrophilen Flüssigkristall der zusammen mit Tetradecane eine hexagonale Struktur ausbildet. Zusätzlich soll diese Struktur erhalten bleiben wenn Tetradecane im Überschuss vorhanden ist. (2) Die Suche nach einem geeigneten Stabilisierer, der es erlaubt den eben genannten Flüssigkristall zu dispergieren und zu stabilisieren. (3) Charakterisierung der entwickelten Emulsion und die Überprüfung ihrer Stabilität. All diese Ziele wurden erreicht und es konnte ein hydrophiler Flüssigkristall mit kommerziellen kurzkettigen Polyethylen Glycol Alkyl Ether (so genannte Brij) und zusätzlich mit einem Triblock-copolymer (Pluronic L64) mit hohem Molekulargewicht hergestellt werden. Dieser Flüssigkristall wurde dann dispergiert und erfolgreich mit einem selbst synthetisierten Triblock-copolymer, einem kommerziell erhältlichen Stabilisierer und auch kommerziell erhältlichen hydrophobisierten Silika Nanopartikeln stabilisiert.

Weiters wurde im Zuge dieser Dissertation ein Projekt durchgeführt dass zum Ziel hatte ISAsomes in einer Weise zu modifizieren, dass sie durch einen Trigger einen Phasentransfer zeigen würden. Zu diesem Zweck wurde die Reaktion von Aminen mit CO_2 zu Carbamat untersucht. Ein Amin dass zur Herstellung des Flüssigkristalls verwendet wurde, würde seine Kopfgruppen Fläche drastisch verändern wenn die Carbamat-reaktion stattfände. Dies hätte eine Änderung der Krümmung zur Folge und damit einen möglichen Phasentransfer. Oleylamin (OLA), 2-Dimethylaminoethanol (DMAE) and 2-(Dibutylamino)ethanol (DBAE) wurden als funktionelle Moleküle zu diesem Zweck getestet. Oleylamin zeigte ein zu geringe Reaktivität und die generell niedrigen Konzentrationen an Amin die eingesetzt wurden um den gewünschten

Flüssigkristall zu erzeugen waren nicht ausreichend um einen Phasentransfer zu induzieren. Jedoch zeigten DMAE und DBAE höhere Reaktivitäten gegenüber CO_2. Obwohl auch hier kein eindeutiger Phasentransfer feststellbar war, wurden immerhin ein klares Verschieben des q-Wertes und eine Neuordnung von zuvor bereits ungeordneten Phasen nach dem durchblasen mit CO_2 beobachtet. Dieses Projekt konnte nicht vollständig beendet werden und besitzt großes Potential für eine weitere Publikation in naher Zukunft.

Abschliessend werden dieser Dissertation zwei Publikationen angehängt die im Zusammenhang mit dem Hauptprojekt als Vorbereitung dazu durchgeführt wurden. Die erste Publikation führte zu einem besseren Verständnis für das Verhalten der Lipide in den ISAsomes, durch die Untersuchung der Transfercharakteristika zwischen zwei verschiedenen flüssig-kristallinen Phasen. Weiters konnte die Transferrate durch das Einbetten der Emulsion in ein Hydrogel kontrolliert werden. Die zweite Publikation erläutert die Bildung von Emulsionen mit Hilfe von Partikeln (so genannte Pickering Emulsionen). Dabei wurden auch erfolgreich intakte flüssig-kristalline Phasen emulgiert. Dies wurde durch die Hydrophobisierung der Silika-Nanopartikel mit Ölsäure erreicht.

Chapter I - Basics

Table of Contents

Introduction

This thesis deals with the possibilities and further development of internally self-assembled particles, also known as ISAsomes. These systems are usually formed as oil-in-water (O/W) emulsion and can contain a variety of liquid crystal (LC) phases. They were studied extensively over the past decades and still are a subject of research due to their numerous possible applications. ISAsomes can act as carriers for many different substances which make it intriguing for the food, pharmaceutical, cosmetic and agricultural industries [1–4]. A more detailed description of ISAsomes can be found in the theory part of this work.

Since the group of Otto Glatter is active in this field since many years, this work is divided into four chapters which cover different aspects of the ISAsome systems.

Chapter III is the main body of this work and describes the development of a water-in-oil (W/O) emulsion containing reverse hexosomes which resulted in a publication in Langmuir [5]. Monoglycerides form lipophilic liquid-crystalline phases when mixed with water. The corresponding liquid-crystalline nanostructures coexist with excess water, which is a necessary condition for the formation of internally nanostructured dispersed particles. These nanostructures can comprise bicontinuous cubic phases, inverted hexagonal phases, and inverted micellar cubic phases. The dispersed particles are therefore named cubosomes, hexosomes, or micellar cubosomes. Such dispersions are usually stabilized by hydrophilic high-molecular-weight tri-block copolymers. Another way to stabilize such dispersions is by forming so-called Pickering or Ramsden emulsions using nanoparticles as stabilizers.

In this contribution, we explore the possibility of forming and stabilizing inverted or reverse systems; i.e. dispersions of hydrophilic liquid-crystalline phases in an excess-oil phase like tetradecane. Our aim was to change from oil-in-water emulsions to water-in-oil emulsions, where the water phase is a liquid-crystalline phase in equilibrium with excess oil, and where the oil is nonpolar; e.g., an alkane. This work consists of three parts: 1. to find a hexagonal hydrophilic liquid-crystalline phase that can incorporate a

certain amount of tetradecane, but can also coexist with excess tetradecane in case of higher oil concentration; 2. to find a suitable stabilizer – either polymeric or nanoparticle type – that can stabilize the emulsion without destroying the hexagonal liquid-crystalline phase and, finally, 3. to check the stability of this reverse-hexosome emulsion. We found out that it is possible to create the hexagonal hydrophilic liquid-crystalline phase with short-chain non-ionic surfactants like polyethylene glycol alkyl ethers, or with high-molecular-weight triblock copolymers of type A-B-A. Furthermore, it is possible to successfully stabilize the reverse hexosomes with low hydrophilic–lipophilic balance (HLB) triblock copolymers – either synthesized in our laboratory or commercially available ones – as well as with hydrophobized, commercially available silica nanoparticles.

Chapter II was a project that was carried out in cooperation with Stefan Salentinig from EMPA in St. Gallen Switzerland. The goal of this project was to modify a closed liquid crystal phase (e.g. hexagonal, emulsified microemulsion) in such way that it would react to a trigger and transfer into an open liquid crystal phase like bicontinuous cubic, or to be dissolved. This could then be used as a carrier system for burst-release experiments in many different applications. This project is focused on CO_2 as external trigger, since it is inexpensive and easily available. It can change the properties of molecules that possess CO_2 active moieties such as amines, amidine or guanidine.

The starting point was the ISAsome emulsion consisting of the monoglyceride GMO – tetradecane – water – F127. Through the replacement of tetradecane with an amine, the trigger function was added.

Chapter IV and Chapter V were projects that were carried out in preparation for this Ph.D. thesis parallel to my Master Thesis, and laid the groundwork for the understanding of these ISAsome systems which were developed in Chapter III.

Chapter IV shows a full paper, first author Guillermo Ramón Iglesias [6], which reports on the kinetics of lipid transfer between two different nano-structured phases (one hexagonal LC, the other emulsified microemulsion). The two separately prepared phases were mixed 1:1 v/v. The occurring phase transfer was observed via time-resolved small-angle X-ray scattering (SAXS). The speed of the transfer could be controlled by embedding the ISAsomes into a 3D hydrogel network. Higher gel

concentrations slowed the transfer rate considerably because the free diffusion of the droplets is decreased. This effect could be counterbalanced by the addition of free stabilizer, which increases the rate of lipid transfer.

Chapter V is again a full paper, first author Amin Sadeghpour [7], which investigated the formation of ISAsomes stabilized by silica particles, so called Pickering emulsion. It was possible to formulate stable emulsions with a hydrodynamic radius of about 100 nm, with intact liquid crystal phases (hexagonal, micellar cubosomes, emulsified microemulsion). The size was important in order to be comparable to the systems stabilized with molecular stabilizers, which are about 100 nm. To achieve this, silica particles were partly hydrophobized with oleic acid without changing their stability. This project gave insight into a different form of emulsion stabilization and the important parameters that have to be considered to achieve a stable emulsion. The gathered knowledge was also used in Chapter III.

Theory

Liquid Crystals (LC)

History

The discovery of liquid crystals happened late in the 19th century by Austrian botanical physiologist *Friedrich Reinitzer*, who investigated different derivatives of cholesterol. He discovered that this derivatives show two melting points, and in cooperation with *Otto Lehmann* and *von Zepharovich*[8], he described the intermediate appearance as crystalline [9]. He further described that these molecules reflect circular polarized light and alter the polarization direction of light. This coined the name for a material class called cholesteric liquid crystals.

Liquid crystals were further investigated and many compounds were discovered and described which exhibit the aforementioned properties. However it remained a scientific curiosity until the late 1960's when Joel E. Goldmacher and Joseph A. Castellano, after important developments by Richard Williams and George H. Heilmeier [10], could find a liquid crystal system that would replace the cathode ray vacuum tube used in old television sets. The technique they developed is used until today to develop materials with specific properties.[11]

Since then many advances aside from the electric industries have been made in the field of liquid crystals.

Definition

Liquid crystals are a deviation from the basic states of matter gas, liquid and solid. In detail the difference lies in the transfer between the ordered or anisotropic solid phase to the non-ordered or isotropic liquid phase. Liquid crystalline materials show some form of order in this gap, whereas standard molecules simply exhibit a single melting point

that separates the solid from the liquid state. The different structures that are formed are called nematic phases, smectic phases and chiral phases (see Figure I-1).
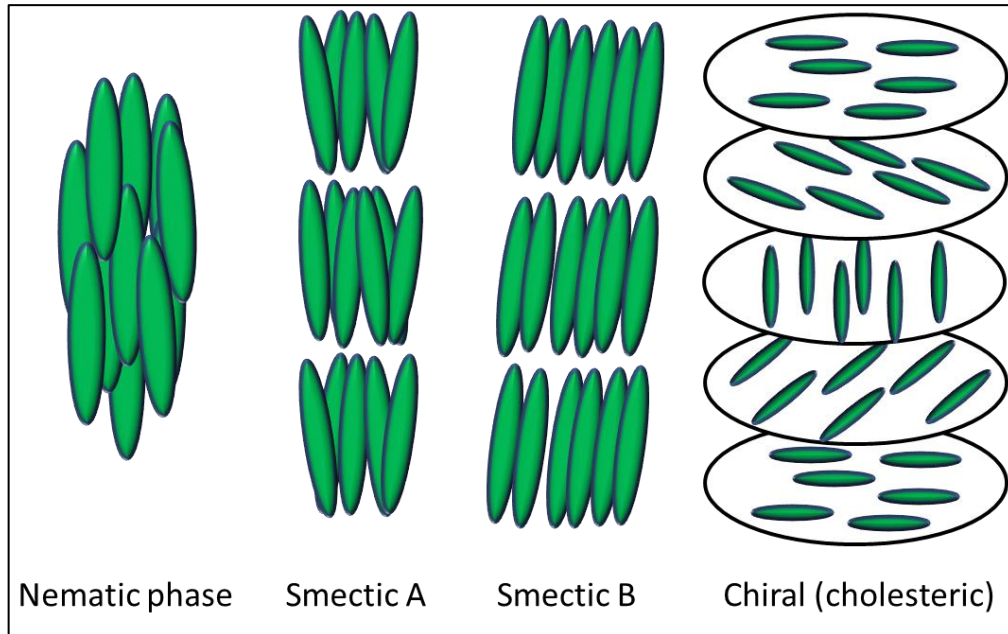
Figure I-1. Schematic of different thermotropic crystals.

Nematic, or thread like phases, appear uniaxial, which means that the molecules self-align along one preferred axes, which leads to the formation of rods or cylinders.[12]

Smectic phases are formed at lower temperatures than nematic phases. They form layers in various degrees of order by which they are classified into smectic A, smectic B, etc.[13]

Chiral phases consist of chiral molecules. These molecules do not contain elements of symmetry. The most famous chiral phase is the aforementioned cholesteric liquid crystal. The chirality of the molecules leads to an asymmetric packaging. This means that a single layer is ordered in one direction in the plane but the order in the plane of the following layer is twisted at a finite angle. This leads to a spiral twist, or a clock like movement of the in-plane direction of the self-assembled molecules.[14]

Liquid crystals can be separated into three categories:

- **Thermotropic liquid crystals**

This class of liquid crystals shows different structures depending on the temperature. The two main classes in thermotropic LC are discotic LC (disc-shaped) and calamitic LC (rod-shaped). Discotic LC phases tend to form columnar phases of long range positional order. Calamitic LC usually form lamellar or smectic phases of long range positional order.

- **Metallotropic liquid crystals**

Metallotropic liquid crystals are a class of inorganic compounds which show formation of liquid crystals when they are combined with organic molecules.[15]

- **Lyotropic liquid crystals**

Lyotropic liquid crystals form different structures depending on their composition. They consist of two or more components of which at least one has to possess liquid crystal properties. Usually molecules that possess an intramolecular amphiphilic property exhibit such lyotropic LC phases. The formed structures and sequences are primarily dependent on the size of the hydrophilic head group and less on the length of the lipophilic chain. However many molecules with lyotropic characteristics also show thermotropic characteristics.

This work is focusing on lyotropic liquid crystals.

Lyotropic Liquid Crystals
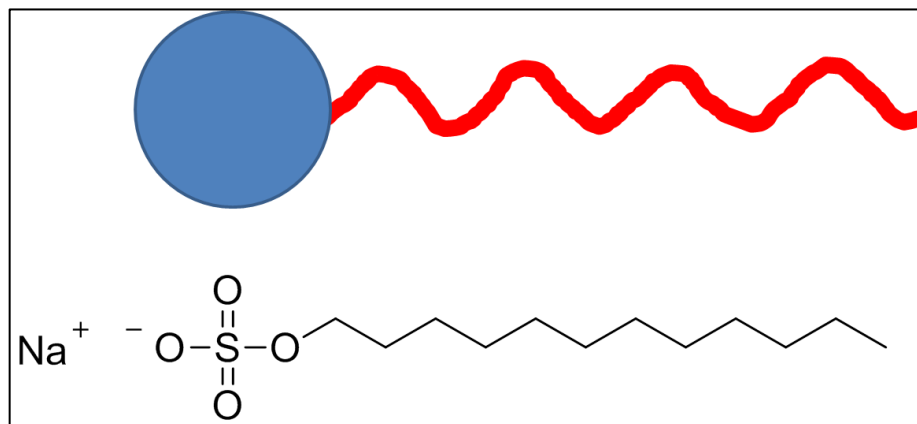
Figure I-2. Upper part: simple schematic of an amphiphilic molecule with a hydrophilic head (blue circle) and a lipophilic tail (red line); lower part: sodium dodecyl sulfate, an example for a widely used surfactant.

Amphiphilic molecules show a hydrophilic and a lipophilic property (see Figure I-2). Examples for such molecules are surfactants, lipids, copolymers, and proteins. These molecules possess the ability to associate in aqueous solution into different structures depending on the conditions such as concentration, temperature, pH, ionic strength or presence of an oil. Furthermore these structures can be controlled by changing the solution conditions, which opens up numerous applications for such systems. An important characteristic of such equilibrium structures is that they form without any energy input, so no ultra-sonication or stirring is necessary.

To understand this self-assembly we look at the concentration dependence of the nonionic surfactant Pluronic F127, which is a block copolymer (ethyleneoxide$_{106}$ − propyleneoxide$_{70}$ − ethyleneoxide$_{106}$) in water (see Figure I-3).[16]
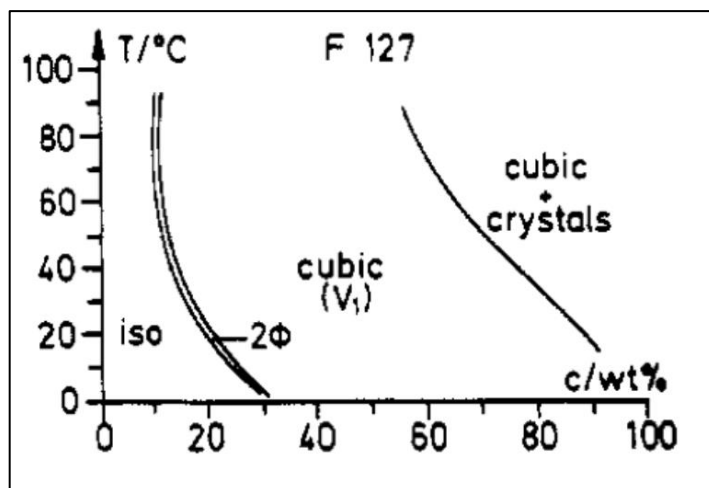
Figure I-3. Phase diagram of the nonionic surfactant Pluronic F127, x-axis shows increasing concentration, y-axis shows increasing temperature. iso: isotropic (not ordered, free surfactant); 2 ϕ describes the presence of free surfactant and micelles. The figure is reproduced from Wanka et.al [16]

At low concentrations the surfactant molecules are freely diffusing as monomers through the aqueous phase. When a certain concentration threshold, also known as critical micelle concentration (*cmc*) is surpassed the surfactant molecules form micelles in equilibrium with free monomers. When the concentration is further increased wormlike micelles are formed. Energetically the formation of one very long worm would be favored, but that is not what happens. In reality the formation of many worms can be observed although the formation of an endcap of the worm is energetically more demanding than the continuous growth. The reason for this is entropy, which acts as a balancing force. To further understand these association phenomena into more complex structures it is necessary to understand the forces between the amphiphilic molecules within the aggregates and how these are affected by the solution conditions. For macroscopic phase separation the driving force is simply the repulsion between hydrophilic and lipophilic phases. This repulsive force is also present between amphiphilic molecules between the hydrophilic heads and the lipophilic tails. Since they are covalently bond to each other, they can only separate locally in a so-called micro phase separation which leads to the formation of complex structures. Beside the hydrophilic/lipophilic repulsion also steric repulsion between all parts of the molecules (excluded volume effect). Charge repulsion of ionic head groups is also a contributing force to the formation of structures. Another contributing factor is the ability of the head

group to bind water molecules. This increases the effective head group area which has influence on the curvature and the resulting structure formed. The amount of water molecules that can be bound is also a function of the temperature.

One important parameter to analyze this behavior is the critical packing parameter (*CPP*, see Eq.I-1), where v is the volume of the hydrocarbon chain or chains which are assumed to be fluid but not compressible. a_0 is the effective head group area and l_c is the maximum length the chains can extend.

$$CPP = \frac{v}{a_0 l_c}$$ Eq. I-1

This dimensionless *CPP* can be used to estimate the packing behavior of the molecules. The effect of the different headgroup sizes is shown in Figure I-4.
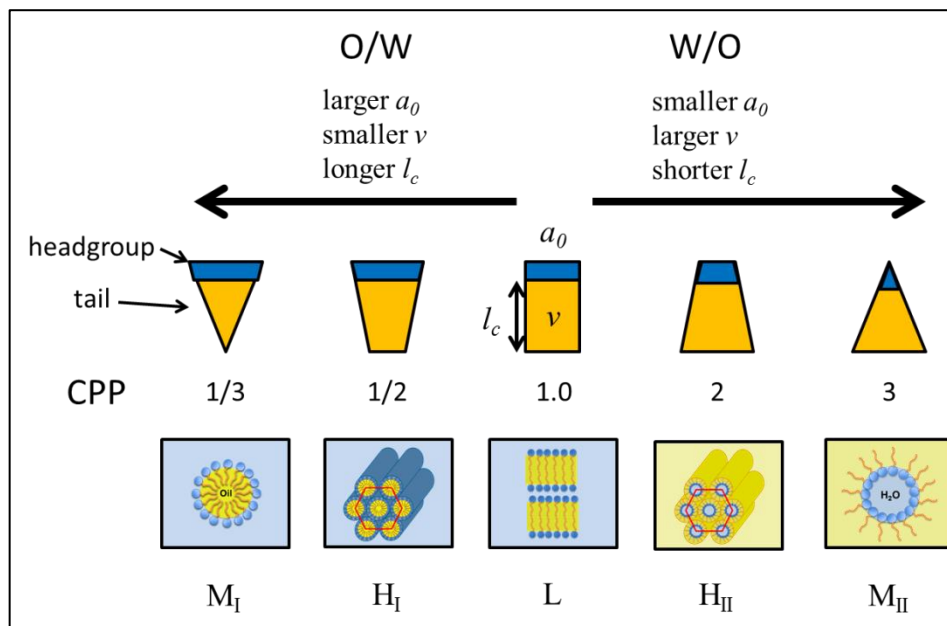
Figure I-4. Packing geometry of amphiphilic molecules described by the dimensionless critical packing parameter *CPP* which is dependent on the head group area a_0 (blue regions), the volume of the chains v (yellow regions) and the maximum length of the chains l_c, The phases represented in the lower row are micellar (M_I), hexagonal (H_I), lamellar (L), inverse hexagonal (H_{II}) and inverse micellar (M_{II}). Figure adapted from Israelachvilli[17].

Although different structures can be formed that fit one *CPP*, entropy will favor the structure with the fewest necessary molecules (smallest aggregation number).[17]

If we apply the *CPP* on the aforementioned Pluronic F127 we can explain the phase diagram. When the *cmc* is reached we start at a low *CPP* (Figure I-4, left side), which means the head group of the surfactant molecules are fully hydrated and therefore the head group area is maximized. When the concentration is further increased, the head group area is decreased, because water is equally distributed to the added surfactant molecules. This leads to a higher *CPP* (Figure I-4, middle) and therefore to a change in curvature and structure. With increasing concentration of the surfactant the interactions between aggregates become more important and lead to the formation of more complex structures. In the case of F127 a cubic phase is formed.

Emulsions

Definition

The term emulsion derives from the Latin word 'mulgeo' (milk) and describes in the easiest form a system of two immiscible fluids where one is dispersed into the other one.

Other known forms of dispersed systems are foam (e.g. whipped cream) where gas is dispersed in a liquid, and suspensions (e.g. blood, latex) where a solid is dispersed in a liquid. A further distinction can be made according to the size and stabilization of emulsion into:

- Macroemulsion – which are in the size range of 0.1 µm to 5 µm
- Nanoemulsion – they are in the range of 20 nm to 100 nm and are only kinetically stable (energy input is needed).
- Microemulsion – they occur in the size range of 5 nm to 50 nm and they are thermodynamically stable (self-assembly). They form without energy input. This is only possible with amphiphilic molecules that create a very low surface tension so thermal energy (kT) is enough to form an emulsion.

Common emulsions do not form spontaneously and therefore some form of energy input, like shaking, stirring, or ultra-sonication, is necessary to disperse one liquid into the other. Two main types of emulsions are water-in-oil (W/O) and oil-in-water (O/W). O/W emulsions are the most present emulsions and are used in many areas of industry and also nature. The most famous product is milk but emulsions are also used in paints, glue, agricultural formulations, etc.

Plain mixtures of two immiscible fluids would arguably not remain in a dispersed state, but separate into two phases. The speed of the phase separation is dependent on the size of the dispersed droplets, the interfacial tension, the density difference of the two fluids and the viscosity of the continuous phase. To avoid the phase separation there is usually a third component added, a so called emulsifier, which works as a stabilizer. These components are usually amphiphilic molecules, but also nanoparticles like SiO_2 are possible. For the formation of a stable emulsion the properties of the stabilizer are crucial. The stabilizer has first to lower the interfacial tension between water and oil to low values and second it has to migrate fast to the newly formed interface and form a monolayer to prevent the recurrence of coalescence. Large proteins, high molecular weight polymers or amphiphilic particles might be good stabilizers, but since the diffusion is slow, small amphiphilic molecules are superior.

Countless different molecules are suitable as stabilizers, but they differ in their structure and molecular weight. One way to classify the different molecules is the hydrophilic-lipophilic balance or HLB[18,19] (see Eq.I-2). This is valid for non-ionic surfactants and used to find the right stabilizer or stabilizer mixture to form an emulsion.

$$HLB = 20 * \left(\frac{M_{hydrophilic}}{M_{total}} \right)$$
Eq. I-2

$M_{hydrophilic}$ is the molar mass of the hydrophilic headgroup and M_{total} the molar mass of the entire molecule. A higher molar mass of the headgroup or, shorter tails (lower total mass) means that the HLB will be high. Surfactants with a high HLB usually form O/W emulsions, due to their better solubility in water. Vice versa surfactants with a low HLB are used to form W/O emulsions due to their better solubility in oil (see Figure I-5).
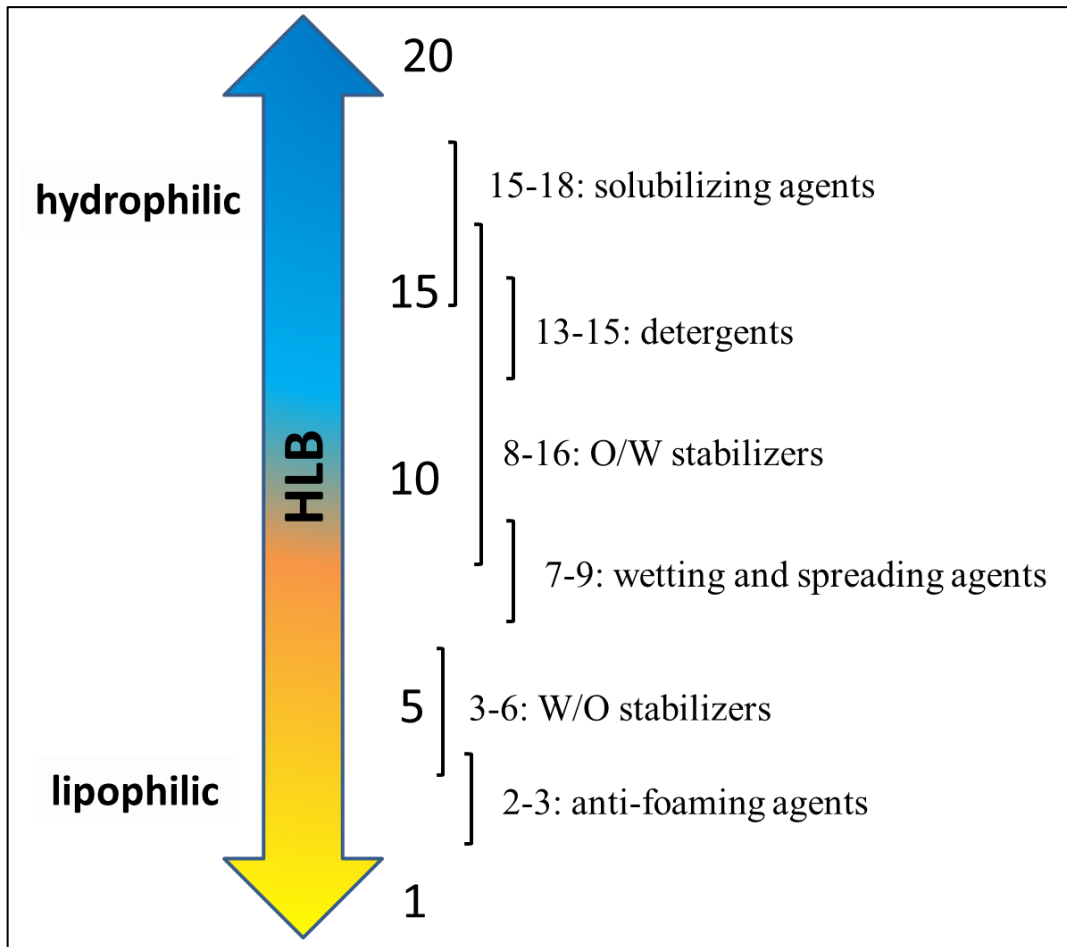
Figure I-5. Hydrophilic-lipophilic balance (HLB) scale and respective stabilizer function.

The disadvantage of the HLB, although a powerful tool, is that it ignores charged groups, and gives no insight into the phase volume ratios that can be emulsified, or the concentration of the emulsifier needed

If the formed emulsion is a W/O or an O/W emulsion depends on the volume ratio of the liquids, the emulsifying agent and its concentration in connection with temperature. The most important parameter however is the solubility of the emulsifier or in the case of solid stabilizers the wettability as can already be seen in the HLB.

As described by Wilder Dwight Bancroft, the phase where the emulsifier is more soluble will be the continuous phase.[20]

The applicability of emulsions is mostly dependent on their long term stability. This stability is dependent on several parameters such as temperature, density difference,

type and concentration of the stabilizer, droplet size, and the distribution of the droplet size. Stabilization with uncharged stabilizers, such as nonionic surfactants is purely steric. Stabilization with charged stabilizers, such as CTAB, show a larger repulsive potential due to the electrostatic force. However the emulsion can be easily destabilized by adding salt and therefore neutralizing the charge.

The destabilization of emulsions is driven by attractive interactions. The most important attractive interaction force is the van der Waals force. This force is only active at very short distances which can be overcome by the polymer layer of a surfactant or the hydrophilic head group of the surfactant.

Besides the intrinsic van der Waals force there is also an artificial attractive interaction that can lead to the destabilization of emulsions - the attractive depletion interaction[21,22].

Stabilized particles or droplets act as hard spheres, which means they cannot go through each other or overlap. Depletion interaction is introduced by the addition of non-adsorbing molecules or particles, so-called depletants, which have a size much smaller than the dispersed particles. These depletants are moving freely in between the dispersed particles. However, when two of the dispersed particles come close together the depletants are pushed aside from the area in between the particles (depletion zone). As a consequence that the small depletants can no longer penetrate this depletion zone they push on the outer side of the large particles and hence create an osmotic pressure. This results in the flocculation of all large particles.

There are several ways an emulsion can degrade (see schematic in Figure I-6):

- **Creaming, Sedimentation**

A creaming or sedimentation process, depending on the viscosity difference between the two fluids, usually occurs when the Brownian motion is exceeded by an external force like centrifugation or simply gravitation. The droplets gather closely packed but are still surrounded by the stabilization layer and the continuous phase. Such degradation can often be reversed by little energy input, e.g. hand shaking.

- **Flocculation**

Flocculation describes the assembly of droplets into flocs without changing the individual droplet size. The reason for the flocculation is the van der Waals attraction

which occurs when no sufficient repulsive forces like charges are present on the droplet surface.

- **Ostwald ripening**

This process occurs because larger particles are thermodynamically favored. More precisely the surface tension creates a pressure on the dispersed phase (Laplace pressure) which is inverse proportional to the droplet size. This means that the Laplace pressure is higher in smaller droplets and therefore molecules are transferred from smaller to larger particles. It also means that Ostwald ripening is primarily dependent on the polydispersity of the emulsion. In monodisperse emulsions the Laplace pressure is equal and therefore no Ostwald ripening takes place. Furthermore this process does not require direct contact by the droplets, but occurs by transport of molecules of the dispersed phase through the continuous phase. The rate of Ostwald ripening is therefore dependent on the solubility of the dispersant in the continuous phase.

- **Coalescence**

Coalescence is the process when two parent droplets merge into one daughter droplet. This happens via four steps- contact that allows attractive interaction, drainage of the continuous phase film between the droplets, the rupture of the film, and the collapse of the droplets. The limit of coalescence is the complete phase separation into two distinct liquid phases.

- **Phase inversion**

Phase inversion is the process where the dispersed phase changes into the continuous phase. This change can be achieved by temperature change, addition of salt, changing the volume fraction of the phases or by induction of a flow. This is of course dependent on the used emulsion system. [23] This phenomenon is used to produce emulsions with very fine droplets (nanoemulsions) and used in the industry to produce cosmetic and pharmaceutical products.
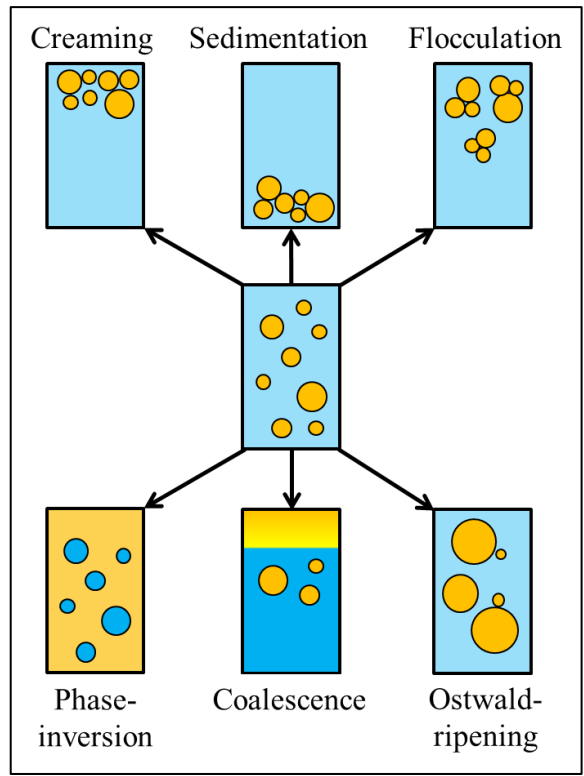
Figure I-6. Schematic of degradation processes of emulsions.

ISAsomes

Internally self-assembled particles (or ISAsomes) are soft matter colloidal systems. They describe the confinement of a lyotropic liquid crystal which is stabilized in an emulsion. The first nanostructured emulsions were developed by the group of Gustafsson[24,25] in 1996/97. They achieved the formation of an emulsion containing cubic and hexagonal LC structures. Additional structures using a similar system were found by Yaghmur et al.[26] in 2005, who introduced the term ISAsomes.

These emulsions consist of a continuous phase, in most cases water, and a dispersed phase which contains a liquid crystal structure or sometimes a microemulsion. The LC structure is formed by the interaction of amphiphilic molecules in combination with a co-solvent which is usually oil, e.g. almond oil, tetradecane, etc. Such emulsions are intensively investigated because their internal nano-structures have a large interfacial area and the possibility to incorporate hydrophilic, lipophilic as well as amphiphilic molecules at low viscosity make them to ideal delivery systems. The amphiphilic molecule that is responsible for the formation of the LC structures is also called the primary surfactant (PS). As mentioned before the LC phase is formed by self-assembly and is in a thermodynamic equilibrium. The emulsion however is stabilized kinetically, which means an energy input is necessary. The long term stability is ensured by the use of stabilizers such as nonionic polymers, proteins or particles. A schematic depiction of the formation of ISAsomes can be found in Figure I-7.
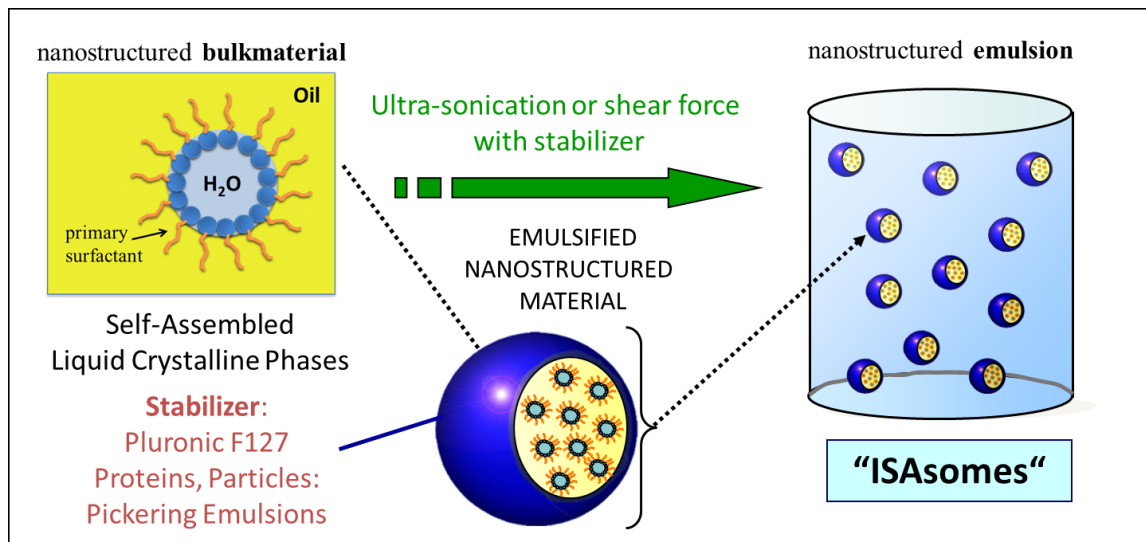
Figure I-7. Schematic of the emulsification of a LC phase into hierarchically organized particles. The graph was adapted from de Campo et al.[27]

A major characteristic that allows the formation of an emulsion is that these liquid crystals are stable against dilution by the continuous phase. The bulk phase, primary surfactant or primary surfactant and oil, will take up water to a certain degree. Beyond this point all added water is present as excess water. Since these systems are also dependent on temperature this results in a phase separation line, beyond which the nanostructure is still stable (see Figure I-8).
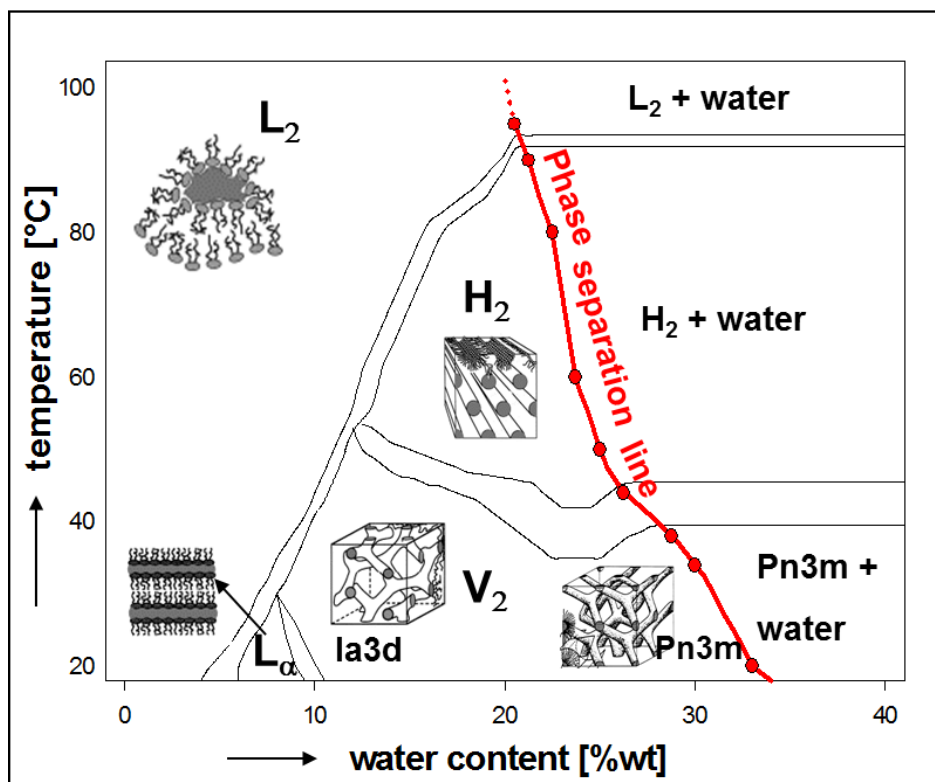
Figure I-8. Phase diagram of the monolinolein/water system showing the phase separation line. The graph was taken from de Campo et al.[28]

As can be seen from Figure I-8 monoglycerides show liquid crystalline phases when in contact with water. Richer phase diversity at room temperature is exhibited when an alkane is added and the ratio of monoglyceride/alkane is varied. As an example the system of monolinolein – tetradecane – water – F127 is shown in Figure I-9.
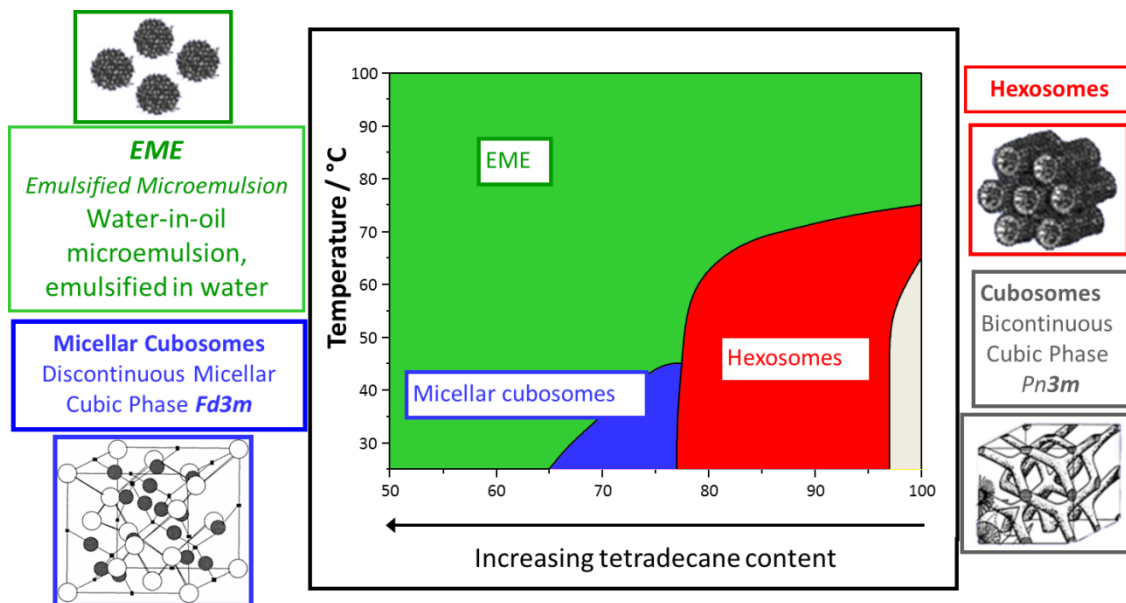
Figure I-9. Phasediagram of the monolinolein – tetradecane – water – F127 emulsion dependent on temperature and ratio of monolinolein/tetradecane (x-axis). The graph was adapted from Guillot et al.[29]

The produced emulsion is usually named after the LC phase it contains. Hexosomes contain a hexagonal phase, cubosomes a cubic phase, etc. In order to be able to act as a carrier the used LC phase has to be closed. This is the case for the emulsified microemulsion, micellar cubosomes and hexosomes[30] depicted in Figure I-9. Only cubosomes are open, which means that incorporated hydrophilic molecules would leak out quickly. Although the cubosomes and hexosomes are both tubular systems it is yet not fully explained why one is open and the other is not. A possible explanation is given by the results of Sagalowicz et al.[31] (Figure 7 in the publication) who shows cryo-TEM pictures of hexosomes. On these pictures the hexagonal tubes appear to be closed in hexagonally ordered ring systems.

However if lipophilic molecules are incorporated they are taken up by the monolinolein and oil in the LC and would be better stabilized.

The advantages of ISAsomes are the low viscosity, which makes them versatile for numerous applications and the adaptability. The internal nanostructure can be modified in many different ways. The internal size can be tuned to maximize the loading capacity[32] and other functionalities e.g. pH sensitivity can be added by incorporating functional molecules[33].

Methods

Preparation methods

The whole thesis revolves around the development of reverse ISAsomes (see Chapter III) which means the dispersion of a hydrophilic liquid crystal in a continuous oil phase. Hence the following preparation methods are focused on the production of the reverse W/O system.

Definition of the sample composition

Bulk samples are non-dispersed samples. The binary mixtures of primary surfactant (PS) which is used to form the LC phase, and water are described by δ, which denotes the weight ratio between the primary surfactant and water.

$$\delta = \frac{mass\ (PS)}{mass\ (PS + water)} * 100 \qquad\qquad \text{Eq. I-3}$$

Ternary mixtures are formed by addition of tetradecane to the binary systems, where the oil content is given in weight percent. Ternary mixtures can be one-phase systems for low tetradecane content, and they eventually form two-phase systems at higher amounts of tetradecane.

Dispersions can only be formed from such two-phase ternary systems which consist of the bulk (primary surfactant, water and tetradecane) and additional stabilizer. They are characterized by β, which defines the stabilizer content relative to the mass of the dispersed binary phase, and Φ, which describes the overall content of the dispersed phase.

$$\beta = \frac{mass\ (stabilizer)}{mass\ (PS + water)} * 100 \qquad\qquad \text{Eq. I-4}$$

$$\Phi = \left[\frac{mass\ (PS + water)}{mass\ (PS + water + TD + stabilizer)}\right] * 100 \qquad \text{Eq. I-5}$$

Binary surfactant–water systems

Since the surfactants E4–E9 and L64 are commercial products and not highly purified, the phase behavior, especially the formation of LC phases, had to be controlled by preparing the corresponding bulk samples. The primary surfactant and water were weighed in a 4 mL vial with different ratios (δ values). The mixtures were heated to 80°C for 5 min to melt any occurring LC phase and ensure homogeneous mixing before cooling to room temperature while vortexing (RS-VA 10, Phoenix Instrument, Garbsen, Germany). The cooling was accelerated by an airgun to avoid phase separation. The samples were left at room temperature for at least 24 h to equilibrate before structural characterization.

Ternary surfactant–water–oil systems

Tetradecane was added with increasing concentration to the binary mixtures with fixed δ values. The samples were heated to 80°C to melt any LC and allow the oil to be incorporated into the LC upon cooling. The cooling was again accelerated by an airgun during vortexing to ensure homogeneity.

Dispersions

Dispersions are produced by adding the fourth component, the stabilizer, to the two-phase ternary system and by applying shear forces (ultra-sonication). This makes it possible to disperse the LC in excess tetradecane. The primary surfactant, water, tetradecane and a 5 wt% stock solution of stabilizer dissolved in tetradecane were weighed into 4 mL vials. The samples were ultrasonicated for 10 min. The ultra-sonication device (Vibra-Cell, Sonics & Materials, Newtown, CT, USA) was equipped with a tapered tip and used at 120 W (30% amplitude of the maximum power of 400 W) in pulsed mode (0.2 s pulses in between 2 s breaks). The samples were placed in a water bath during ultra-sonication to facilitate heat dissipation. The samples were

characterized by dynamic light scattering, polarization microscopy and small-angle X-ray scattering after one hour of equilibration time.

Polarization Microscopy

Polarization microscopy was carried out on a Leica DM2500 M microscope with two polarization filters to show anisotropy of certain liquid-crystal phases from their optical birefringence. The centrifuged sample was squeezed to a thin layer of about 100 μm and investigated in transmittant light mode, with a 20x/0.40 objective. The mounted camera was a Sony[TM] DXC-390P. The pictures were recorded using the software Sarfusoft 2.1 (Nanolane, France).

Dynamic Light Scattering (DLS)

DLS was used to determine the mean hydrodynamic radius of the dispersion droplets. The DLS equipment consisted of a diode laser (Coherent Verdi V5, $\lambda = 532$ nm) and a goniometer with single-mode fiber detection optics (OZ from GMP, Zürich, Switzerland). The data was acquired by an ALV/SO-SIPD/DUAL photomultiplier with pseudo-cross correlation and an ALV 7004 Digital Multiple Tau Real Time Correlator (ALV, Langen, Germany). The correlation functions were determined and stored by the ALV software package. The light-scattering signal was measured ten times for 30 s at a scattering angle of 90° at 25 °C and the resulting correlation functions were averaged. The mean hydrodynamic radius R_H was calculated by means of the cumulant method[66].

Small Angle X-ray Scattering (SAXS)

The SAXS equipment consisted of a high-flux SAXSess camera (Anton Paar, Graz, Austria) connected to a Debyeflex 3003 X-ray generator (GE-Electric, Germany) operating at 40 kV and 50 mA with a sealed-tube Cu anode. The Goebel-mirror focused and Kratky-slit collimated X-ray beam was line-shaped (17 mm horizontal dimension at the sample). The scattered radiation was measured in the transmission mode and

recorded by a one-dimensional MYTHEN-1k microstrip solid-state detector (Dectris, Switzerland), within a q range of 0.1–6 nm^{-1}. The magnitude of the scattering vector q is given by $q = 4\pi(\sin\theta)/\lambda$, with 2θ being the scattering angle with respect to the incident beam and λ the wavelength of the X-rays, 0.154 nm. All measurements were conducted at 25°C.

References

1. Ubbink, J., Burbidge, A. & Mezzenga, R. Food structure and functionality: a soft matter perspective. *Soft Matter* **4,** 1569–1581 (2008).

2. Mezzenga, R., Schurtenberger, P., Burbidge, A. & Michel, M. Understanding foods as soft materials. *Nat. Mater.* **4,** 729–740 (2005).

3. Tomsic, M., Guillot, S., Sagalowicz, L., Leser, M. E. & Glatter, O. Internally self-assembled thermoreversible gelling emulsions: ISAsomes in methylcellulose, kappa-carrageenan, and mixed hydrogels. *Langmuir* **25,** 9525–34 (2009).

4. Salentinig, S., Sagalowicz, L. & Glatter, O. Self-assembled structures and pK a value of oleic acid in systems of biological levance. *Langmuir* **26,** 11670–11679 (2010).

5. Pirolt, F., Glatter, O. & Trimmel, G. Reverse Hexosome Dispersions in Alkanes—The Challenge of Inverting Structures. *Langmuir* **34,** 8379–8387 (2018).

6. Iglesias, G., Pirolt, F., Sadeghpour, A. & Glatter, O. Lipid Transfer in Oil-in-Water Isasome Emulsions: Influence of Arrested Dynamics of the Emulsion Droplets Entrapped in a Hydrogel. *Langmuir* **29,** 15496–15502 (2013).

7. Sadeghpour, A., Pirolt, F. & Glatter, O. Submicrometer-sized Pickering emulsions stabilized by silica nanoparticles with adsorbed oleic acid. *Langmuir* **29,** 6004–12 (2013).

8. Lehmann, O. Über fließende Krystalle. *Zeitschrift für Phys. Chemie* **4,** 462–472 (1889).

9. Reinitzer, F. Beiträge zur Kenntniss des Cholesterins. *Monatshefte für Chem.* **9,** 421–422 (1888).

10. Heilmeier, G. H., Zanoni, L. A. & Barton, L. A. Dynamic scattering in nematic liquid crystals. *Appl. Phys. Lett.* **13,** 46–47 (1968).

11. Goldmacher, J. E. & Castellano, J. A. Electro-optical compositions and devices.

12. Rego, J. A., Harvey, J. A. A., MacKinnon, A. L. & Gatdula, E. Asymmetric

synthesis of a highly soluble 'trimeric' analogue of the chiral nematic liquid crystal twist agent Merck S1011. *Liq. Cryst.* **37,** 37–43 (2010).

13. Diele, S. *et al.* Liquid Crystalline Structures of the 2-(trans-4-n-alkylcyclohexyl)propan-1,3-diols. *Mol. Cryst. Liq. Cryst. Inc. Nonlinear Opt.* **166,** 131–142 (1989).

14. de Gennes, P. G. & Prost, J. *The Physics of Liquid Crystals*. *Opt. Acta Int. J. Opt.* **22,** (1993).

15. Martin, J. D. *et al.* Metallotropic liquid crystals formed by surfactant templating of molten metal halides. *Nat. Mater.* **5,** 271–275 (2006).

16. Wanka, G., Hoffmann, H. & Ulbricht, W. Phase Diagrams and Aggregation Behavior of Poly(oxyethylene)-Poly(oxypropylene)-Poly(oxyethylene) Triblock Copolymers in Aqueous Solutions. *Macromolecules* **27,** 4145–4159 (1994).

17. Israelachvili, J. N. *Intermolecular and Surface Forces*. *J. Chem. Inf. Model.* **53,** (2011).

18. Griffin, W. C. Classification of Surface-Active Agents by 'HLB'. *J. Cosmet. Sci.* **1,** 311–326 (1949).

19. Griffin, W. C. Calculation of HLB Values of Non-Ionic Surfactants. *J. Cosmet. Sci.* **1,** 249–256 (1954).

20. Bancroft, W. The Theory of Emulsification, IV. *J. Phys. Chem.* **7,** (1912).

21. Asakura, S. & Oosawa, F. Interaction between Particles Suspended in Solutions of Macromolecules. *J. Polym. Sci.* **33,** 183–192 (1958).

22. Cowell, C., Li-In-On, R. & Vincent, B. Reversible flocculation of sterically-stabilised dispersions. *J. Chem. Soc. Faraday Trans. 1 Phys. Chem. Condens. Phases* **74,** 337–347 (1978).

23. Preziosi, V., Perazzo, A., Caserta, S., Tomaiuolo, G. & Guido, S. Phase inversion emulsification. *Chem. Eng. Trans.* **32,** 1585–1590 (2013).

24. Gustafsson, J., Ljusberg-Wahren, H., Almgren, M. & Larsson, K. Cubic Lipid-Water Phase Dispersed into Submicron Particles. *Langmuir* **12,** 4611–4613 (1996).

25. Gustafsson, J., Ljusberg-Wahren, H., Almgren, M. & Larsson, K. Submicron Particles of Reversed Lipid Phases in Water Stabilized by a Nonionic Amphiphilic Polymer. *Langmuir* **13,** 6964–6971 (1997).

26. Yaghmur, A., Campo, L. De & Sagalowicz, L. Emulsified microemulsions and oil-containing liquid crystalline phases. *Langmuir* 569–577 (2005).

27. de Campo, L. *et al.* Five-component food-grade microemulsions: structural characterization by SANS. *J. Colloid Interface Sci.* **274,** 251–267 (2004).

28. De Campo, L. *et al.* Reversible phase transitions in emulsified nanostructured lipid systems. *Langmuir* **20,** 5254–5261 (2004).

29. Guillot, S. *et al.* Direct and indirect thermal transitions from hexosomes to emulsified micro-emulsions in oil-loaded monoglyceride-based particles. *Colloids Surfaces A Physicochem. Eng. Asp.* **291,** 78–84 (2006).

30. Phan, S., Fong, W. K., Kirby, N., Hanley, T. & Boyd, B. J. Evaluating the link between self-assembled mesophase structure and drug release. *Int. J. Pharm.* **421,** 176–182 (2011).

31. Sagalowicz, L. *et al.* Crystallography of dispersed liquid crystalline phases studied by cryo-transmission electron microscopy. *J. Microsc.* **221,** 110–121 (2006).

32. Chemelli, A., Maurer, M., Geier, R. & Glatter, O. Optimized loading and sustained release of hydrophilic proteins from internally nanostructured particles. *Langmuir* **28,** 16788–16797 (2012).

33. Salentinig, S., Tangso, K. J., Hawley, A. & Boyd, B. J. pH-driven colloidal transformations based on the vasoactive drug nicergoline. *Langmuir* **30,** 14776–14781 (2014).

Chapter II - CO_2 Driven Colloidal Phase Transitions

Table of Contents

Introduction

Colloidal systems which can alter their structure and properties when exposed to certain triggers including temperature[1,2], ultrasound[3], enzyme[4,5], light[6,7] and pH[8–11] are widely studied, especially in the pharmaceutical industry for targeted drug delivery and in the oil industry for extraction and cleaning processes.

The aim of this project was to design a LC system with a closed structure, e.g. emulsified micro emulsion (EME), inverse micellar cubosomes (Fd3m), or hexagonal (H_{II}), and add a functionality to trigger a phase transition to an open structure such as, the inverse bicontinuous cubic phase or even dissolve the liquid crystals into vesicles or direct micelles. This phase transitions can be used to release encapsulated active components. Reversibility was a point of interest but not the highest priority. CO_2 was chosen as an external trigger since it is a cheap and easily available substance with biological relevance. It can alter the structure and properties of polymers and surfactant if they are equipped with CO_2 active moieties like amine, amidine or guanidine groups[12–15]. Until now the major role of such systems was to act as polarity switches. The addition of CO_2 leads to higher polarity of the molecules by forming ionic species, and the removal of CO_2 by purging with N_2 or heat treatment would reverse the system to its low polarity state. This allowed numerous applications in solvent-based separation processes, as CO_2 sensor or CO_2 captor.

In this work the reversible transformation of an amine- to a carbamate group upon the reaction with CO_2 was investigated to achieve a phase transition in self-assembled lyotropic liquid crystalline systems. During the reaction with CO_2 the neutral amine group is transformed into the corresponding negatively charged carbamate and a proton (see Figure II-1). The reaction is reversible by heating, purging with N_2 gas or acidification of the solution.[16–19] The charge repulsions among the negatively charged carbamate headgroups at the interface after reaction with CO_2 leads to an increase in the effective headgroup area which decreases the critical packing parameter (*CPP*, see Chapter I – Theory). This ultimately changes the curvature of the O/W interface and may induce a phase transition to more hydrophilic interfaces.
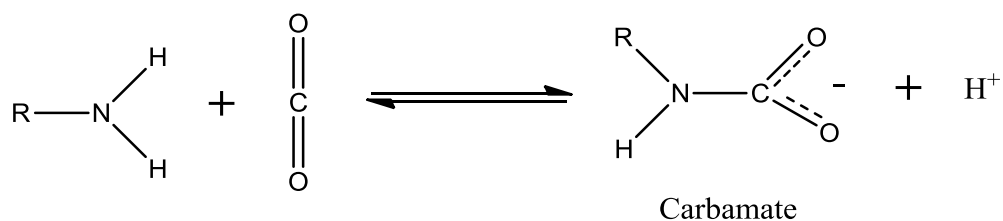
Carbamate

Figure II-1. Scheme of the carbamate formation upon reaction of the amine group with CO_2

Short-chain organic amines such as mono and di-ethanolamine are well researched agents for the capture of CO_2.[16] The amine groups react with the CO_2 to form a carbamate anion and a proton (see Figure II-1). The reaction is reversible by heating, purging with N_2 gas or acidification of the solution.[16–19]

Groundwork has already be done by Salentinig et al.[20] by introducing CO_2 responsive, amine-modified polymer micelles with possible applications in the food, pharma and energy sector. In the scope of this work the transfer of such properties to ISAsomes was attempted by (i) studying the phase diagram of lipid/amine mixtures in the bulk and (ii) investigating the effect of CO_2 on the self-assembly in the dispersed system.

Materials

Oleylamine (OLA), an aliphatic primary amine, was purchased from Sigma Aldrich Co. LLC. As primary surfactant we used technical grade monoglyceride, glycerol monooleate (GMO) as the commercial grade product Dimodan MO 90/D and monolinolein Dimodan U/J (DMU). Both were purchased from Danisco A/S, Braband, Denmark. 2-Dimethylaminoethanol (DMAE) and 2-(Dibutylamino)ethanol (DBAE) were purchased from Sigma Aldrich (Buchs, Switzerland). Structures of the used monoglycerides and amines are depicted in Figure II-2. L-Tryptophan (Trp) with purity higher than 99% was purchased from Carl-Roth GmbH & Co.KG, Germany. Triblock copolymer Pluronic F127 was a gift from BASF (Mount Olive, New Jersey, USA). Deionized water was used for all experiments. Sodium hydroxide pellets were purchased from Sigma Aldrich (Switzerland) and hydrochloric acid (37%) was purchased from VWR Chemicals (USA).
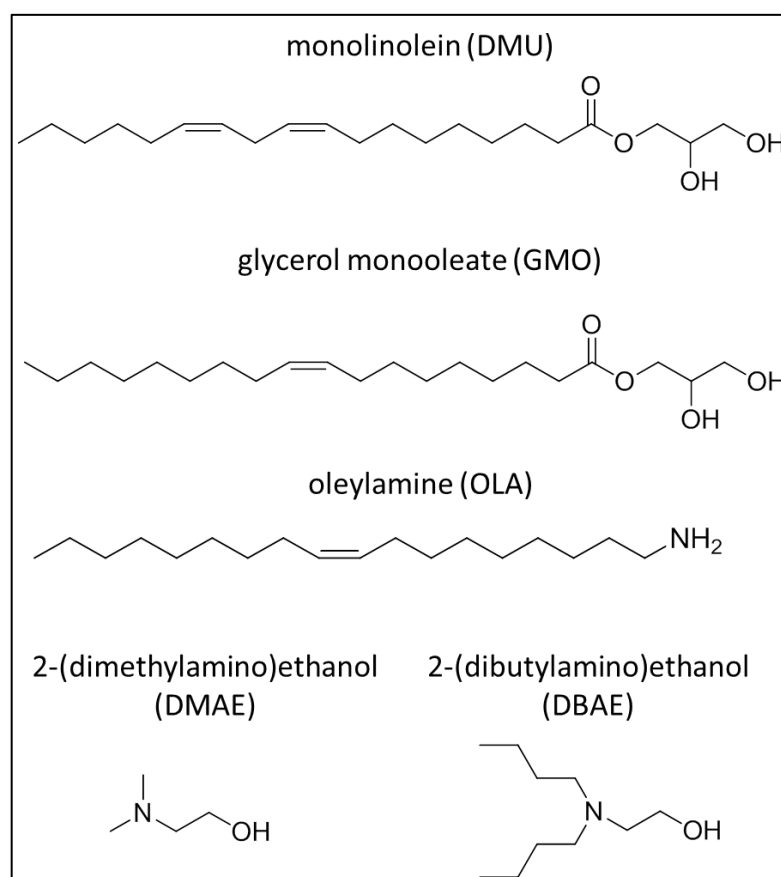
Figure II-2. Structure of the used monoglycerides and amines.

Sample Preparation

Bulk

Bulk samples consisted of GMO – OLA – water. The bulk samples were heated to 100°C for 5 min. and mixed by vortexing. During vortexing the samples were cooled with an airgun to increase the cooling rate and ensure homogenization. The GMO/OLA ratio is defined by the δ-value described in Eq. II-1.

$$\delta = \frac{mass\ (GMO)}{mass\ (GMO + OLA)} * 100 \qquad \text{Eq. II-1}$$

The overall amount of the oil phase (GMO + OLA) used in the sample is defined by ϕ (see Eq. II-2).

$$\phi = \left[\frac{mass(GMO + OLA)}{mass(GMO + OLA + water)}\right] * 100 \qquad \text{Eq. II-2}$$

ϕ was kept at 60 % for the bulk samples.

Dispersions

Dispersions of GMO – OLA, stabilized by the triblock copolymer Pluronic F127 were prepared. Deionized water containing 1 wt% F127 was used as stock solution for all samples. The amount of used F127 relative to the dispersed phase (GMO + OLA) is defined by β.

$$\beta = \left[\frac{mass(F127)}{mass(GMO + OLA)}\right] * 100 \qquad \text{Eq. II-3}$$

The samples were sonicated using a tip sonicator (tapered tip) for 5 minutes (Pulse: 0.5 ON/ 1.5 OFF at a power of 120 W). During the sonication the samples were placed in a water bath to facilitate heat dissipation. ϕ was kept at 10 % for the dispersions. The characterization of the samples was performed with small angle x-ray scattering (SAXS) and polarization microscopy.

CO$_2$ purging

All samples were purged with CO_2 at approximately 3-5 bar for 2 minutes. Since the sample vials were open, a low pressure was used to avoid splashing of sample, excessive foam formation and increased evaporation of water. When too much water is evaporated the sample composition would have been compromised.

Characterization

All samples were characterized with in-house methods. Structures were investigated by small angle X-ray scattering (SAXS). The SAXS patterns of inverse hexagonal phases were characterized by the mean lattice parameter *a* (see Eq. II-4). This parameter is derived from the relative positions of the corresponding Bragg reflections in the SAXS spectra by the following relation:

$$a = \frac{4\pi}{\sqrt{3}q_{peak1}}$$ Eq. II-4

where q_{peak1} is the q value of the first peak in the spectrum[21]. The parameter describes the size of the unit cell of the respective structure.

The birefringence of the hexagonal phase was investigated with a polarization microscope. Respective particle sizes were measured by dynamic light scattering (DLS). Details concerning all methods can be found in Chapter I of this thesis.

Results

OLA - Bulk Screening

The first step was to incorporate the Oleylamin into a liquid crystalline two-component system with well-studied phase behavior. Since OLA and oleic acid have the same alkyl chain structure, we used the phase diagram of the GMO/oleic acid system as guideline and replaced the oleic acid with OLA[11] to achieve specific structures.
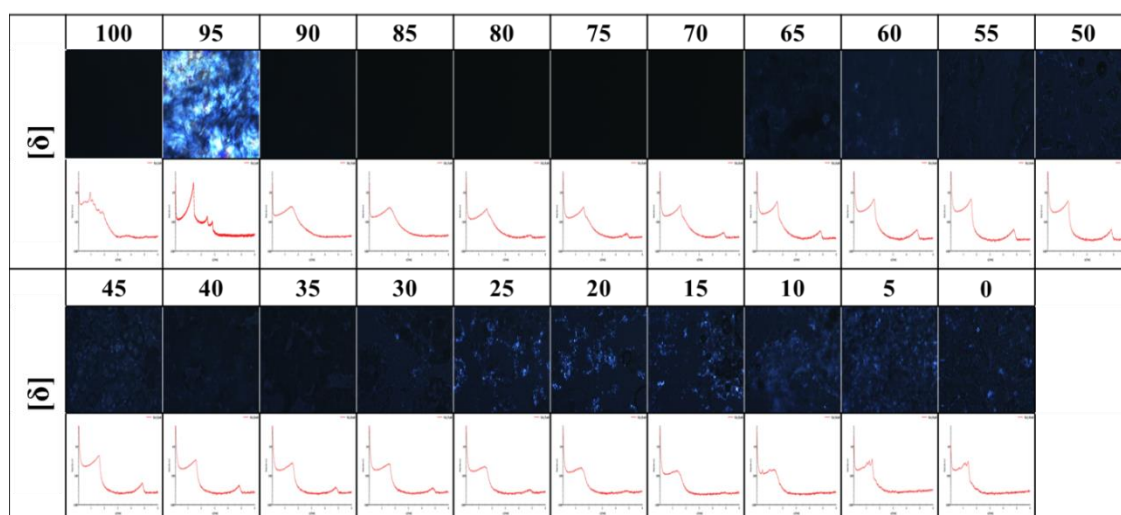
Figure II-3. Screening results for the binary GMO/OLA bulk phase; Upper row: polarization microscope pictures; Lower row: SAXS curves; the sample composition was $\phi = 60$ wt% oil phase (GMO + OLA), 40 wt% H_2O.

Bulk samples of GMO and OLA were prepared at defined δ between 0 and 100. Figure II-3 shows the characteristic SAXS pattern of a bicontinuous cubic phase (Pn3m type) at a water saturated δ_{100}, in agreement with previous studies[22]. The inverse hexagonal phase was found at δ_{95}. This is supported by the birefringence that can be seen in the polarization microscopy image. Between δ_{90} and δ_{85} a broad single peak at $q = 1.5$ nm^{-1} can be observed in the SAXS curves, indicative of an inverse microemulsion. At δ values between 80 and 15 the formation of a lamellar phase was discovered and at δ_{10}

and δ_5 the formation of a mixed phase is observed which most likely contains a micellar cubic (Fd3m) and a bi-continuous cubic phase.
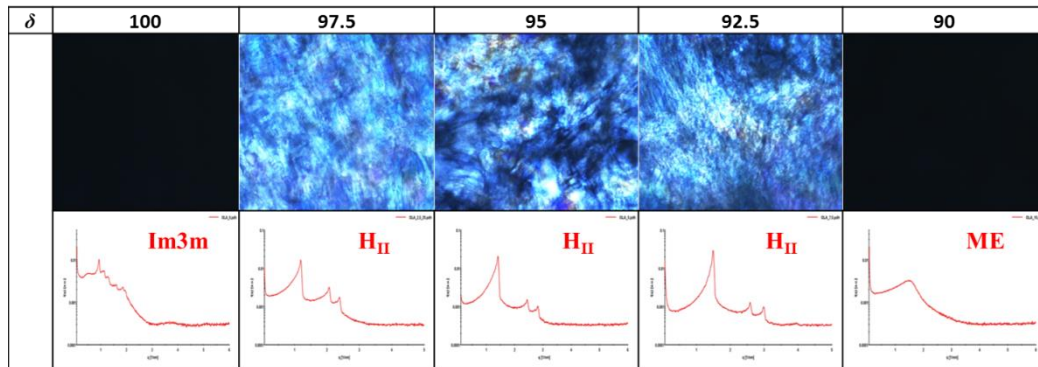
Figure II-4. Results of OLA bulk samples between δ_{100} and δ_{90}; Upper part: polarization microscopy images. Lower part: SAXS spectra of bulk phases, Im3m - type of cubic phase, H_{II} - inverse hexagonal phase, ME - micro emulsion.

Figure II-4 shows a more detailed investigation of nanostructures between δ_{100} and δ_{90}. The polarization microscope pictures clearly show the presence of the inverse hexagonal phase by birefringence. The influence of increasing OLA amounts on the hexagonal phase is elaborated in Figure II-5.
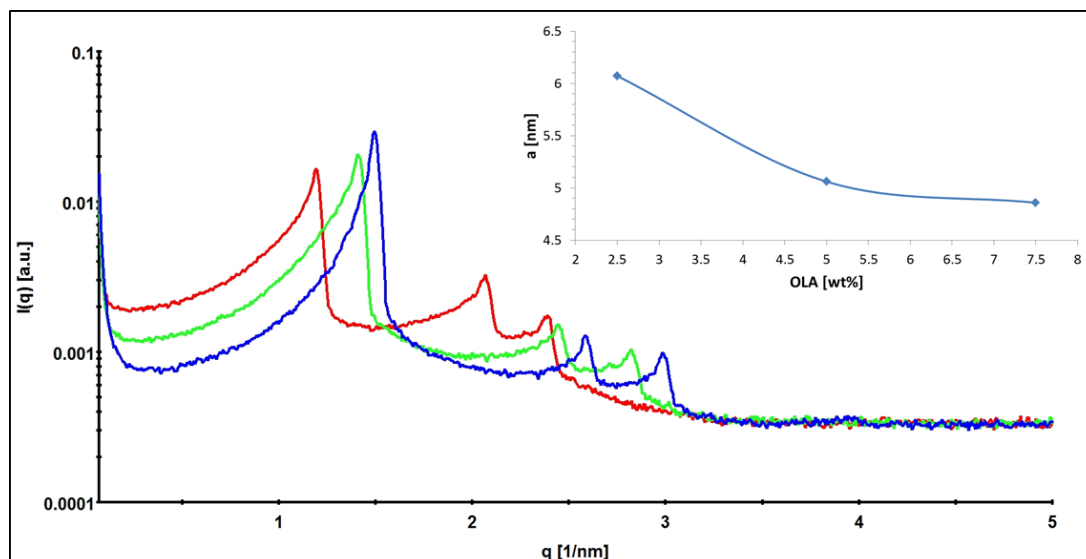
Figure II-5. SAXS spectra of OLA bulk samples $\delta_{97.5}$ (red), δ_{95} (green) and $\delta_{97.5}$ (blue). The box shows the decrease of the lattice parameter *a* with increasing OLA content in the system.

The Bragg reflections from the inverse hexagonal phase shift to higher q-values upon increasing the δ value from 92.5 to 97.5. The corresponding lattice parameter decreases from 6.1 nm at $\delta_{92.5}$ to 4.9 nm at $\delta_{97.5}$.

To further investigate the effect of temperature on the self-assembled structures, a temperature scan between 20°C and 50°C was conducted (see Figure II-6).
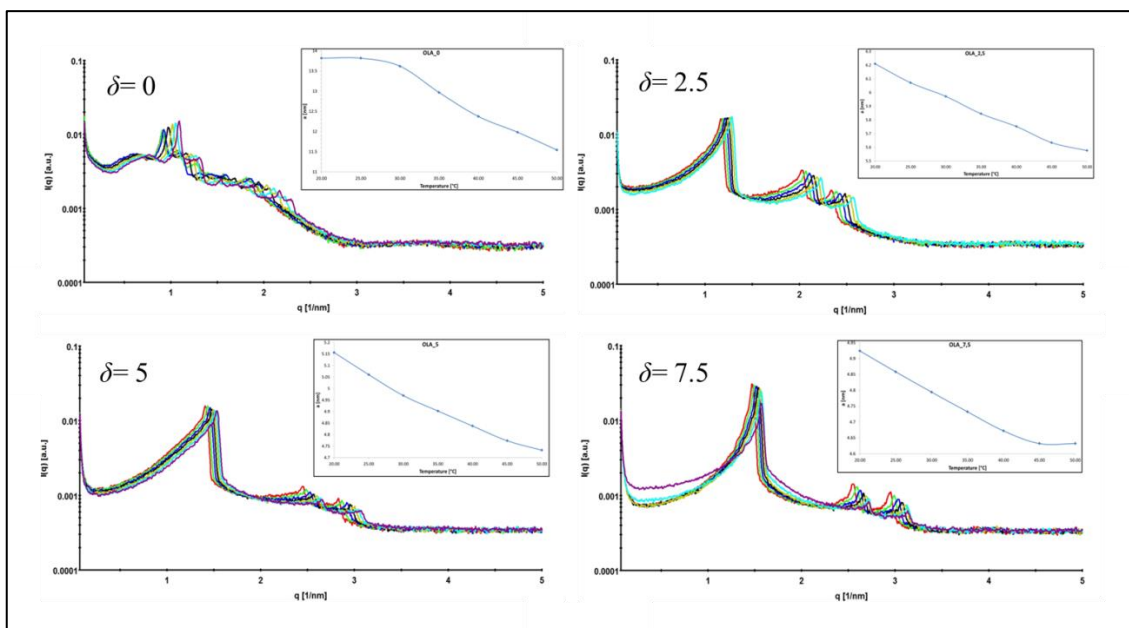
Figure II-6. SAXS spectra and corresponding lattice parameter *a* (inset) upon increasing temperature from 20°C to 50°C in 5 °C steps for the bulk samples at $\delta = 0$, 2.5, 5, 7.5

No phase transformations were observed within this temperature range. The lattice parameter *a* is decreasing with increasing temperature in all samples. This is similar to the so-called 'breathing mode'[2]. Upon heating water is expelled out of the liquid crystal and the mobility of the alkyl chains increases, which impacts on the CPP and ultimately the lattice parameter. This effect is reversed when the system is cooled back to room temperature.

Additionally it was studied if Dimodan U (DMU) could be used instead of GMO. DMU is the commercial form of monolinolein. Similar to GMO (oleic acid ester), DMU is a monoglyceride with the difference of an additional unsaturated carbon bond (linoleic acid ester). This leads to an increase in splay of the hydrophobic carbon chain and possible changes in the interaction with OLA[23]. For this purpose two bulk samples were prepared and compared to the GMO samples (Figure II-7).
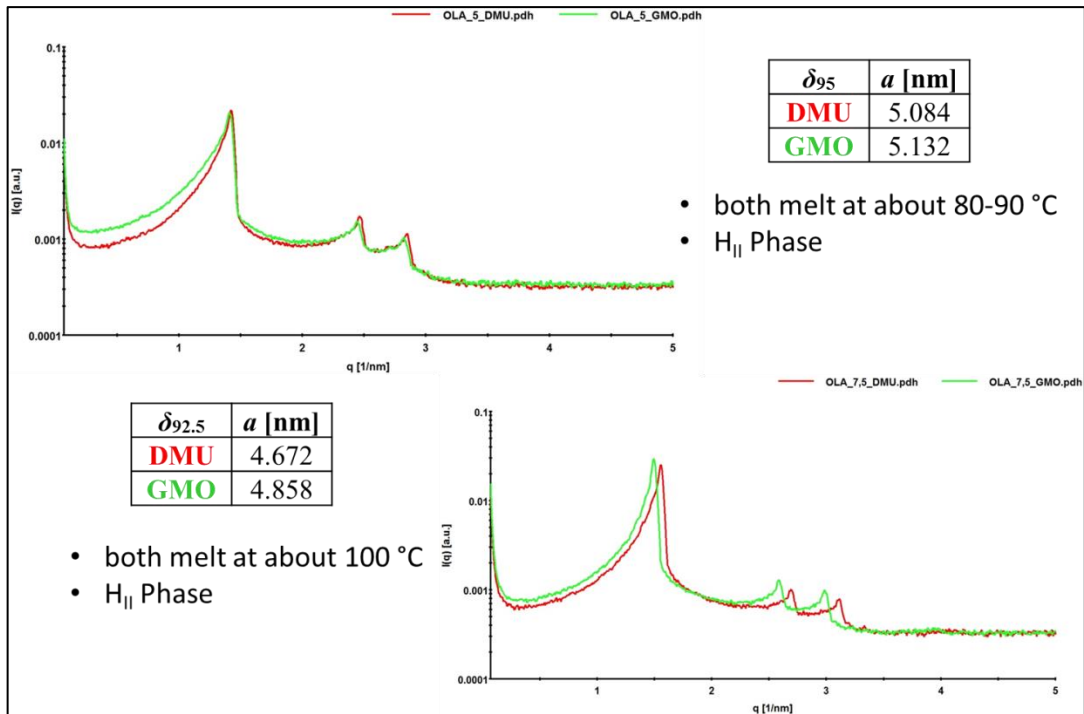
Figure II-7. SAXS graphs of the bulk phases with different primary surfactants: Dimodan U (DMU) compared to glycerol monooleate (GMO)

The SAXS results show that the structure is also stable with DMU and only a slight decrease in the lattice parameter a compared to GMO could be detected. This decrease is attributed to the monoglyceride since the δ_{100} bulk phases (pure monoglyceride saturated with water) of both monoglycerides exhibit a difference in lattice parameter of 0.89 nm for the Pn3m phase. The lattice parameter for δ_{100} GMO is 9.49 nm and the lattice parameter for δ_{100} DMU is 8.6 nm [24].

To investigate the effect of CO_2 on the structure, low-viscous dispersions of the self-assembled structures were prepared from the highly viscous bulk phases. The lower viscosity of the dispersions allows bubbling with CO_2 gas, and monitoring of the structural transformations with SAXS. Initially, dispersions were prepared from previously prepared and equilibrated bulk-phases. Since the bulk samples consist of 60 wt% oil phase and 40 wt% water, this led to $\phi = 60$. Four dispersions were produced from the bulk-phases: δ_{95} (GMO), $\delta_{92.5}$ (GMO), δ_{95} (DMU) and $\delta_{92.5}$ (DMU). The SAXS curves of the respective samples are depicted in Figure II-8.
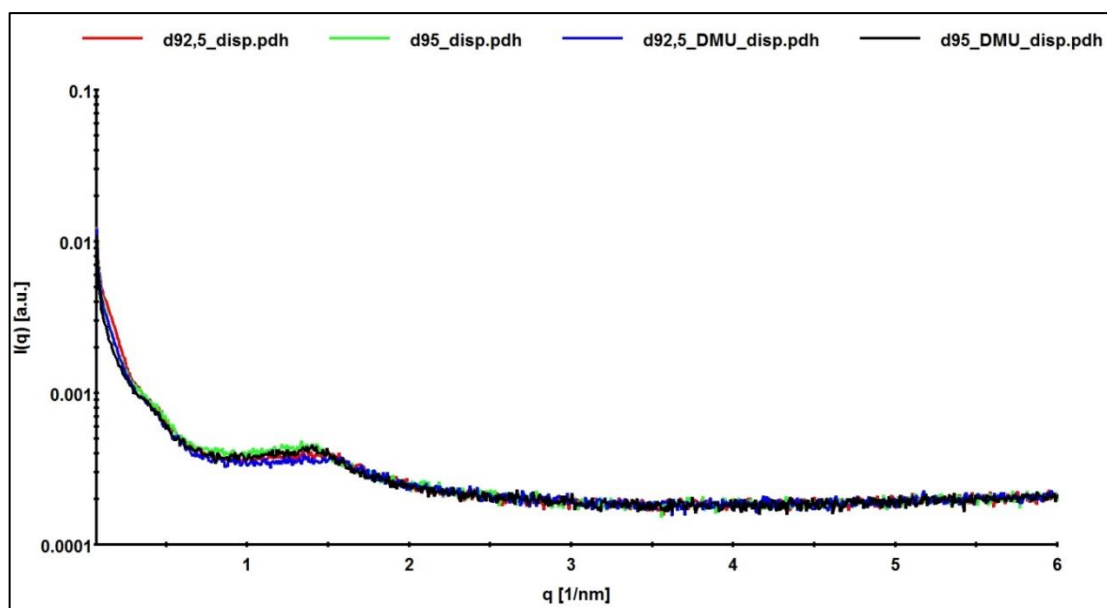
Figure II-8. SAXS results of dispersions prepared from the bulk-samples

All samples (GMO and DMU) did not form the expected hexosomes but instead a scattering pattern indicative for an emulsified microemulsion (EME) was found with a broad correlation peak around $q \sim 1.5$ nm^{-1}. The reason for this might be that the already formed bulk phase is rather stable against dispersion and the energy input by ultra-sonication was not sufficient to homogeneously disperse the material into particles. Also already present CO_2 that was dissolved in water or was incorporated during the sonication process could lead to the reorganization into an EME. The DLS results showed hydrodynamic radii (R_H) between 40 and 60 nm for all samples.

Control experiments (see Appendix) were conducted to check the condition of the primary surfactants. The experiments revealed that the direct sonication of the hydrated bulk phases into dispersions is not working sufficiently. However when the single components are mixed directly before the sonication process the resulting ISAsomes showed the expected nano structure.

Based on this finding, new dispersions were produced (i) under normal conditions (environmental air, no N_2 flow), and (ii) under N_2-flow (Figure II-9) to investigate the effect of CO_2 integration from air during preparation.
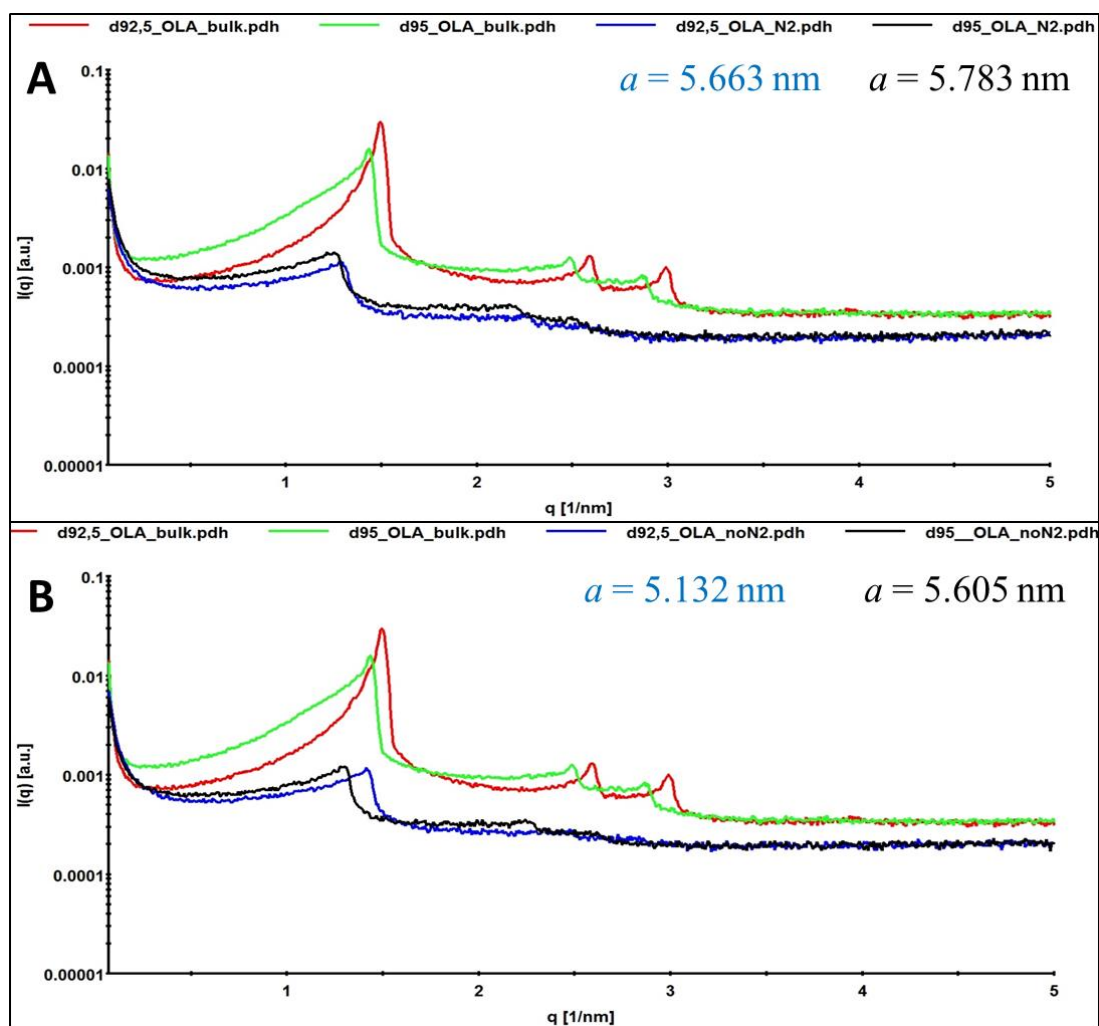
Figure II-9. OLA- Dispersions ($\delta_{92.5}$ – blue, δ_{95} – black) produced under N_2-flow (A) and under air (B); bulk phases ($\delta_{92.5}$ – red, δ_{95} – green) for comparison

The SAXS data presented in Figure II-9 show a difference in lattice parameter between the dispersions produced under environmental air and dispersions produced under N_2 flow. The reaction of the OLA amine group with CO_2 from air (which is approximately 0.04 v/v %) during the production under environmental conditions could already induce the reaction of some amine groups to negatively charged carbamate groups. However the first test showed that larger lattice parameters are reached for the samples, which were produced under N_2-flow. A difference in lattice parameter of about 0.5 nm for $\delta_{92.5}$ and almost 0.2 nm for δ_{95} was found. A possible explanation for this finding is that charge attraction among protonated and positively charged amine groups with the negatively charged carbamates could result in the shrinking of the effective headgroup area at the interface. Similar observations were reported for the integration of positively

charged peptides into negatively charged oleic acid self-assemblies, with a shrinking of the effective headgroup area upon addition of low peptide concentration, followed by an gradual increase of the area at higher peptide content.[25]

OLA – CO$_2$- Response

The dispersions produced under N$_2$-flow were bubbled with CO$_2$ to investigate the change in the self-assembled structure in the system. (Figure II-10)
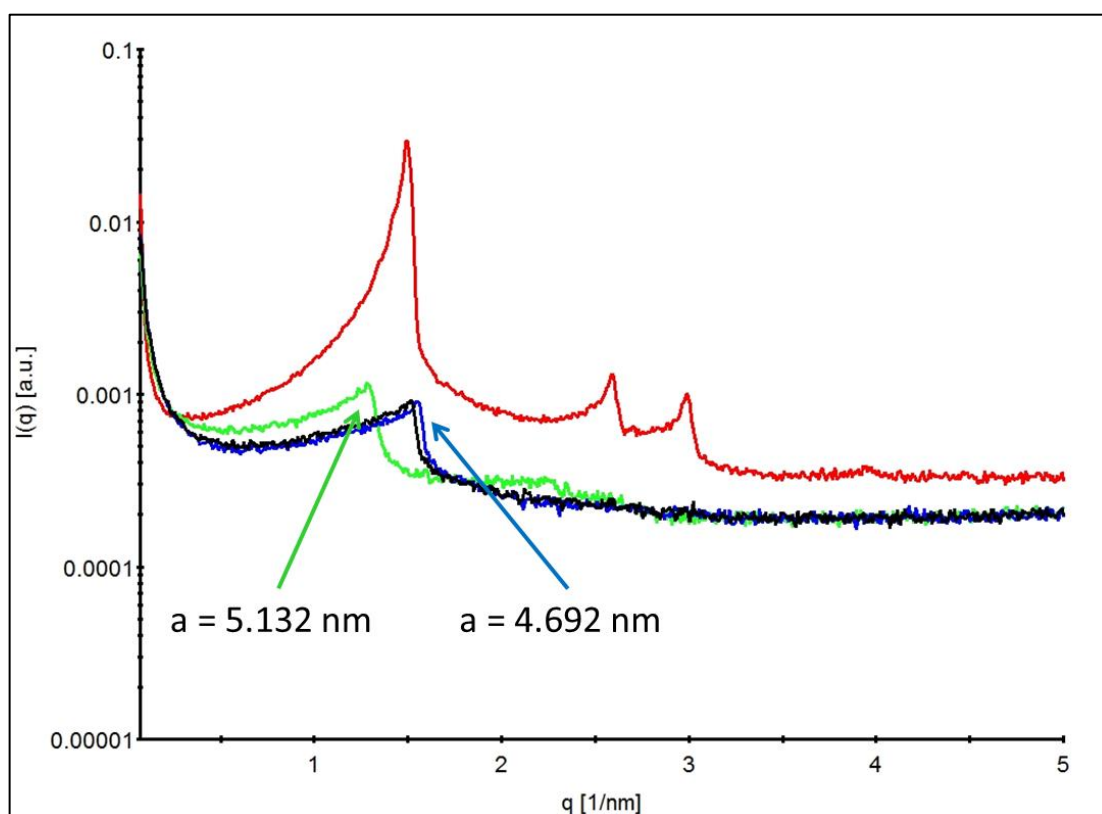
Figure II-10. Red: $\delta_{92.5}$ bulk phase. Dispersions $\delta_{92.5}$: green - produced under N$_2$-flow, 0 days old; blue - produced under N$_2$-flow, 1 day old; black - produced under N$_2$-flow, 1 day old and bubbled with CO$_2$.

The SAXS curves show the newly produced $\delta_{92.5}$ dispersion with H$_{II}$ structure and a corresponding lattice parameter of 5.13 nm. This decreases within one day to 4.69 nm

(blue curve). The following purge with CO_2 with approximately 3-5 bar over 2 minutes had only a negligible effect on the lattice parameter. A possible explanation is that the CO_2 from environmental air was enough to trigger the carbamate reaction and lead to the decrease in the lattice parameter in one day. The derived difference of about 0.5 nm is in agreement with the difference in the samples which were produced under N_2 flow and under environmental air.

To investigate the effect of CO_2, a δ_{90} bulk sample (several days after preparation) was bubbled (see Figure II-11). The sample was characterized directly before and after the purging with CO_2. This sample was chosen because an EME bulk phase is still fluid and therefore easy to bubble with CO_2. The hexagonal bulk phase is a highly viscous liquid crystal phase.
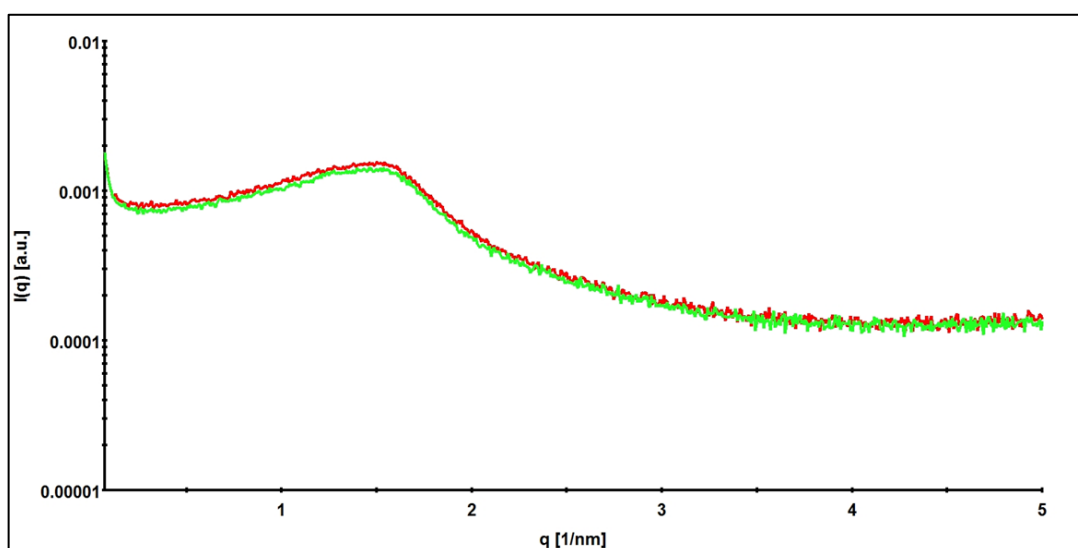
Figure II-11. δ_{90} bulk sample. red – untreated sample; green – after bubbling with CO_2

No considerable change could be detected after bubbling with CO_2. The expectation was to change the curvature which would lead to the formation of the hexagonal phase that can be found at $\delta_{92.5}$. Again the assumption is that the CO_2 present in the air during the production was enough to already trigger the carbamate reaction.

The reaction of an amine with CO_2 to carbamate should be reversed by heating or purging with N_2. To test this, dispersions which showed the transformation from

hexagonal to EME over the course of 20 days were heated to 100°C for 2 minutes, and cooled under N_2- flow to avoid contamination with air (see Figure II-12).

As expected a part of the dispersion was phase separated (the separated oil is visibly sticking on the glass wall), but a second SAXS measurement of the sample showed, that the dispersion maintained the inverse micellar structure. The loss of part of the emulsion is attributed to the loss of the amphiphilic character of the stabilizer F127. At high temperatures near the cloud point the poly ethylene oxide part is dehydrated and the molecule becomes lipophilic. This is detrimental to the stabilization effect and leads to phase separation.[26] Once the lipid is stuck to the glass wall it cannot return into the nano structure. Only a repeated energy input can return the lipids, which is observable by the increase in intensity in the black curve. The heat treatment and following cooling under N_2-flow showed no significant effect on the phase (blue curve). Also a second dispersion process with ultra-sonication did not induce significant changes in the SAXS pattern (black curve).
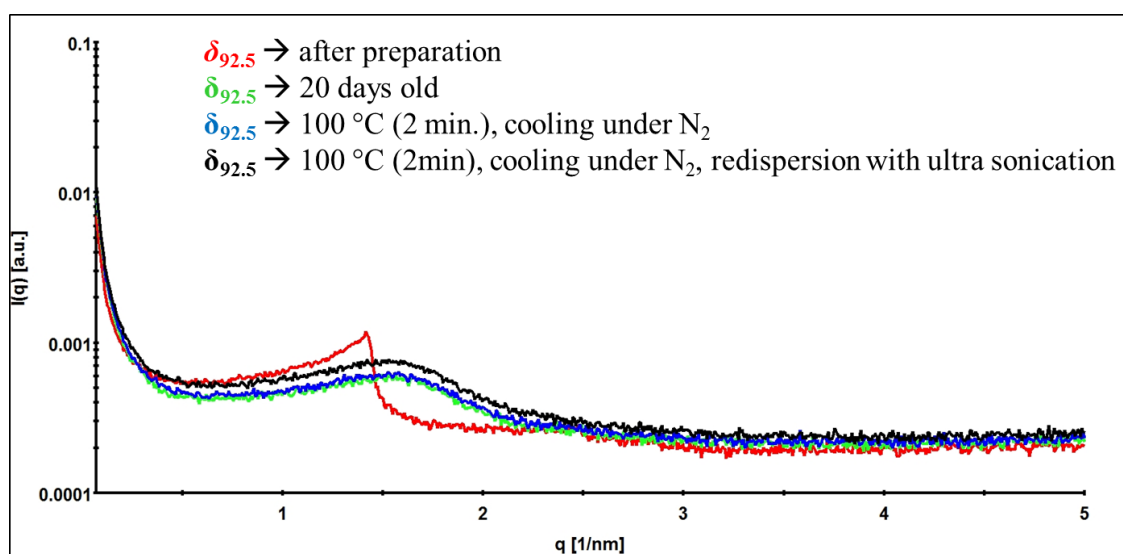
Figure II-12. Heat treatment of already prepared dispersion $\delta_{92.5}$ prepared under air

The same experiment was carried out with the dispersion which was produced under N_2- flow. It showed the same transition (Figure II-13).
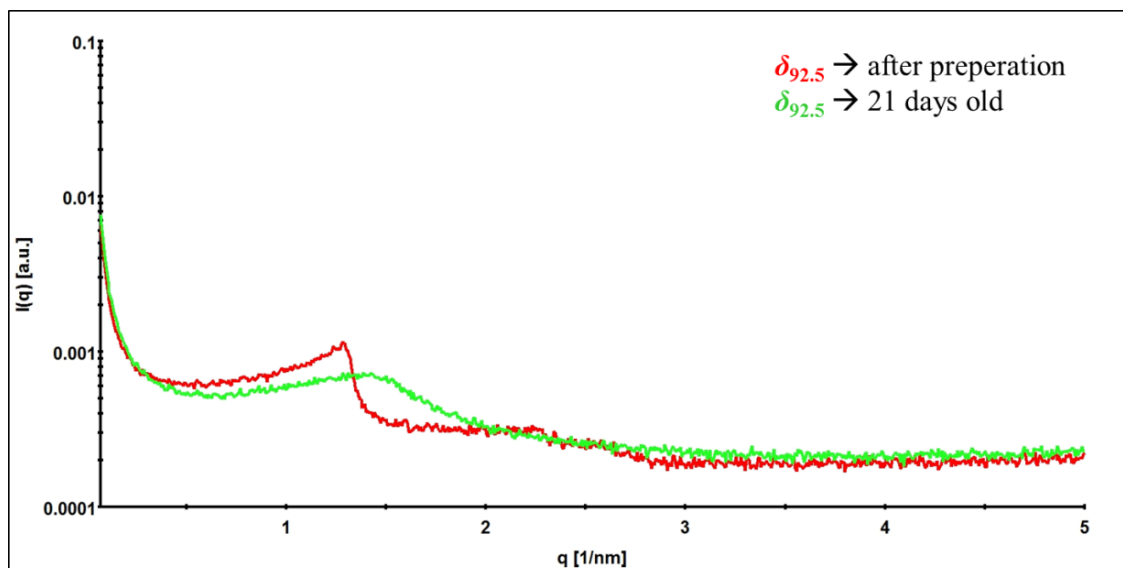
Figure II-13. Response of the nanostructure in a dispersion $\delta_{92.5}$ which was produced under N_2- flow

OLA – Influence of the pH

In the next step the influence of the pH on the phase was tested. OLA has a pKa value of about 10.7. This means that at a pH of 10.7 about half of the amine species will be deprotonated. When the pH value increases two units, about 99 % of the amine groups will be deprotonated and uncharged. The reaction equilibrium shifts to the side of the carbamate. At low pH the amine group is positively charged (protonated) and the equilibrium is on the side of the free CO_2. Two dispersions were altered with HCl (1M) to show a pH of 3.6 and NaOH (1M) to show a pH of 11.7 (see Figure II-14, Figure II-15). Again one can see that the lattice parameter and the order of the hexagonal structure decreased considerably over time from 5.60 nm to 4.63 nm, which might be an effect of a slow transition of CO_2 into the phase. When the pH is adjusted to 11.7 the hexagonal structure is destroyed and an EME is formed. The high pH could have led to the breaking of the ester bonds of GMO and facilitated the subsequent phase transition.
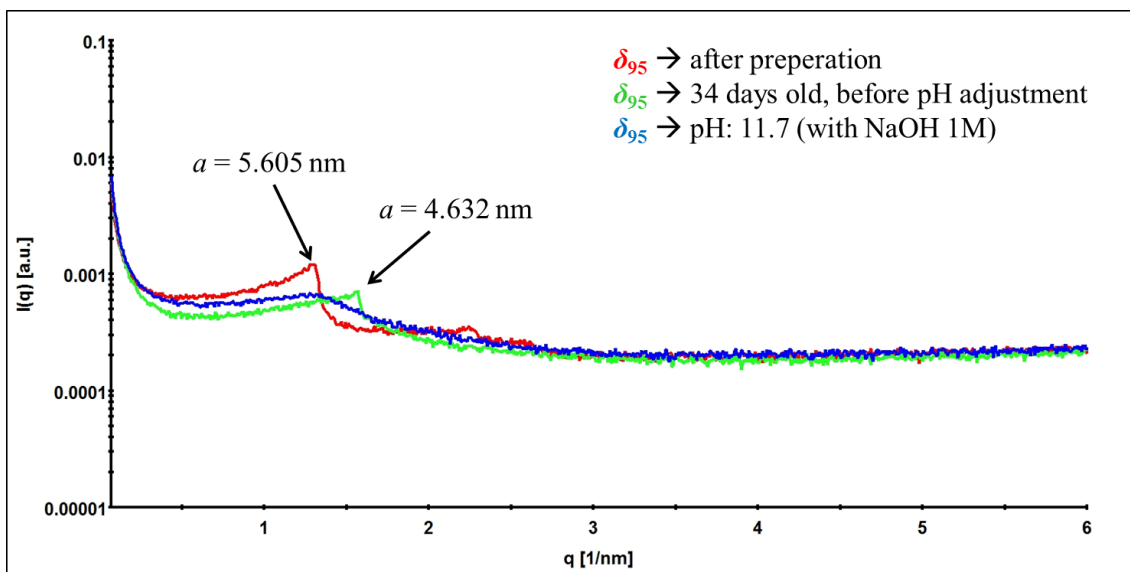
Figure II-14. Effect of the pH 11.7 on the hexagonal phase, δ_{95}

A difference was observed for the dispersion where the pH was adjusted to 3.6. The sample showed an increase in lattice parameter (from 4.69 nm to 5.28 nm). The addition of the HCl did not destroy the hexagonal phase but decreased the order considerably and the coexistence of an EME cannot be excluded.
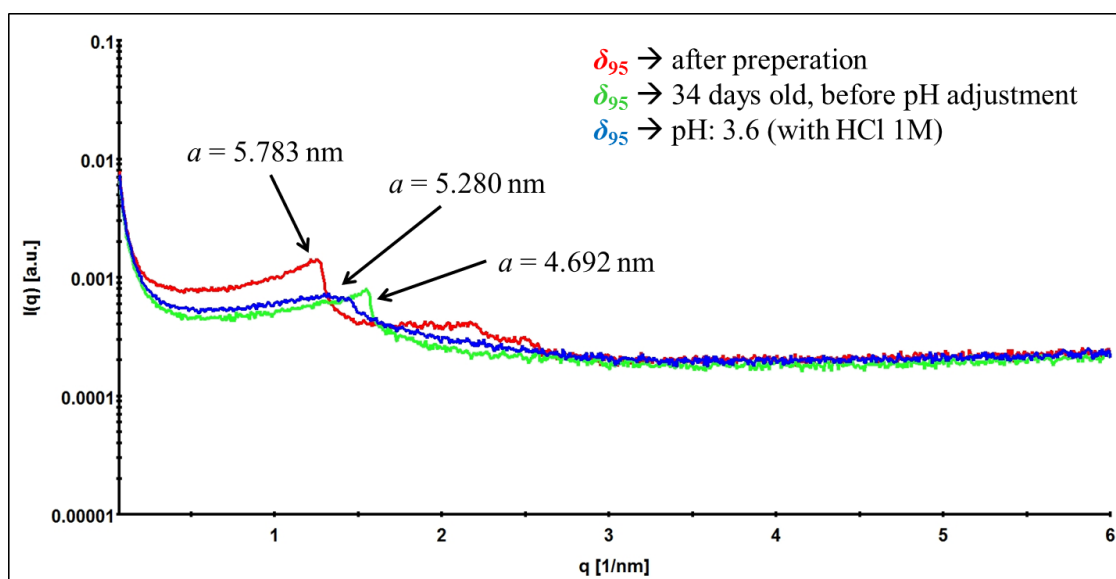
Figure II-15. Effect of the pH 3.6 on the hexagonal phase, δ_{95}

The hexagonal phase is destroyed when the pH is high and the order is significantly decreased at low pH. The reason for the transfer from hexagonal phase to an EME at high pH might be the breaking of the ester bond of GMO.

New Amines – DMAE, DBAE

Oleylamine showed transformations in the self-assembled nanostructure, but reacted rather slow. This could be related to the hydrophobic character of this amine or even the modified thermodynamic conditions at the confined oil-water interface inside the nanostructure. Therefore, 2-Dimethylaminoethanol (DMAE) and 2-(Dibutylamino)ethanol (DBAE) were tested because of their more hydrophilic character compared to OLA and their high reactivity with CO_2 as presented in previous studies.[27,28]

To check the suitability as functional molecules for structural transformations in ISAsomes, we investigated the solubility and prepared bulk samples with these components.

In the solubility experiments it was shown that DMAE is soluble in water and tetradecane, whereas DBAE is mostly soluble in tetradecane. This is in agreement with the corresponding logP values of -0.5 for DMAE and +2.9 for DBAE (calculated with ALOGPS 2.1).

DMAE, DBAE – Bulk

Bulk samples were prepared as described in the Materials section of this work. After 12 h equilibration time, the samples were characterized by SAXS and polarization microscopy (Figure II-16).
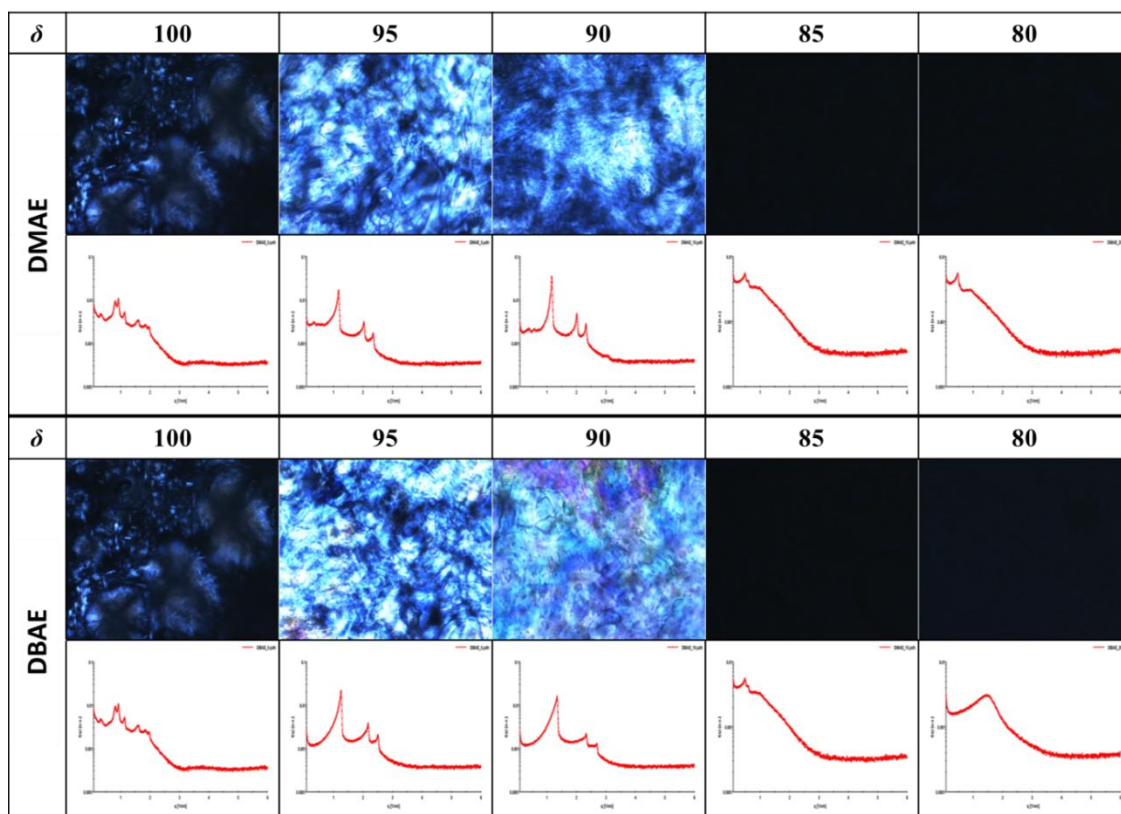
Figure II-16. Screening results of the bulk samples between δ_{100} to δ_{80}; 60 wt% DMU + (DMAE, DBAE), 40 wt% H$_2$O; upper row: polarization microscopy images, lower row: scattering curves from SAXS.

The results show the hexagonal phase equal to the results with oleylamine, between δ_{95} and δ_{90} (content of 5 wt% and 10 wt% of the new amines). To elucidate the situation in this area, further samples containing 2 wt% (δ_{98}) and 3 wt% (δ_{97}) of DMAE and DBAE were produced and characterized. The combined results are shown in Figure II-17.
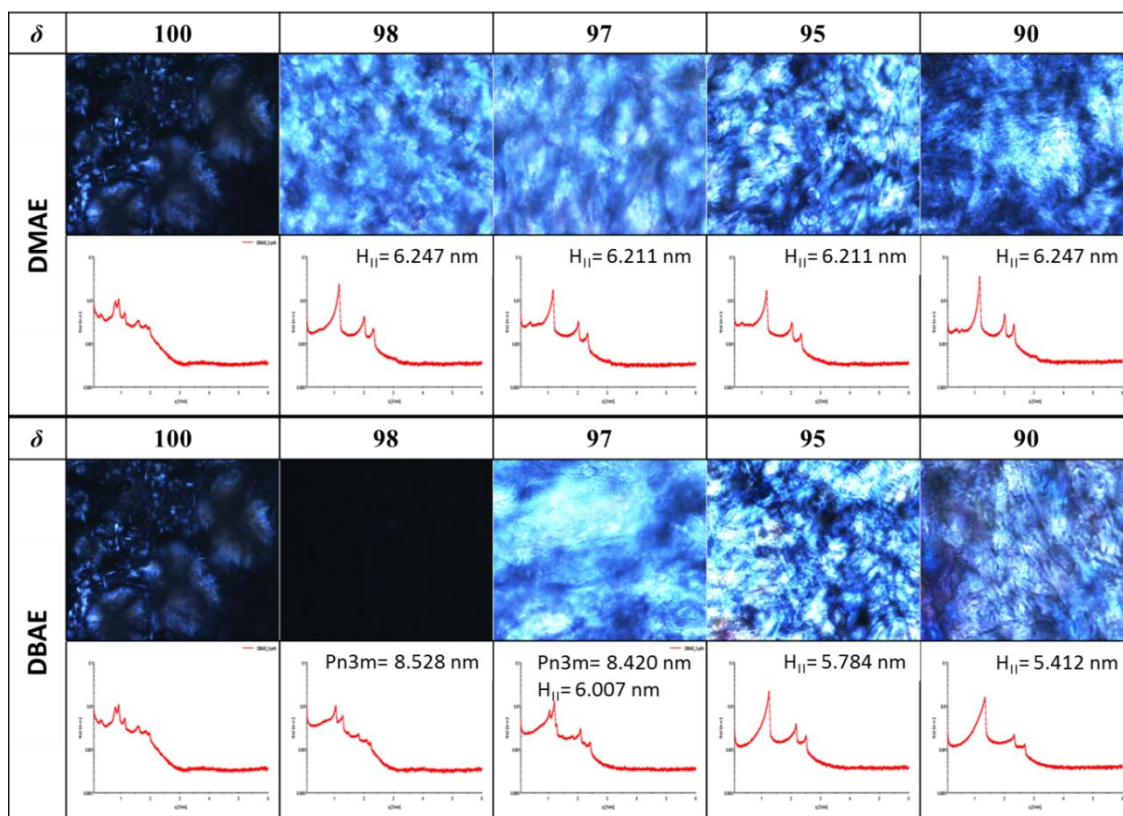
Figure II-17. Screening results of the bulk samples between δ_{100} to δ_{90}; 60 wt% DMU + (DMAE, DBAE), 40 wt% H_2O; upper row: polarization microscopy images, lower row: scattering curves from SAXS.

The results indicate that DMAE has a stable hexagonal phase between δ_{98} and δ_{90}. DBAE on the other hand shows the SAXS pattern of a pure Pn3m phase at δ_{98} and a mixed H_{II}/Pn3m phase at δ_{97} (Figure II-18). At δ_{95} and δ_{90} DBAE shows a hexagonal phase, which decreases in lattice constant with higher content of the amine.
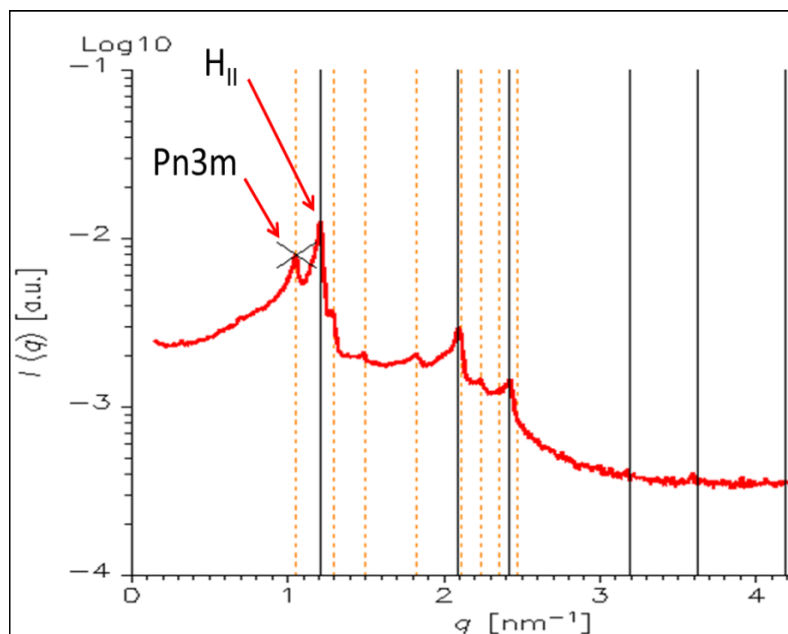
Figure II-18. Space Group Indices of the bulk sample DBAE δ_{97}; solid lines: peak positions of hexagonal phase; dashed lines: peak positions of cubic phase (Pn3m)

The lattice parameter *a* for DMAE is stable with increasing amine concentration in contrary to the influence of OLA and DBAE. This is illustrated in Figure II-19.
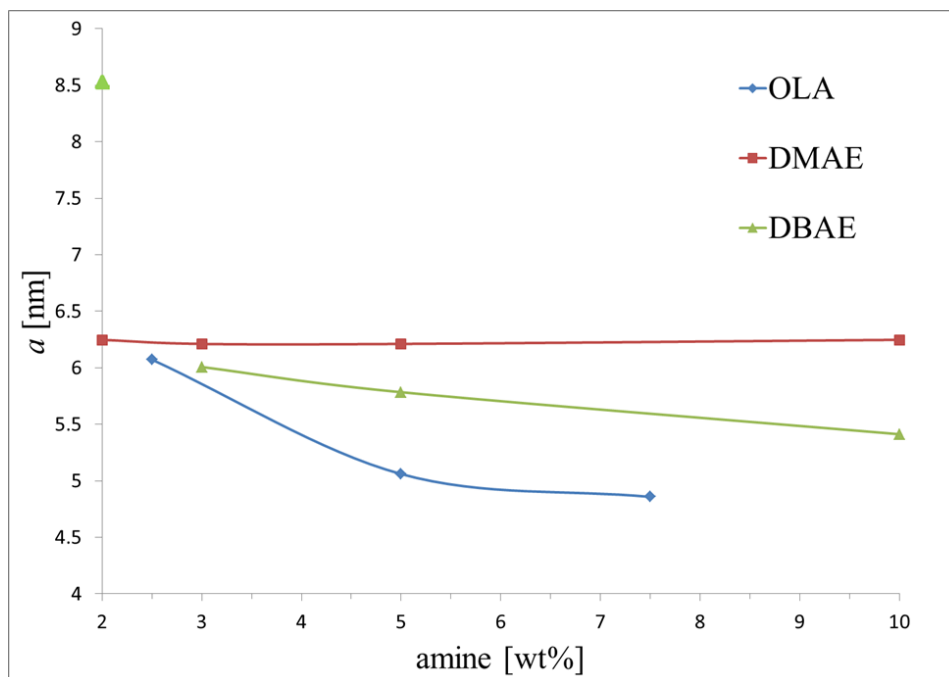
Figure II-19. Influence of an increasing amine concentration (OLA, DMAE, DBAE) on the hexagonal lattice parameter *a* [nm] of the bulk phases.

The reason for the constant lattice parameter with increasing DMAE content might be the more hydrophilic character of the molecule. Only a finite amount might be incorporated into the liquid crystal phase and all additional added DMAE may be dissolved in the aqueous phase. The stronger effect of DBAE on the lattice parameter can be attributed to the higher lipophilic character and bulkier sidechains of the molecule.

DMAE and DBAE – Dispersion

Dispersion samples were prepared as described in the materials section of this work. The milky dispersions were characterized by DLS, depolarized DLS, polarization microscopy and SAXS.

The polarization microscope did not provide indication for the presence of an anisotropic phase in the dispersion. The low lipid concentration ($\varphi=10$) of the dispersion in combination with a decreased order of the liquid crystal (see following figures) could be responsible for the missing birefringence. The DLS results are summarized in Table II-1.

Table II-1. R_H of the dispersion samples was characterized by DLS. * calculated by 2nd cumulant fit, using an averaged correlation function; ** Polarizers were adjusted to crossed position based on minimum scattering intensity with a reference sample of Latex spheres at 120 mW Power, Minimum adjusted to < 1 kHz

Sample	R_H [nm]*	depol [kHz]**
DMAE δ_{98}	81.32 ± 0.20	4
DMAE δ_{97}	70.96 ± 0.14	4
DBAE δ_{97}	136.81 ± 0.58	14.8
DBAE δ_{95}	131.66 ± 0.36	19

DBAE appears to have an influence on the mean droplet size of the emulsion. The reason could be the higher lipophilicity of the molecule.

The SAXS results are depicted in Figure II-20.
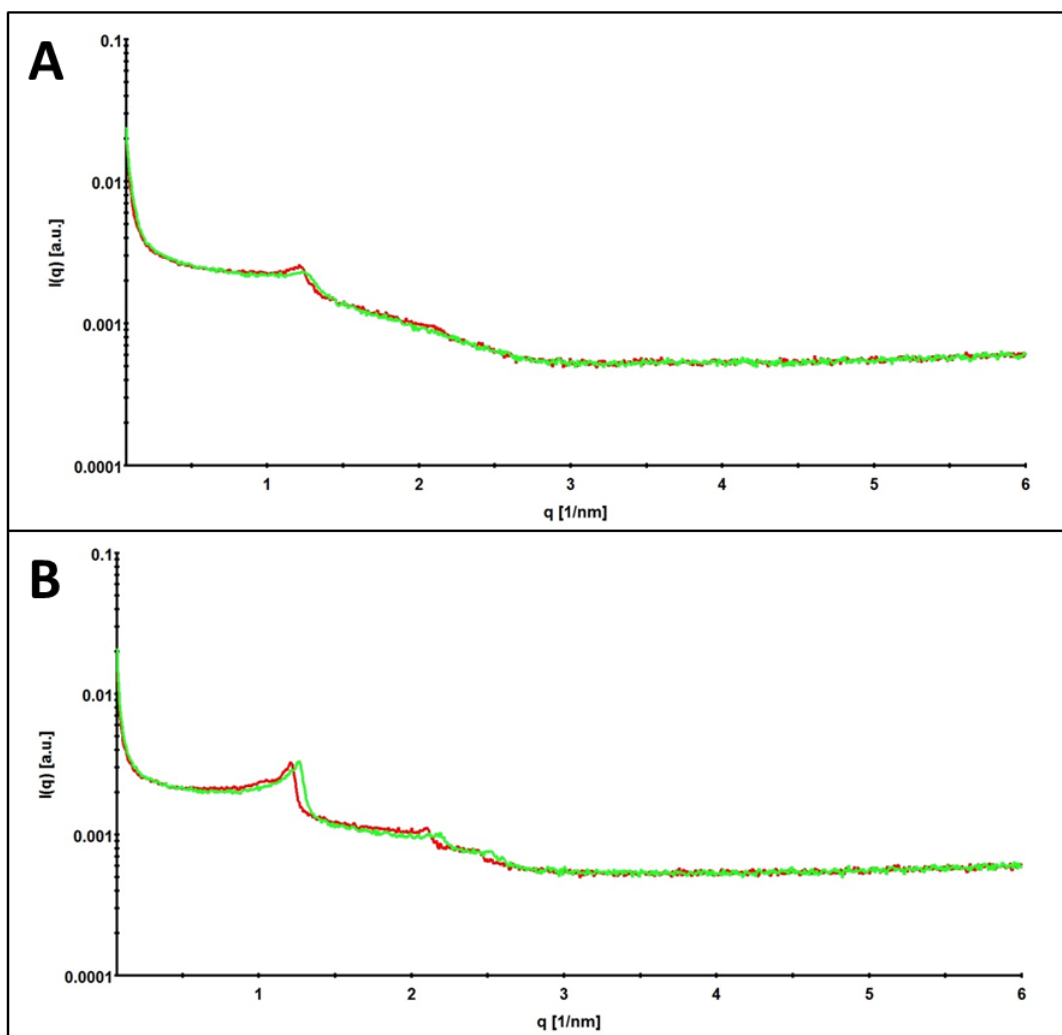
Figure II-20. SAXS results from the dispersion- samples. DMAE (A): δ_{98} – red, δ_{97} – green; DBAE (B): δ_{97} – red, δ_{95} – green

The scattering curves show a hexagonal phase with a lattice parameter of 5.99 nm for δ_{97} DBAE and 5.74 nm for δ_{95} DBAE, which corresponds well to the findings in the bulk phase.

The weak and broad Bragg peaks in the δ_{98} DMAE curve indicate the presence of a not well-ordered hexagonal phase with a lattice parameter of 5.99 nm. The δ_{97} DMAE dispersion appears to be an even less ordered hexagonal phase with a lattice parameter of 5.83 nm. All dispersions showed a structural change over several days (see Figure II-21 and Figure II-22). It is clearly visible that both DBAE samples transferred from a hexagonal phase to an EME phase. The DMAE δ_{98} sample also converted to an EME however the order of the EME was nearly lost completely in the δ_{97} sample.
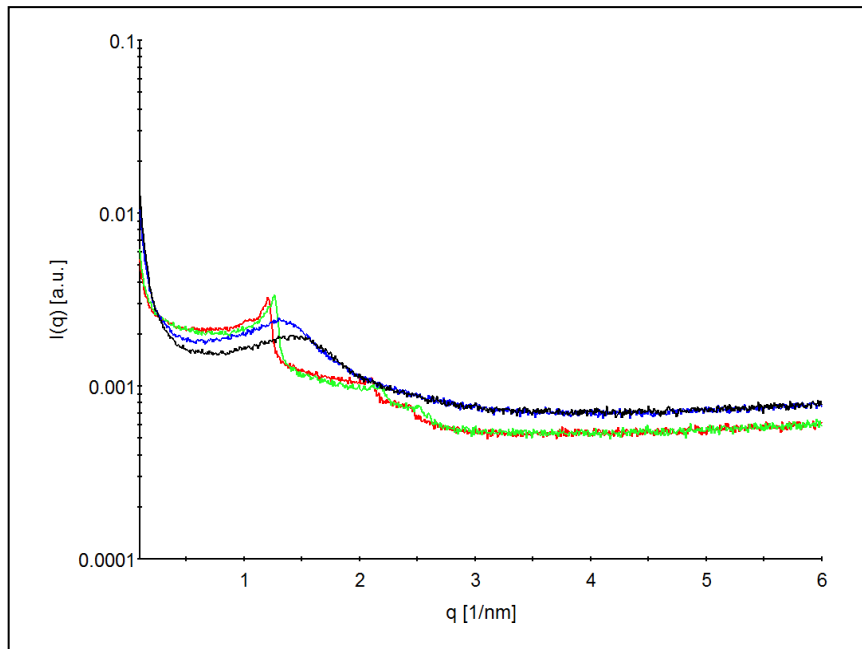
Figure II-21. DBAE δ_{97} (red and blue) and δ_{95} (green and black); structural change over time in the dispersions
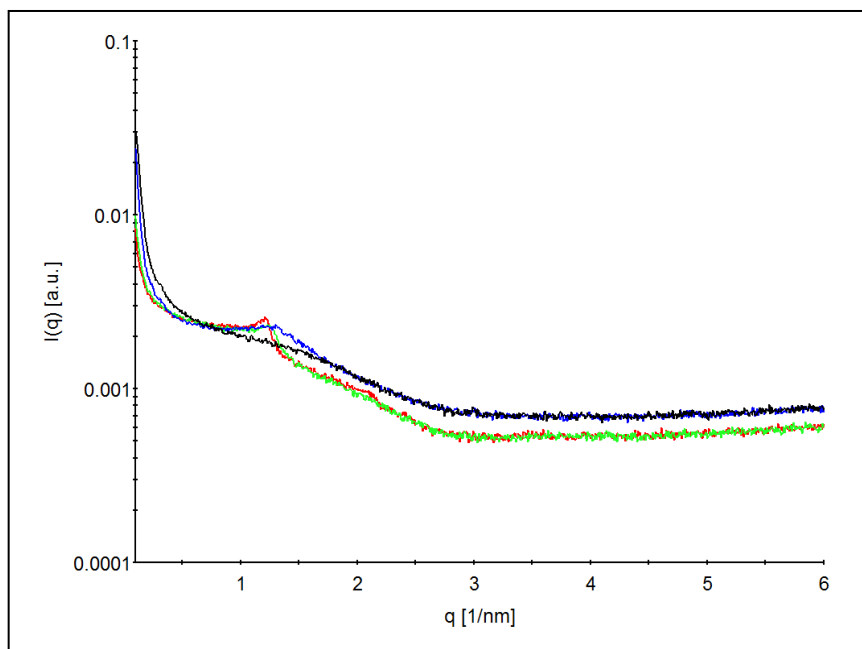
Figure II-22. DMAE δ_{98} (red and blue) and δ_{97} (green and black); structural change over time in the dispersions

DMAE and DBAE – CO$_2$-Response

Since we suspected that the CO$_2$ present in the air during and after the production of the samples led to the transition from the hexosomes to EME, the samples were bubbled with N$_2$ for 2 minutes and characterized again (see Figure II-23 and Figure II-24).
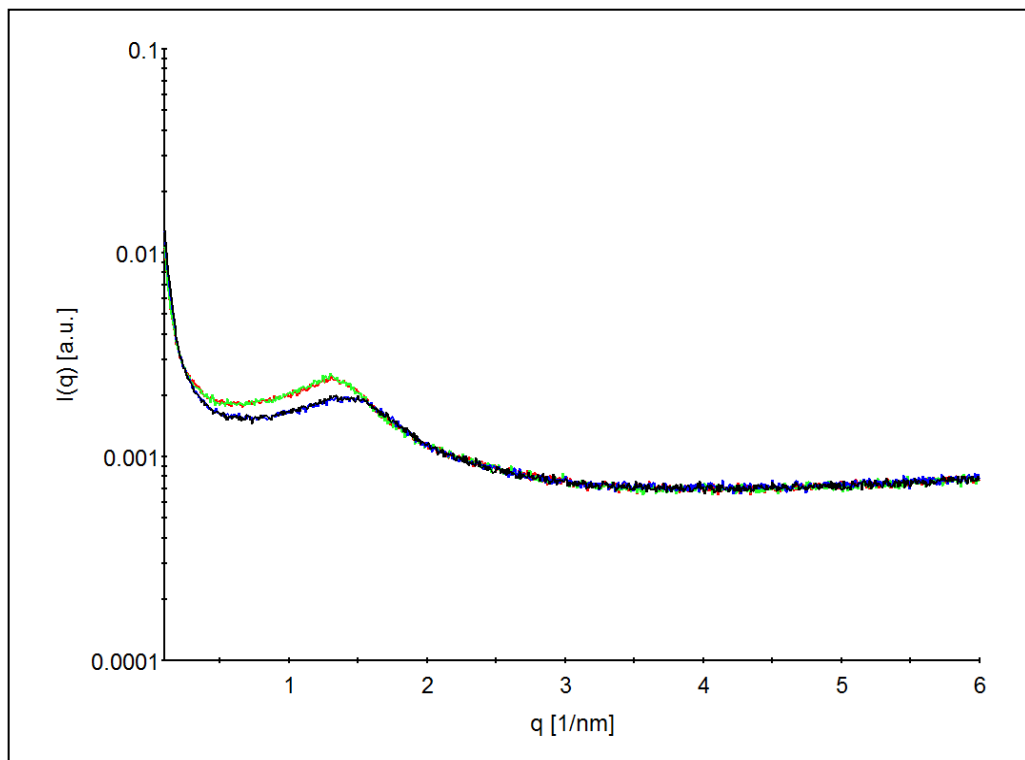
Figure II-23. DBAE dispersions before (δ_{97}-red, δ_{95}-green) and after bubbling with N$_2$ (δ_{97}-blue, δ_{95}-black).
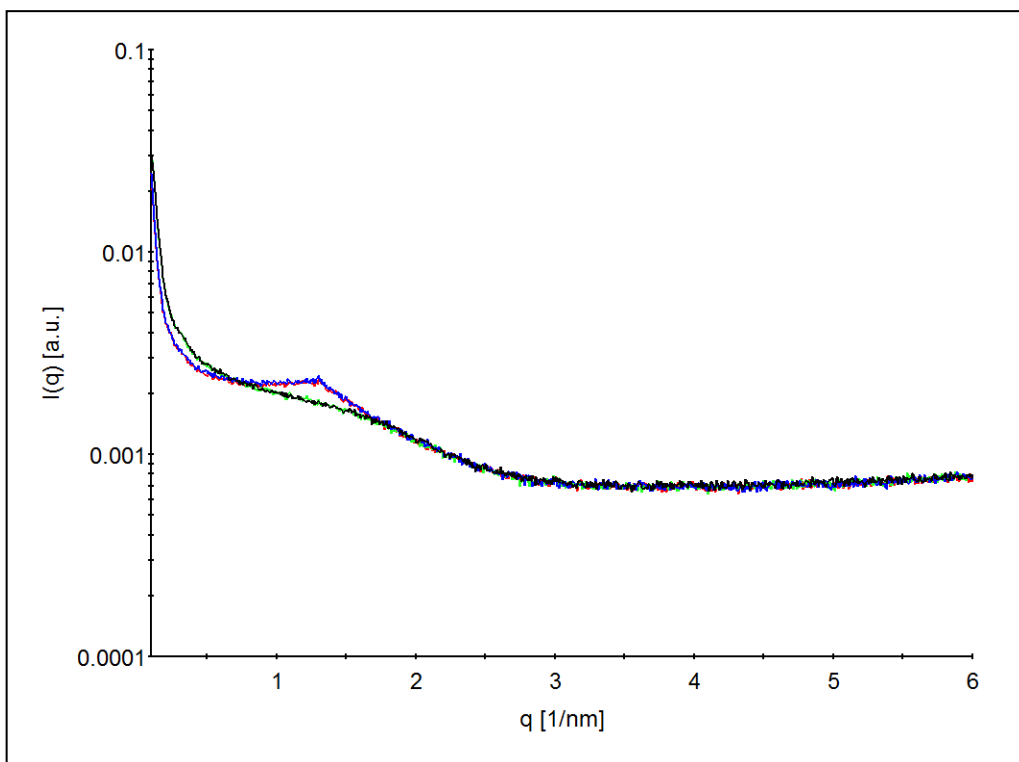
Figure II-24. DMAE dispersions before (δ_{98}-red, δ_{97}-green) and after bubbling with N_2 (δ_{98}-blue, δ_{97}-black).

The purge with N_2 had no effect on the structure concerning the DMAE samples. However the DBAE samples showed a slight shift in q-value, indicating a decrease of the lattice parameter for the EME. Subsequently bubbling with CO_2 was attempted to see if an interaction takes place (see Figure II-25 and II-30).
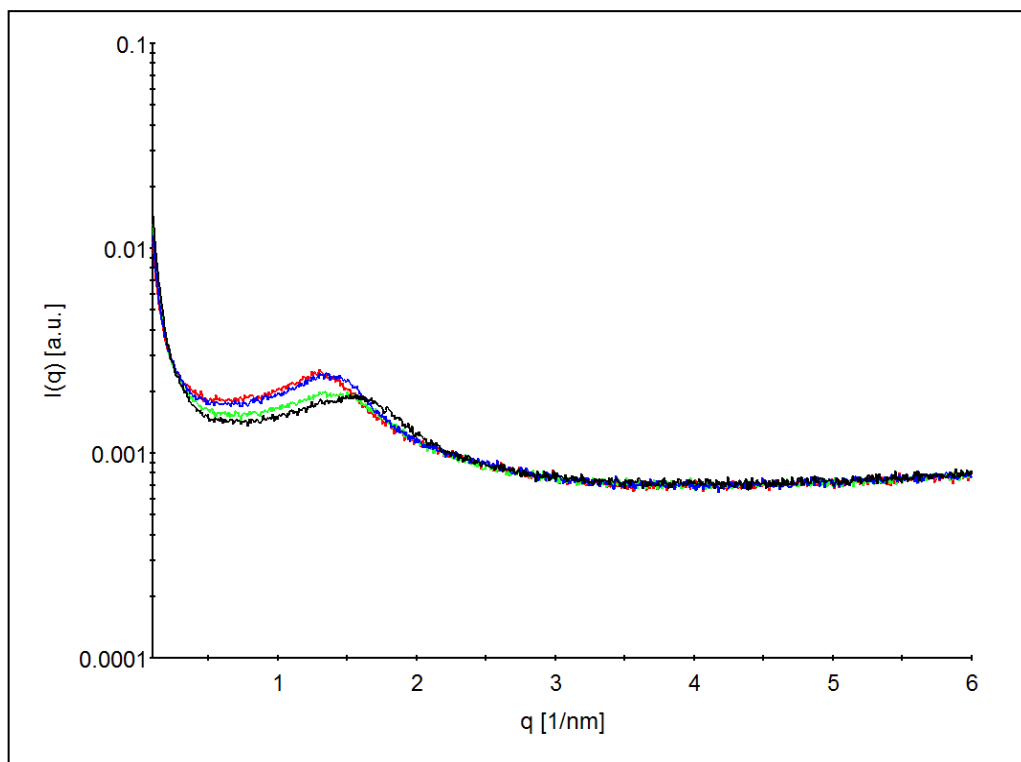
Figure II-25. DBAE dispersions before (δ_{97}-red, δ_{95}-green) and after bubbling with CO_2 (δ_{97}-blue, δ_{95}-black).

Both DBAE dispersions showed a slight shift to higher q- values which indicates interaction with the CO_2 although it was not enough to trigger any phase transition.
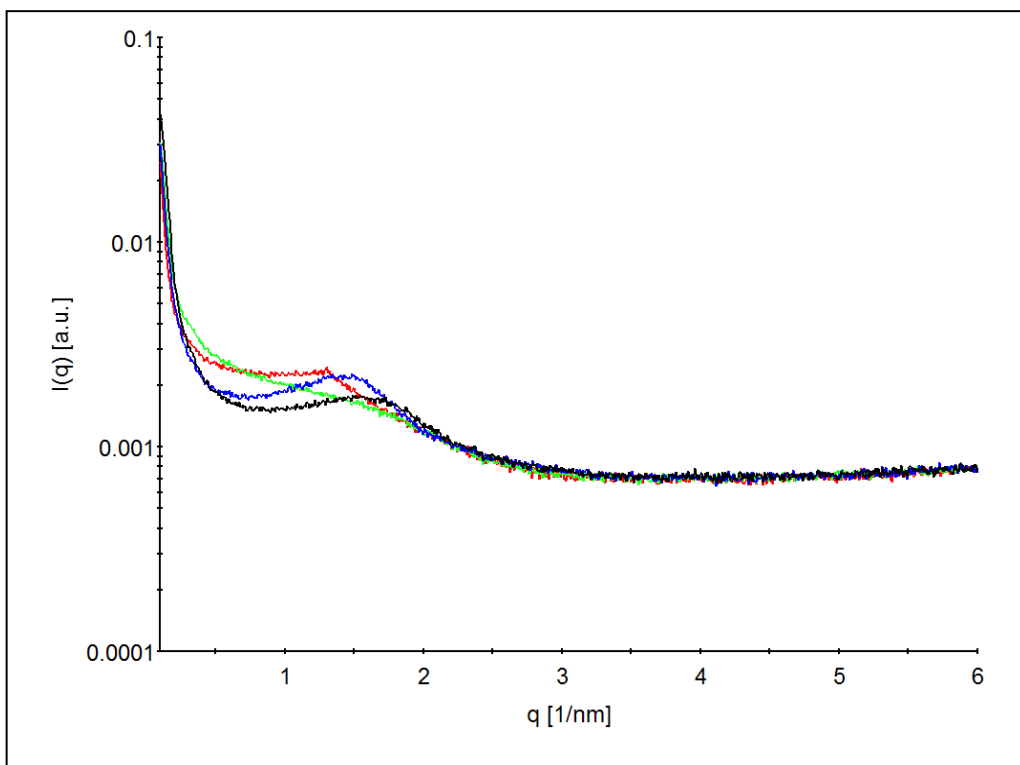
Figure 26. DMAE dispersions before (δ_{98}-red, δ_{97}-green) and after bubbling with CO_2 (δ_{98}-blue, δ_{97}-black).

The DMAE dispersions show a considerable reaction to CO_2. The system reverted from a relatively disordered EME to an ordered EME. In the case of the δ_{97} DMAE dispersion the very weakly ordered EME changed into a clear-ordered EME after the bubbling with CO_2.

Conclusion

To achieve the goal of a CO_2 responsive ISAsome system the incorporation of different amine molecules was investigated. For all tested amines an inverse hexagonal structure was found at high δ – values in the bulk phases. This would allow the application as a carrier system, since the inverse hexagonal phase is closed (see Chapter I- Theory) and furthermore as burst-release system with the added trigger function by CO_2.

In addition to OLA, the amines DMAE and DBAE were investigated for their suitability as CO_2-responsive functional molecules to trigger nanostructural transformations. Their shorter alkyl chain compared to OLA was supposed to decrease solubility in the lipid domain and therefore increase accessibility for the CO_2 at the interface. However, the phase behavior was similar to that of oleylamine between δ_{98} and δ_{90}.

ISAsomes containing the inverse hexagonal phase could be produced with all three investigated amines (OLA, DMAE and DBAE). The production of emulsions under normal condition and under N_2 flow showed a clear difference in lattice parameter for the $\delta_{92.5}$ OLA dispersion (difference of 0.53 nm) and δ_{95} OLA dispersion (difference of 0.18 nm). This confirmed that CO_2 is captured by the amines. Furthermore it indicates that already CO_2 that is present in air is enough to trigger the carbamate formation. This assumption was fortified by the dispersion which was produced under N_2 flow and showed a decrease in the lattice parameter of 0.44 nm when stored under normal conditions for one day.

All dispersions transitioned from the inverse hexagonal phase to an EME within days. Further tests with DMAE and DBAE dispersions showed that purging with N_2, which is supposed to remove the captured CO_2 from the nano structure, led to a shift to lower q-values for the EME. Subsequent purging with CO_2 resulted in a shift back to q-values that were observed before purging with N_2. Furthermore the DMAE, which showed a decreased order of EME before purging with N_2, regained its order after purging with CO_2. Clear switch ability could be found for these short-chain amines.

In sum, this study pioneers CO_2 switchable lyotropic liquid crystalline nanomaterials. The detailed insights into nanostructure formation and transformation in response to

CO_2 may provide essential knowledge for the rational design of CO_2 responsive drug delivery systems.

Outlook

The next suggested steps would be a series of control experiments to investigate the kinetics of this transition from H_{II} to EME using time-resolved on-line SAXS. Furthermore the continuation of the preliminary results to modify the liquid crystal structure with tryptophan to be closer at the phase boundary might lead to a system which is more sensitive to CO_2 as a trigger. We suspect that the low fraction of amine present in the sample and a slow uptake of CO_2 are responsible for the fact that the system shows no immediate phase transition.

A possible continuation of this project might lie in the testing of other short-chain amines which show high reactivity with CO_2 but also might allow the incorporation into the liquid crystal phase in higher concentrations.

Appendix

Preliminary Results

To check the condition of the primary surfactant new bulk phases with model substances were produced with δ = 92.5, one with oleic acid (OA) and one with tetradecane (see Figure II-27).
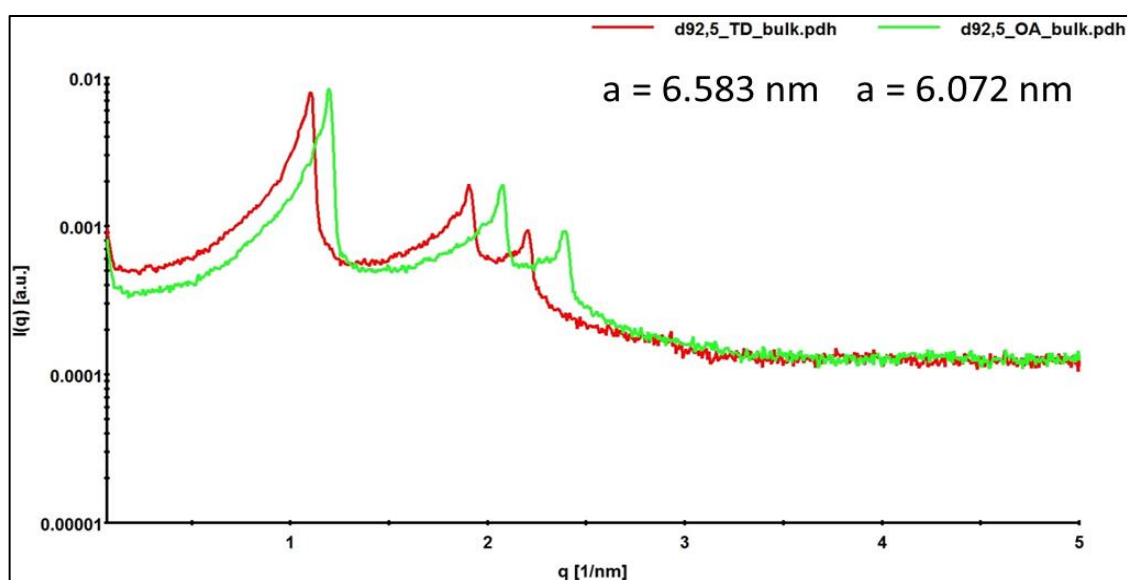
Figure II-27. Bulk phases of known systems with tetradecane and oleic acid (OA)

The bulk samples show the hexagonal phase as expected and the derived lattice parameters are in agreement with literature.

New dispersions were produced by mixing the starting materials without prior homogenization of the bulk phase materials. ϕ was kept at 10 (β = 9) which allows the comparison to results gathered in previous projects. The resulting SAXS graphs can be found in Figure II-28.
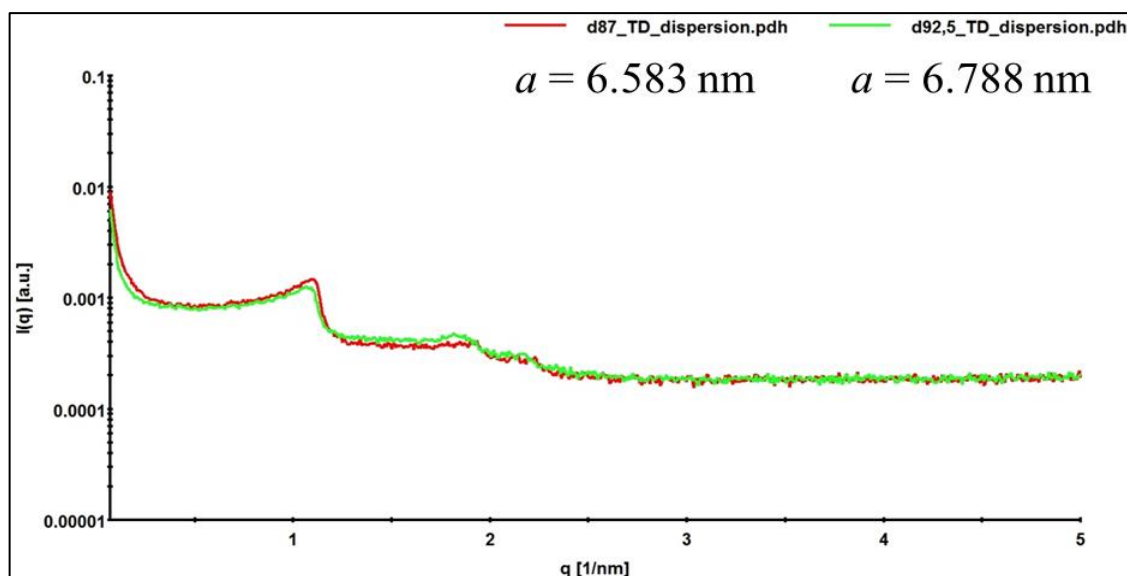
Figure II-28. Dispersions prepared directly from starting material with DMU – tetradecane – water – F127 with $\delta = 87$ (red) and 92.5 (green)

The hexagonal phase is clearly visible with a unit cell size of 6.58 nm for δ_{87} and 6.79 nm for $\delta_{92.5}$ in the newly prepared dispersions. The newly produced dispersions showed R_H of about 100 nm, which is in the same range than previous ISAsome samples.

It can be concluded that the ultra-sonication setup is working properly, and that there might be difficulties to build the dispersion from using the bulk phase.

Modification of the LC

The respective liquid crystal phases are usually found within a defined range of composition of primary surfactant and oil. In the GMO / OLA system, H_{II} structure was found between $\delta = 92.5$ and $\delta = 97.5$. Since we suspect that the uptake of CO_2 is a very slow process we tried to modify the hexagonal phase to be closer to the phase boundary, where only small amounts of CO_2 would be sufficient to initiate a phase transition.

For this purpose it was tried to incorporate the amino acid tryptophan (Trp) into the ISAsomes loaded with tetradecane in order to push the system closer to the phase boundary, so the CO_2 would act more effectively as a trigger. The amphiphilic character

of tryptophan leads to the integration in the layer of GMO and therefore to an expansion of the structure [29]. The tryptophan was dissolved in the water phase at 50°C. First a test on the standard DMU – tetradecane – water system was carried out (see Figure II-29).

$\delta_{92.5}$	a [nm]
no Trp	4.858
Trp	5.205
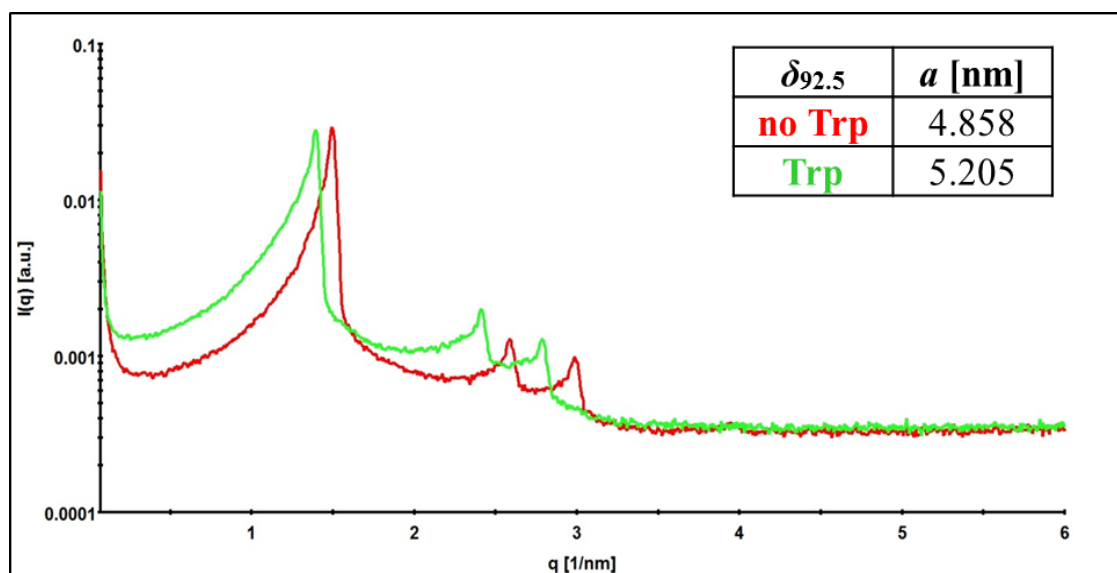
Figure II-29. $\delta_{92.5}$ bulk samples (DMU – tetradecane – water); red- no Trp; green – 2 wt% Trp

The incorporation of Trp leads to an increase of the lattice parameter. Based on this observation we tried to produce an OLA-containing bulkphase (DMU, OLA, H_2O) and Trp (see Figure II-30).
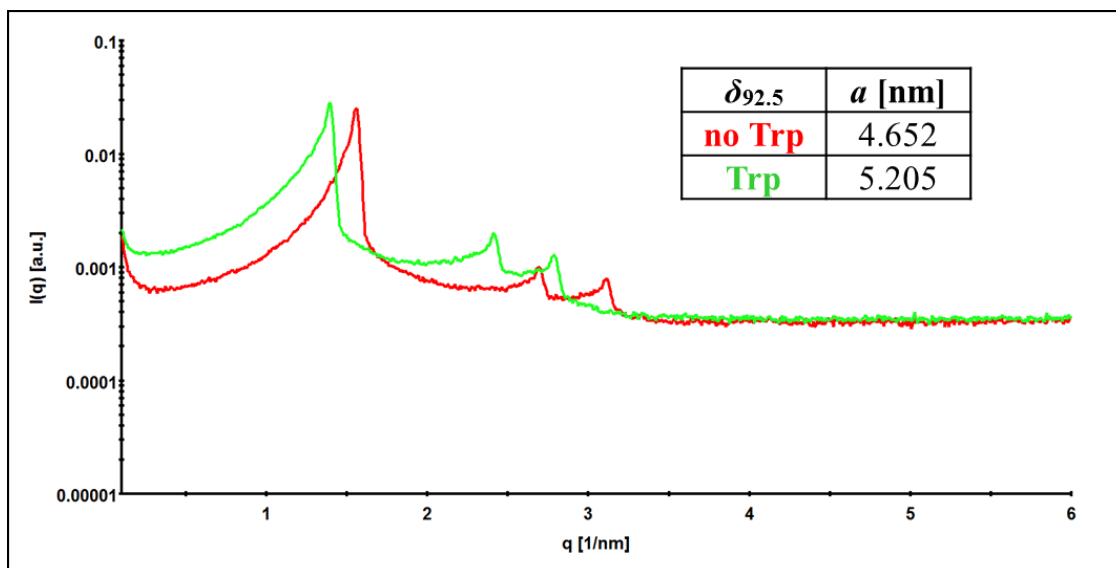
Figure II-30. $\delta_{92.5}$ bulk phase (DMU – OLA – water); red – no Trp; green – 2 wt% Trp

The increase of the lattice parameter was similar to the sample with tetradecane. However the modified samples showed a yellow color within 15 minutes indicating some interaction of the amine with the Trp. The reason for this has yet to be found.

References

1. Yaghmur, A., Campo, L. De & Sagalowicz, L. Emulsified microemulsions and oil-containing liquid crystalline phases. *Langmuir* 569–577 (2005).

2. de Campo, L. *et al.* Reversible phase transitions in emulsified nanostructured lipid systems. *Langmuir* **20,** 5254–61 (2004).

3. Munshi, N., Rapoport, N. & Pitt, W. G. Ultrasonic activated drug delivery from Pluronic P-105 micelles. *Cancer Lett.* **118,** 13–19 (1997).

4. Salentinig, S., Phan, S., Hawley, A. & Boyd, B. J. Self-assembly structure formation during the digestion of human breast milk. *Angew. Chemie - Int. Ed.* **54,** 1600–1603 (2015).

5. Salentinig, S., Sagalowicz, L., Leser, M. E., Tedeschi, C. & Glatter, O. Transitions in the internal structure of lipid droplets during fat digestion. *Soft Matter* **7,** 650–661 (2011).

6. Tangso, K. J. *et al.* Novel Spiropyran Amphiphiles and Their Application as Light-Responsive Liquid Crystalline Components. *J. Phys. Chem. B* **117,** 10203–10210 (2013).

7. Zhao, Y. Rational design of light-controllable polymer micelles. *Chem. Rec.* **7,** 286–294 (2007).

8. Negrini, R. & Mezzenga, R. PH-responsive lyotropic liquid crystals for controlled drug delivery. *Langmuir* **27,** 5296–5303 (2011).

9. Salentinig, S. *et al.* PH-responsive micelles based on caprylic acid. *Langmuir* **30,** 7296–7303 (2014).

10. Salentinig, S., Tangso, K. J., Hawley, A. & Boyd, B. J. pH-driven colloidal transformations based on the vasoactive drug nicergoline. *Langmuir* **30,** 14776–14781 (2014).

11. Salentinig, S., Sagalowicz, L. & Glatter, O. Self-assembled structures and pK a value of oleic acid in systems of biological levance. *Langmuir* **26,** 11670–11679 (2010).

12. Jessop, P. G., Mercer, S. M. & Heldebrant, D. J. CO2-triggered switchable solvents, surfactants, and other materials. *Energy Environ. Sci.* **5,** 7240–7253

(2012).

13. Jessop, P. G. Independent virus development outside a host. *Nature* **436,** 1102 (2005).

14. Liu, Y. Switchable Surfactants. *Science (80-.).* **313,** 958–960 (2006).

15. Han, D., Tong, X., Boissière, O. & Zhao, Y. General strategy for making CO2-switchable polymers. *ACS Macro Lett.* **1,** 57–61 (2012).

16. Lewis, T., Faubel, M., Winter, B. & Hemminger, J. C. CO2 capture in amine-based aqueous solution: Role of the gas-solution interface. *Angew. Chemie - Int. Ed.* **50,** 10178–10181 (2011).

17. Jackson, P., Fisher, K. J. & Attalla, M. I. Tandem mass spectrometry measurement of the collision products of carbamate anions derived from CO 2 capture sorbents: Paving the way for accurate quantitation. *J. Am. Soc. Mass Spectrom.* **22,** 1420–1431 (2011).

18. Jackson, P., Beste, A. & Attalla, M. Insights into amine-based CO2 capture: an ab initio self-consistent reaction field investigation. *Struct. Chem.* **22,** 537–549 (2011).

19. Jackson, P., Beste, A. & Attalla, M. I. CO2capture in aqueous ammonia solutions: A computational chemistry perspective. *Phys. Chem. Chem. Phys.* **14,** 16301–16311 (2012).

20. Salentinig, S., Jackson, P. & Hawley, A. Amine-Functionalized CO 2 Responsive Triblock Copolymer Micelles—A Small-Angle X-ray Scattering Study. *Macromolecules* **48,** 2283–2289 (2015).

21. Freiberger, N. & Glatter, O. Small-angle scattering from hexagonal liquid crystals. *J. Phys. Chem. B* **110,** 14719–14727 (2006).

22. Pitzalis, P. *et al.* Characterization of the liquid-crystalline phases in the glycerol monooleate/diglycerol monooleate/water system. *Langmuir* **16,** 6358–6365 (2000).

23. Fong, C., Le, T. & Drummond, C. J. Lyotropic liquid crystal engineering-ordered nanostructured small molecule amphiphile self-assembly materials by design. *Chem. Soc. Rev.* **41,** 1297–1322 (2012).

24. Yaghmur, A., de Campo, L., Sagalowicz, L., Leser, M. E. & Glatter, O. Emulsified microemulsions and oil-containing liquid crystalline phases. *Langmuir* **21,** 569–577 (2005).

25. Gontsarik, M., Mohammadtaheri, M., Yaghmur, A. & Salentinig, S. pH-Triggered nanostructural transformations in antimicrobial peptide/oleic acid self-Assemblies. *Biomater. Sci.* **6,** 803–812 (2018).

26. Alexandridis, P. & Alan Hatton, T. Poly(ethylene oxide)-poly(propylene oxide)-poly(ethylene oxide) block copolymer surfactants in aqueous solutions and at interfaces: thermodynamics, structure, dynamics, and modeling. *Colloids Surfaces A Physicochem. Eng. Asp.* **96,** 1–46 (1995).

27. Conway, W. *et al.* CO2 absorption into aqueous amine blended solutions containing monoethanolamine (MEA), N,N-dimethylethanolamine (DMEA), N,N-diethylethanolamine (DEEA) and 2-amino-2-methyl-1-propanol (AMP) for post-combustion capture processes. *Chem. Eng. Sci.* **126,** 446–454 (2015).

28. Hwang, S. J., Kim, J., Kim, H. & Lee, K. S. Solubility of Carbon Dioxide in Aqueous Solutions of Three Secondary Amines: 2-(Butylamino)ethanol, 2-(Isopropylamino)ethanol, and 2-(Ethylamino)ethanol Secondary Alkanolamine Solutions. *J. Chem. Eng. Data* **62,** 2428–2435 (2017).

29. Chemelli, A., Conde-Valentin, B., Uhlig, F. & Glatter, O. Amino Acid Induced Modification of Self-Assembled Monoglyceride-Based Nanostructures. *Langmuir* **31,** 10377–10381 (2015).

Chapter III

Reverse Hexosome Dispersions in Alkanes – The Challenge of Inverting Structures

LANGMUIR

Reverse Hexosome Dispersions in Alkanes—The Challenge of Inverting Structures

Franz Pirolt,[†] Otto Glatter,*,[‡] and Gregor Trimmel[†]

[†]Institute for Chemistry and Technology of Materials and [‡]Institute for Inorganic Chemistry, Graz University of Technology, Stremayrgasse 9, 8010 Graz, Austria

S *Supporting Information*

ABSTRACT: Monoglycerides form lipophilic liquid-crystalline (LC) phases when mixed with water. The corresponding LC nanostructures coexist with excess water, which is a necessary condition for the formation of internally nanostructured dispersed particles. These nanostructures comprise bicontinuous cubic phases, inverted hexagonal phases, and inverted micellar cubic phases. The dispersed particles are therefore named cubosomes, hexosomes, or micellar cubosomes. Such dispersions are usually stabilized by hydrophilic high-molecular-weight triblock (TB) copolymers. Another way to stabilize such dispersions is by forming the so-called Pickering or Ramsden emulsions using nanoparticles as stabilizers. In this contribution, we explore the possibility of forming and stabilizing inverted or reverse systems, that is, dispersions of hydrophilic LC phases in an excess oil phase like tetradecane. Our aim was to change from oil-in-water emulsions to water-in-oil emulsions, where the water phase is a LC phase in equilibrium with excess oil and where the oil is nonpolar, for example, an alkane. This work consists of three parts: (1) to find a hexagonal hydrophilic LC phase that can not only incorporate a certain amount of tetradecane but can also coexist with excess tetradecane in the case of higher oil concentration, (2) to find a suitable stabilizer—either polymeric or nanoparticle type—that can stabilize the emulsion without destroying the hexagonal LC phase, and finally (3) to check the stability of this reverse hexosome emulsion. We discovered that it is possible to create a hexagonal hydrophilic LC phase with short-chain nonionic surfactants such as polyethylene glycol alkyl ethers or with high-molecular-weight TB copolymers of type A—B—A. Furthermore, it is possible to successfully stabilize the reverse hexosomes with low hydrophilic—lipophilic balance TB copolymers—either synthesized in our laboratory or commercially available ones—as well as with hydrophobized, commercially available silica nanoparticles.
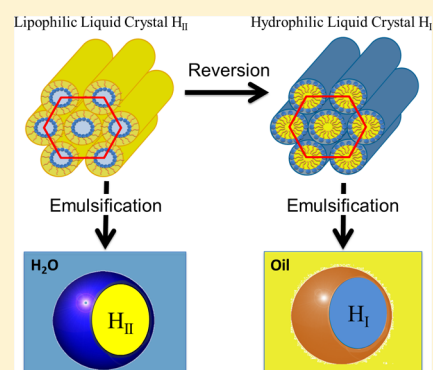
INTRODUCTION

Monoglycerides form liquid-crystalline (LC) phases when mixed with water.[1–3] The structure formed depends on the type of monoglycerol, temperature, and water content. The fully hydrated monoglycerides such as monooleate and monolinoleate form a variety of self-assembled structures.[4–6] Phytantriol(3,7,11,15-tetramethylhexadecane-1,2,3-triol) exhibits a lyotropic phase behavior similar to monoolein.[7–10] The corresponding LC nanostructures coexist with excess water, which is necessary for forming internally structured dispersed particles.[11–21] These nanostructures comprise bicontinuous cubic phases, inverted hexagonal phases, inverted micellar cubic phases, or water-in-oil (W/O) microemulsions; the dispersed particles are therefore named cubosomes,[3] hexosomes,[22] micellar cubosomes,[23] and emulsified microemulsions,[24] or more generally speaking, isasomes, where the isa suffix denotes "internally self-assembled" particles.[25] Such dispersions are usually stabilized by hydrophilic high-molecular-weight triblock (TB) copolymers PEO$_n$PPO$_m$PEO$_n$, such as poloxamer 407 or Pluronics F127 or Synperonic FE/ F127.[12,13] These polymers, although very hydrophilic, can still penetrate the LC nanostructure. The bicontinuous cubic phase

can change from *Pn*3*m* symmetry to *Im*3*m* with some attached vesicles[12,20,26–28] while the hexosomes are hardly influenced and the micellar cubosomes can transform into emulsified microemulsions at a very high polymer concentration.[28] The transformation from *Pn*3*m* symmetry to *Im*3*m* can be avoided by replacing F127 with F108[29] or Myrj 59;[30] however, F127 is still the most frequently used polymer for stabilizing isasomes.[31] Oil-in-water (O/W) emulsions can also be stabilized by complexes of oppositely charged polyelectrolytes, although stable emulsions with relatively large droplets can only be found in a limited pH range.[32] As yet, there are no known applications for such oppositely charged polyelectrolytes in the stabilization of LC systems. Another way to stabilize dispersions of LC materials is by forming the so-called Pickering[33] or Ramsden[34] emulsions, in which the dispersions are stabilized by nanoparticles made from different materials.[35–41] Such particles can range from silica[42] to laponite,[43,44] soot,[45] or proteins.[46,47] As in the case of polymeric stabilizers,

the molecules forming the LC phase to be dispersed may interact (adsorb) with the Pickering particles. Such an adsorption process may change the composition and structure of the LC phase.

Until now, we have discussed the dispersion of hydrophobic LC phases in the excess water phase. In this contribution, we explore the possibility of the formation and stabilization of inverted or reverse systems, that is, dispersion of hydrophilic LC phases in an excess oil phase, such as an alkane. This means changing from O/W emulsions to W/O emulsions, with the restrictions that the water phase to be dispersed should be an LC phase in equilibrium with excess oil and that the oil should be nonpolar, that is, an alkane. Although the literature is very rich in the description of O/W emulsions,[48,49] for all kinds of oils, there are far fewer contributions on W/O emulsions,[50−52] especially where the oil is nonpolar.[53−55] In fact, there have been no reports of a stabilized W/O emulsion containing an LC phase until now; only W/O emulsions without stabilizers based on continuous LC oil phases were reported.[56] For stabilized particles (Pickering emulsions), it is essential to control the surface properties.[57]

This work was split into three parts: first, we had to find a hydrophilic LC phase that could incorporate a certain amount of alkanes but coexist with excess alkane at higher oil concentrations. Basically, the LC phase can show bicontinuous cubic, hexagonal, or discontinuous, micellar cubic structures, which can be clearly identified by the corresponding Miller indices[58] in a small-angle X-ray scattering (SAXS) pattern. In the case of a very weak order, the system may only clearly show the first-order peak. In such cases, it is of great advantage to use polarized light microscopy to identify the phase. Only hexagonal phases show a depolarized signal in light microscopy, whereas cubic phases do not (they only show black images under crossed polarizers). Therefore, we focused on hexagonal LC phases, specifically on creating hexosomes of hydrophilic LC phases in oil. To distinguish between usual O/W hexosomes and our W/O ones, we use the term *reverse hexosomes* for the latter. It must be kept in mind that hexosomes are O/W emulsions regularly based on an inverse lipophilic hexagonal (H_{II}) phase, but for historical reasons, they are just called hexosomes. We prepared W/O emulsions containing a "normal" hydrophilic hexagonal phase (H_I), and we call them reverse of the hexosomes.

We selected tetradecane as our alkane, being liquid at ambient temperature (melting temperature 5.5 °C) but having a low enough vapor pressure (0.0155 hPa at 25 °C) to avoid compositional inaccuracies because of evaporation during sample handling. Second, we sought a convenient stabilizer for forming stable W/O dispersions. We initially looked for a suitable emulsifier for just water-in-tetradecane and then we used the successful candidates to solubilize the LC phase. Short-chain surfactants might have enabled the formation of stable water-in-tetradecane emulsions; however, they were excluded, as it is well-known from the original work on cubosomes and hexosomes that such small amphiphilic molecules will intercalate into the LC phase and change or even destroy the internal nanostructure. Therefore, we looked for high-molecular-weight polymeric stabilizers with relatively low hydrophilic−lipophilic balance (HLB) or for relatively hydrophobic particles for Pickering systems. Third, those stabilizers that gave stable water-in-tetradecane emulsions were tested to see if they could also give stable dispersions containing the hydrophilic LC phase in tetradecane without

destroying the LC nanostructure. In this contribution, we report on LC phases based on nonionic industrial-grade surfactants and on TB copolymers stabilized by either long-chain polymeric stabilizers—laboratory-synthesized and commercial ones—or by specially selected hydrophobic nanoparticles.

■ EXPERIMENTAL SECTION

The aim of this work was to develop a system containing a hydrophilic LC phase dispersed and stabilized in excess alkane. A primary surfactant is needed to form the LC phase, whereas a second surfactant is needed to disperse and stabilize that LC phase. We refer to the second surfactant as the stabilizer, which may be either a molecular stabilizer or a nanoparticle stabilizer. Molecules such as polyethylene glycol alkyl ethers (C_iE_j)[59] or various poloxamers[60] are known to form LC phases in excess oil. Highly purified C_iE_j and L64 have shown a promising phase behavior in previous studies.[59,61] They formed LC phases in the presence of water and could be swelled by oils; they also formed stable two-phase systems in excess oils such as toluene and decane. Because of financial restrictions and for better applicability, we generally used commercially available technical-grade chemicals.

Materials. Various C_iE_j samples, product name Genapol LA 040−090 (E4−E9), were provided by Clariant (Germany). All of the surfactants received consisted of a medium alkyl chain length of 12−16 carbons (C_{12}−C_{16}). The samples differed in the number of ethylene oxide units (E4−E9). Pluronic L64 (L64) and tetradecane ≥99% were purchased from Sigma-Aldrich (Switzerland). Pluronic L64 is a TB copolymer (A−B−A) consisting of a propylene oxide core (30 units) and two ethylene oxide chains (13 units). The structures are shown in Figure 1.
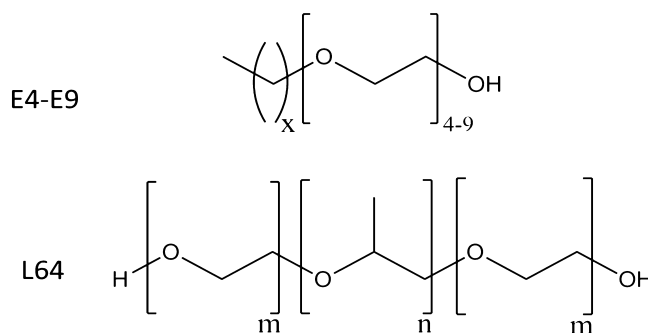
Figure 1. Scheme of primary surfactants used for the formation of the LC phases. E4−E9: *x* = 12−16; L64: *m* = 13, *n* = 30.

Cithrol DPHS (DPHS), provided by Croda (United Kingdom), was used as the molecular stabilizer and Aerosil R711 (R711), provided by Evonik (Germany), was used as the nanoparticle stabilizer for dispersions. The water used in the experiments was deionized by PURELAB Prima by Elga (UK). All surfactants, stabilizers, and tetradecane were used as received.

In addition, two different block copolymers, synthesized by ring-opening metathesis polymerization (ROMP) during this project, were also used as molecular stabilizers. ROMP is a versatile and flexible method for synthesizing block copolymers with various properties and functionalities.[62]

Two different architectures of block copolymers with norbornene backbones were chosen (see Figure 2). The first is a diblock (DB) copolymer with an A−B structure, where A is a long hydrophobic block (dodecyl side chains) and B is a short hydrophilic block (ethylene glycol side chains) with a ratio of 3:1 to mimic the structure of a standard surface-active molecule with low HLB. The second architecture is a TB copolymer of A−B−A structure with a ratio of 3:1:3, which is often used for W/O microemulsions but, in addition, should be soluble in tetradecane.
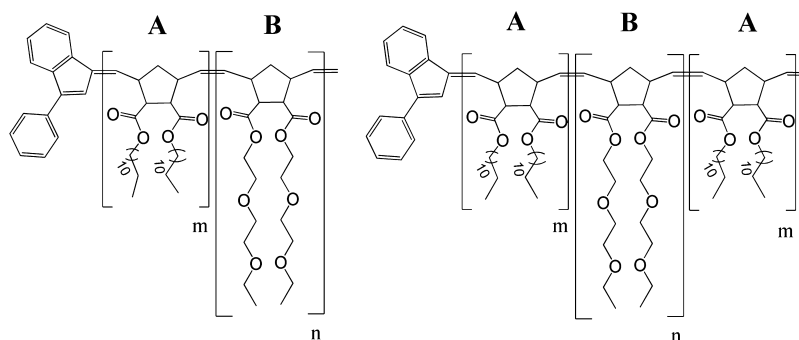
Figure 2. Block copolymers with norbornene backbones synthesized by ROMP. Number of units: $m = 60$, $n = 20$. A—hydrophobic block, B—hydrophilic block. Left: DB (A−B = 3:1); right: TB (A−B−A = 3:1:3).

The polymerization procedure, which uses the Ru catalyst M31[63] as an initiator, is described in detail in the Supporting Information and was adapted from Hollauf et al.[64] For the synthesis of the oligoethyleneglycol-functionalized monomer, a slightly modified literature protocol was used[65] (see also the Supporting Information). The resulting ratio of hydrophobic to hydrophilic blocks in the synthesis was determined via ^1H NMR spectroscopy. The multiplet at 1.40−1.13 ppm represents the hydrophobic dodecyl side chains, whereas the multiplet at 3.75−3.45 ppm represents the hydrophilic ethylene oxide side chains. Integration of the signals gives ratios of 3.5:1 for the DB and 3.5:1:3.5 for the TB. The higher ratio of hydrophobic blocks resulting for DB and TB can be explained by the slower reaction rate of hydrophilic blocks because of the poor solubility in organic solvents.

All the reagents and solvents used for the synthesis were purchased with reagent-grade quality from Sigma-Aldrich (Switzerland) or ABCR (Germany) and used as received. Complex M31 [1,3-bis(2,4,6-trimethylphenyl)-2-imidazolidinylidene]dichloro-(3-phenyl-1*H*-inden-1-ylidene)(pyridyl) ruthenium(II) was obtained from UMI-CORE AG Co.

Preparation Methods. *Definition of the Sample Composition.* Bulk samples are nondispersed samples. The binary mixtures of the primary surfactant (PS) and water are described by δ, which denotes the weight ratio between the primary surfactant and water.

$$\delta = \frac{\text{mass (PS)}}{\text{mass (PS + water)}} \times 100 \qquad (1)$$

Ternary mixtures are formed by the addition of tetradecane to the binary systems, where the oil content is given in weight percent. Ternary mixtures can be one-phase systems for low tetradecane content, and they eventually form two-phase systems at higher amounts of tetradecane.

Dispersions can only be formed from such two-phase ternary systems, which consist of the bulk (primary surfactant, water, and tetradecane) and additional stabilizer. They are characterized by β (eq 2), which defines the stabilizer content relative to the mass of the dispersed binary phase, and Φ (eq 3), which describes the overall content of the dispersed phase.

$$\beta = \frac{\text{mass (stabilizer)}}{\text{mass (PS + water)}} \times 100 \qquad (2)$$

$$\Phi = \left[\frac{\text{mass (PS + water)}}{\text{mass (PS + water + TD + stabilizer)}} \right] \times 100 \qquad (3)$$

Binary Surfactant−Water Systems. Because the surfactants E4−E9 and L64 are commercial products and not highly purified, the phase behavior, especially the formation of LC phases, was controlled by preparing the corresponding bulk samples. The primary surfactant and water were weighed in 4 mL vials with different ratios (δ values, eq 1). The mixtures were heated to 80 °C for 5 min to melt any occurring LC phase and ensure homogeneous mixing before cooling to room temperature while vortexing (RS-VA 10, Phoenix Instrument,

Garbsen, Germany). The cooling was accelerated by an air gun to avoid phase separation. The samples were left at room temperature for at least 24 h to equilibrate before structural characterization.

Ternary Surfactant−Water−Oil Systems. Tetradecane was added with increasing concentration to the binary mixtures with fixed δ values. The samples were heated to 80 °C to melt any LC and allow the oil to be incorporated into the LC upon cooling. The cooling was again accelerated by an air gun during vortexing to ensure homogeneity.

Dispersions. Dispersions are produced by adding the fourth component, the stabilizer, to the two-phase ternary system and by applying shear forces (ultrasonication). This makes it possible to disperse the LC in excess tetradecane. The primary surfactant, water, tetradecane, and a 5 wt % stock solution of the stabilizer dissolved in tetradecane were weighed in 4 mL vials. The samples were ultrasonicated for 10 min. The ultrasonication device (Vibra-Cell, Sonics & Materials, Newtown, CT, USA) was equipped with a tapered tip and used at 120 W (30% amplitude of the maximum power of 400 W) in pulsed mode (0.2 s pulses in between 2 s breaks). The samples were placed in a water bath during ultrasonication to facilitate heat dissipation. The samples were characterized by dynamic light scattering (DLS), polarization microscopy, and SAXS after 1 h of equilibration time.

Polarization Microscopy. Polarization microscopy was carried out on a Leica DM2500 M microscope with two polarization filters to show the anisotropy of certain liquid-crystal phases from their optical birefringence. The centrifuged sample was squeezed to a thin layer of about 100 μm and investigated in transmittance light mode, with a 20×/0.40 objective. The mounted camera was a Sony DXC-390P. The pictures were recorded using the software Sarfusoft 2.1 (Nanolane, France).

Dynamic Light Scattering. DLS was used to determine the mean hydrodynamic radius of the dispersion droplets. The DLS equipment consisted of a diode laser (Coherent Verdi V5, λ = 532 nm) and a goniometer with single-mode fiber detection optics (OZ from GMP, Zürich, Switzerland). These data were acquired by an ALV/SO-SIPD/DUAL photomultiplier with pseudo-cross-correlation and an ALV 7004 Digital Multiple Tau Real Time Correlator (ALV, Langen, Germany). The correlation functions were determined and stored by the ALV software package. The light-scattering signal was measured 10 times for 30 s at a scattering angle of 90° at 25 °C, and the resulting correlation functions were averaged. The mean hydrodynamic radius R_H was calculated by means of the cumulant method.[66]

Small-Angle X-ray Scattering. The SAXS equipment consisted of a high-flux SAXSess camera (Anton Paar, Graz, Austria) connected to a Debyeflex 3003 X-ray generator (GE-Electric, Germany) operating at 40 kV and 50 mA with a sealed tube Cu anode. The Goebel-mirror-focused and Kratky-slit-collimated X-ray beam was line-shaped (17 mm horizontal dimension at the sample). The scattered radiation was measured in the transmission mode and recorded by a one-dimensional MYTHEN-1k microstrip solid-state detector (Dectris, Switzerland), within a q range of 0.1−6 nm^{-1}. The
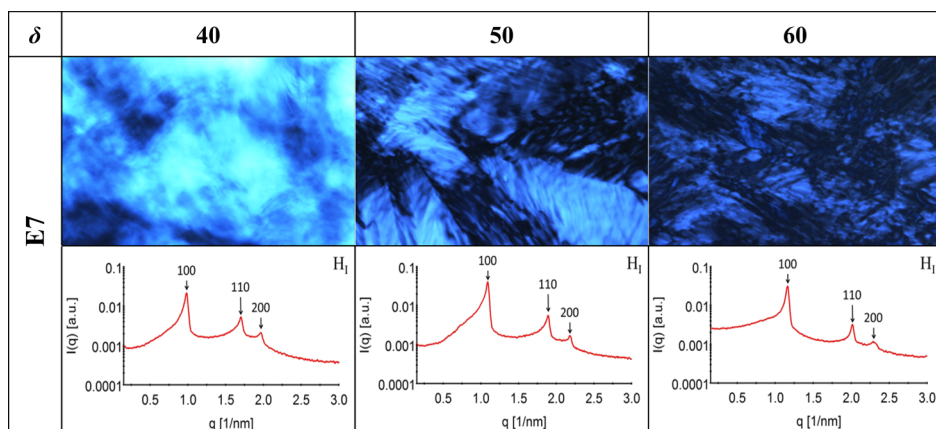
Figure 3. Screening of E7 binary bulk samples at different δ values; the peak indices indicate a hexagonal structure H_I; upper row: polarization microscopic pictures; lower row: SAXS curves (log(intensity) vs q).
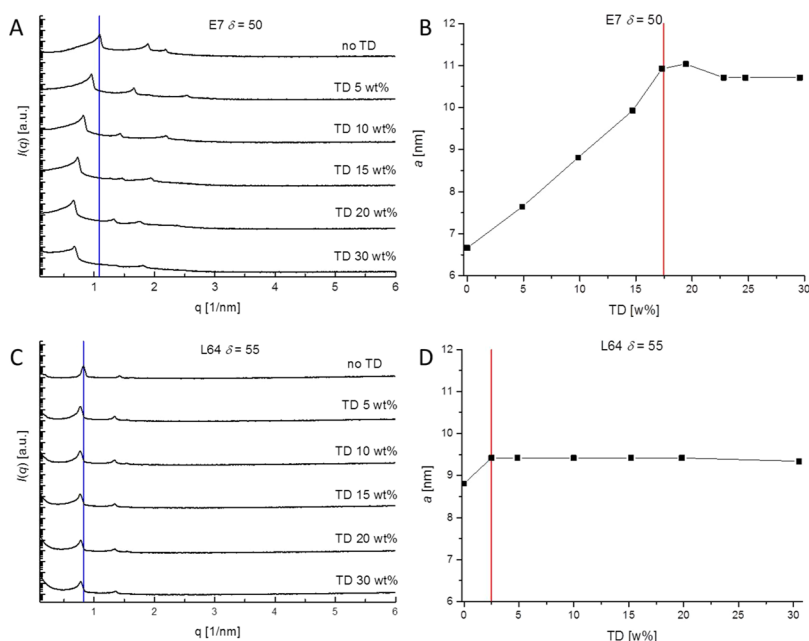
Figure 4. Results of oil loading of the hexagonal bulk phases of E7 at $\delta = 50$ wt % and L64 at $\delta = 55$ wt %. (A,C) Shift of hexagonal phase SAXS peaks to lower q values. TD = tetradecane, the blue line marks the peak position of the sample with no tetradecane. (B,D) Corresponding lattice parameters a, the red line marks the point of saturation with tetradecane.

magnitude of the scattering vector q is given by $q = 4\pi(\sin\theta)/\lambda$, with 2θ being the scattering angle with respect to the incident beam and λ the wavelength of the X-rays, 0.154 nm. All measurements were conducted at 25 °C.

■ RESULTS AND DISCUSSION

Screening of the Bulk Samples. The binary bulk samples of E4−E9 and L64 were prepared as described in the Binary Surfactant−Water Systems section. Their nanostructures were investigated by SAXS and polarization microscopy. Figure 3 shows the resulting SAXS curves and the corresponding polarization microscopic pictures for E7 and L64 measured at 25 °C. E4−E6 showed no hexagonal phase and were not further investigated. E7−E9 showed the existence of a hexagonal phase and were quite similar to each other. E7 was finally chosen as the primary surfactant because it showed the most stable hexagonal phase against temperature variation and the highest uptake of tetradecane relative to E8 and E9 (see the Supporting Information, Figure S5). The cumulative

results for E4−E9 and L64 can be found in the Supporting Information (Figures S1−S3).

Hexagonal structures were found at $40 \leq \delta \leq 60$ for E7 and at $\delta = 55$ for L64, which are in good agreement with previous reports on purified C_iE_j systems.[59] The corresponding phase diagrams from the literature can be found in the Supporting Information (Figure S4). At higher δ values, both the primary surfactants formed L_α phases. E7 showed hexagonal lattice parameters of 7.38 nm ($\delta = 40$), 6.66 nm ($\delta = 50$), and 6.25 nm ($\delta = 60$). L64 showed a hexagonal phase at $\delta = 55$ with a lattice parameter of 8.81 nm.

Oil-Loading Capacity of Bulk Samples. To form an emulsion in a continuous oil phase, the system must form a stable two-phase system with excess oil. The point at which no more oil is incorporated into the LC phase is called the phase-separation point or phase-separation line in a triphasic diagram, beyond which the LC formed no longer swells but is still stable.

The oil-loaded samples were characterized by SAXS to show the behavior of the hexagonal phase upon the uptake of tetradecane. The mean size of the unit cell or lattice parameter for the hexagonal phase can be derived from the SAXS curve by the following relation:[67]

$$a = \frac{4\pi}{\sqrt{3}\, q_{peak1}}$$

(4)

where a is the lattice constant and q_{peak1} is the q value of the first peak in the spectrum. The shift of the first peak toward lower q values with increasing concentration of tetradecane shows the uptake of oil into the hexagonal LC. From Figure 4, one can see that the bulk phase of E7 at $\delta = 50$ incorporates up to 17.5 wt % tetradecane before saturation. The lattice parameter increases from 6.7 nm with no tetradecane present up to 11.0 nm at the phase-separation point. Beyond this point, all additional tetradecane is present as excess oil, the samples show a turbid appearance, and the lattice parameter has a constant value of about 10.7 nm. E8 and E9 show a similar behavior (Supporting Information, Figure S5). L64 shows only a small uptake of 2.5 wt % tetradecane at $\delta = 55$; beyond that, no more tetradecane is incorporated, and the hexagonal phase appears to be stable. The lattice parameter at 8.8 nm without tetradecane increases to 9.4 nm at the plateau.

Dispersions of the LC in the Continuous Excess Oil Phase. The next step is to form a dispersion of the LC in the continuous excess oil phase. To achieve this, the aqueous phase has to be dispersed and stabilized in the alkane phase. Here, the aqueous phase consists of a hydrophilic LC as an aggravating factor. First, one has to find a suitable stabilizer to form a W/O emulsion. Some general aspects to be considered when looking for a stabilizer for hydrophilic LC phases in an alkane are as follows: amphiphilic polymers must have both a high molecular weight to avoid being incorporated into the hydrophilic LC and a dominating lipophilic part (low HLB value[68,69]) to be soluble in the alkane. In the case of particles for Pickering emulsions, nanoparticles must be quite hydrophobic to enable the formation of W/O emulsions.[57]

Various commercially available stabilizers, such as AOT, Pluronics L64, and P123, as well as different polysilanes with structural characteristics similar to that of AOT, were tested. To investigate the applicability of a stabilizer, solubility tests in tetradecane were first conducted, followed by water emulsification tests. All the stabilizers tested showed either insufficient solubility in tetradecane or did not form stable water-in-tetradecane emulsions. The lack of effective strong stabilizing forces, such as electrostatic or steric forces in an alkane, makes it challenging to produce an emulsion that shows long-term stability against coalescence and, finally, phase separation.

Water-in-Tetradecane Emulsions with Molecular Stabilizers: DB Norbornene Copolymer, TB Norbornene Copolymer, and DPHS. After purification and characterization of the two products DB and TB, emulsification tests were conducted using plain water in tetradecane as a first test. After we had already synthesized the DB and TB copolymers, a commercially available block copolymer was brought to our attention: DPHS, which is used for the stabilization of W/O emulsions in the cosmetic industry,[70] also has an A−B−A structure with two hydrophobic poly(12-hydroxystearic acid) A-blocks and a hydrophilic polyethylene glycol B-block (see

Figure 5). Additionally, it has a high average molecular weight ≥5000 g/mol.
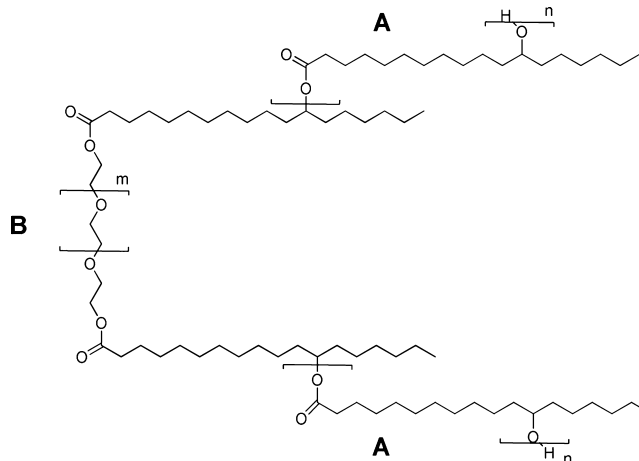
Figure 5. Structure of DPHS adapted from Hassan et al.:[71] (A) hydrophobic poly(12-hydroxystearic acid) with $n = 9$ units and (B) hydrophilic polyethylene glycol with $m = 30$ units, average molecular weight ≥5000 g/mol.

DB, TB, and DPHS showed good solubility in tetradecane. The solutions (1 wt %) of stabilizers in tetradecane were prepared and loaded with water, using the same ultrasonication procedure as described in the Dispersions of the LC in the Continuous Excess Oil Phase section.

The samples were characterized in terms of mean droplet size by DLS (see Table 1). All the three stabilizers were able to stabilize various concentrations of water droplets in tetradecane: DB norbornene copolymer, TB norbornene copolymer, and DPHS.

DB and TB showed micelle formation at a concentration of 0.1 wt % with a mean size of $R_H = 16$ nm, whereas TB micelles only formed at 2 wt % stabilizer concentration; nonetheless,

Table 1. Size of Stabilizer Micelles and Water-Swollen Micelles in Tetradecane[a]

| | R_H [nm] | | | |
| | stabilizer concentration | | | |
stabilizer	0.1 wt %	1 wt %	2 wt %	water content
DB	16.9 ± 0.10	15.6 ± 0.05	15.2 ± 0.05	0 v/v %
TB	X	X	14.7 ± 0.05	
DPHS	95.6 ± 0.3	183.9 ± 0.9	206.3 ± 1.6	
DB	490.5 ± 3.5	121.7 ± 2.0	202.8 ± 1.8	1 v/v %
TB	249.5 ± 2.5	175.6 ± 0.8	220.5 ± 2.8	
DPHS	141.2 ± 1.4	82.1 ± 0.2	84.4 ± 0.3	
DB	680.4 ± 9.9	421.5 ± 3.5	453.6 ± 3.9	5 v/v %
TB	not stable	384.2 ± 8.2	395.2 ± 3.6	
DPHS	463.7 ± 11.0	157.5 ± 0.9	142.2 ± 0.4	

[a]Determination of the hydrodynamic radius R_H by DLS measurements. The first section shows pure micelles with no water, and the following sections show water-swollen micelles with 1 and 5 v/v % water. DB: DB norbornene copolymer, TB: triblock norbornene copolymer, DPHS: Cithrol DPHS X: no signal. Samples with water were ultrasonicated as described in the Dispersions of the LC in the Continuous Excess Oil Phase section.

they were of comparable size (R_H = 15 nm). DPHS shows large R_H values at 1 and 2 wt % because wormlike micelles are formed, which was confirmed by depolarized DLS measurements. When water is added (1 v/v %), the worms swell and transform into spherical micelles, which leads to the smaller radii around 80 nm.

Long-term stability tests were conducted over a period of 20 days at a stabilizer concentration of 1 wt % and three different water concentrations: 1, 5, and 10 v/v %. All of the samples showed stability against phase separation over the test period, but they did also show a tendency to agglomeration and sedimentation. Therefore, before the DLS measurements, the samples were shaken by hand to break up any agglomerates that had formed. Nonetheless, during the measurements, an increase in the mean size of the particles is observable. Thus, it is conceivable that bigger agglomerates were formed again in the sample during the measurement. Higher amounts of water led to larger droplets and faster agglomeration behavior and sedimentation. To summarize, the stabilizers showed that it is possible to stabilize water over a longer period, without any signs of phase separation, such as a clear water layer at the bottom. The corresponding detailed results are summarized in the Supporting Information (Table S1).

Water-in-Tetradecane Emulsions with the Nanoparticle Stabilizer. Along with the polymeric stabilizers, the commercially available particle stabilizer R711 was used to monitor the formation of a stable Pickering emulsion. These SiO_2 particles are partially hydrophobized with 2-propenoic acid 2-methyl-3-(trimethoxysilyl)propylester. Masliyah et al. found that R711 particles only formed W/O emulsions if the particles were suspended in oil first.[72] The same stability tests were conducted for the polymeric stabilizers; however, the fast sedimentation behavior of the droplets (≤5 min) did not allow a reliable determination of the droplet sizes. The system did not phase-separate, but agglomerates were formed rapidly over the course of the measurements. Drelich et al.[73] reported that the emulsions stabilized by R711 particles show larger radii in the micrometer range and, at higher concentrations, form 3D networks of R711 particles, which support emulsion stability.

Reverse Hexosomes: Hexagonal LC Phases Dispersed in Tetradecane. Dispersions were prepared with Φ values of 5 and 10% and characterized by DLS, polarization microscopy, and SAXS. Samples with different δ and β values were prepared. Dispersions prepared with DB as the stabilizer were not stable and did not form a hexagonal phase; therefore, only the results for TB, R711, and DPHS are shown in the following. All the dispersion samples were centrifuged (15 min, 4500 rpm, 25 °C) before the measurement with the polarization microscope and SAXS in order to increase the concentration and, thus, also the signal.

The results for all the samples with E7 as the primary surfactant showed an influence of the stabilizers on the LC. Generally, the higher the β value, that is, the higher the concentration of the stabilizer, the more disturbed was the hexagonal phase; one corresponding example is shown in Figure 6. The graph also shows an extra peak next to the first reflection of the hexagonal phase at a q-value of 0.83. This indicates the coexistence of a lamellar phase. This lamellar phase is the neighboring phase of E7 for δ = 70 (see also Figures S8 and S2 in the Supporting Information). The peak indices are shown in Figure S8.

A δ value of 60, which is the upper limit of the hexagonal phase, was chosen because when a δ value of 50 was used, the
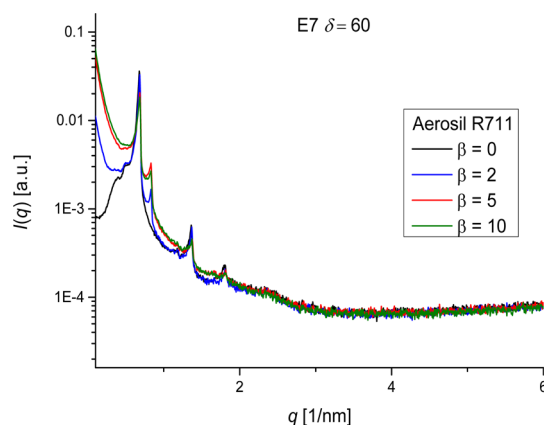
Figure 6. Influence of increasing concentration of the R711 stabilizer on the SAXS signal of the hexagonal phase E7, δ = 60.

hexagonal phase did not form; hence, an interaction between the stabilizer and the primary surfactant is suspected (see the Supporting Information, Figure S6). From the results of all our experimental series, we could see that the system changes in the presence of the stabilizers as if the relative concentration δ of the primary surfactant was lowered. This suggests that the primary surfactant interacts with and adsorbs to the stabilizer until the stabilizer is saturated. This disturbs the hexagonal phase. Figure 6 shows that, in the case of R711, the order of the hexagonal phase decreases with an increasing amount of the stabilizer. This leads to the conclusion that the ratio between the primary surfactant and the stabilizer plays a major role in the stability of the liquid crystal. In other words, there must be sufficient primary surfactant to saturate the stabilizer.

The results for dispersions produced with E7 as the primary surfactant are summarized for the three successful stabilizers found in this study in Figure 7.
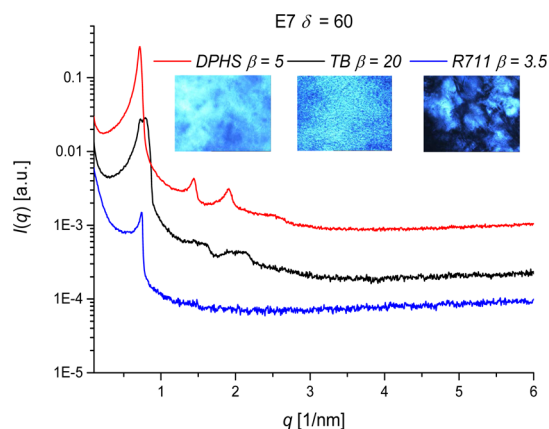
Figure 7. Dispersion results for different stabilizers with E7 as the primary surfactant, Φ = 10. Samples were centrifuged before SAXS measurement and polarization microscopy.

The hexagonal LC was found in all three dispersions in various degrees of order. The different β values were chosen after testing for the best stability and weakest influence on the LC phase. TB showed a lattice parameter of 9.18 nm and an R_H value of 170 nm. The SAXS curve shows relatively broad reflections, which indicate a slightly disturbed order of the hexagonal phase. The sample with R711 shows only the first-order reflection of the hexagonal phase with a lattice parameter

of 9.76 nm, but the polarization microscope confirms the presence of the hexagonal phase. The R_H value of this sample could not be determined because of the fast agglomeration and sedimentation behavior. However, no phase separation was observed. DPHS shows the best stabilization properties of the tested stabilizers in terms of highest stability and least disturbance of the hexagonal phase. The lattice parameter was calculated to be 10.12 nm, and R_H was 190 nm.

The results for dispersions containing L64 as the primary surfactant are summarized in Figure 8.
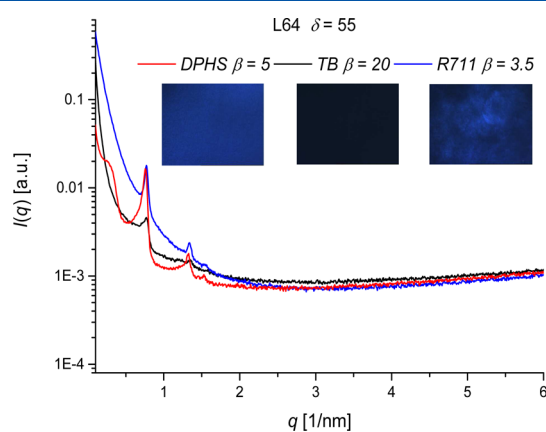
Figure 8. Dispersion results for the primary surfactant L64, $\Phi = 10$; the samples were centrifuged before SAXS measurement and polarization microscopy.

L64 appeared more stable against all stabilizers; hence, the δ value of 55 was used, which corresponds to the hexagonal phase in the binary L64−water sample. The SAXS curve reveals a hexagonal but very disturbed phase for TB with a lattice parameter of 9.34 nm and an R_H value of 117 nm. No polarization effect could be seen under the polarization microscope. However, the SAXS data clearly indicate the presence of the hexagonal phase. The samples stabilized with R711 showed a lattice parameter of 9.42 nm. DPHS showed a lattice parameter of 9.50 nm and an R_H value of 168 nm. The polarization microscope shows a reduced order for both the samples.

Macroscopically, the dispersions stabilized with DPHS showed the best stability. They showed the smallest particle size, lowest polydispersity, and slowest agglomeration and sedimentation behavior.

CONCLUSIONS

We have achieved, for the first time, the formation of a W/O emulsion, with an average droplet size of 160 nm, containing a H_I hexagonal LC phase—reverse hexosomes—and showing sterical stability for more than 7 days. Agglomeration and sedimentation in the dispersions were always fast, but we did not find phase separation within a period of 1 month and the agglomeration was reversible by hand shaking.

Hydrophilic hexagonal LC phases (H_I) can be formed with short-chain nonionic surfactants such as polyethylene glycol alkyl ethers (C_iE_j) or with high-molecular-weight TB copolymer of type A−B−A. We successfully used Genapol LA 070 ($C_{12-16}E_7$) and Pluronics L64 as the primary surfactants; they can form H_I phases, swell by incorporation of a certain amount of tetradecane, and remain stable beyond the phase separation in equilibrium with excess oil.

The stabilization of a hydrophilic H_I LC phase in a nonpolar medium such as tetradecane was a difficult task because the lack of repulsive interactions in such a medium always favors agglomeration rather than stable emulsions. All the tested stabilizers (DB, TB, DPHS, and R711) showed the capability to stabilize different amounts of plain water.

Reverse hexosomes could be formed using the stabilizers TB, DPHS, and R711 but not with DB. One general problem was the interaction of the primary surfactant with the stabilizer. The system changes in the presence of the stabilizers as if the relative concentration δ of primary surfactant was being lowered. This is strong evidence that the primary surfactant interacts with and adsorbs to the stabilizer until the stabilizer is saturated. This disturbs and may even destroy the hexagonal phase H_I. Therefore, it may be necessary to increase the δ value of the system. This interaction between the primary surfactant and stabilizer was stronger for the short-chain primary surfactant E7 than for the long-chain primary surfactant L64. The most stable reverse hexosome dispersions were formed with the stabilizer Cithrol DPHS.

In future, we aim to optimize the order of the hexagonal crystal and the versatility of the system by expanding to other solvents, including natural oils, such as triglycerides. Furthermore, the possibility of incorporating active molecules such as enzymes into the LC phase should be explored.

■ ASSOCIATED CONTENT

ⓢ Supporting Information

The Supporting Information is available free of charge on the ACS Publications website at DOI: 10.1021/acs.langmuir.8b01455.

> Detailed results for the binary primary surfactant−water bulk samples for samples E4−E9, adapted phase diagrams from the literature for E8 and L64, diagram showing the oil-loading capacity for E7−E9, detailed description of the synthesis procedure for the two molecular stabilizers used (DB and TB), spectrum showing the influence of the stabilizers on E7 with a δ value of 50, and detailed results of the long-term stability tests of the ternary tetradecane−stabilizer−water systems (PDF)

■ AUTHOR INFORMATION

Corresponding Author

*E-mail: otto.glatter@tugraz.at.

ORCID ⓘ

Otto Glatter: 0000-0002-4498-4385

Gregor Trimmel: 0000-0001-8922-4163

Notes

The authors declare no competing financial interest.

■ ABBREVIATIONS

DB, diblock copolymer

DLS, dynamic light scattering

DPHS, (PEG-30) dipolyhydroxystearate

LC, liquid crystal
O/W, oil-in-water
PS, primary surfactant
R_H, hydrodynamic radius
ROMP, ring-opening metathesis polymerization
SI, supporting information
SAXS, small-angle X-ray scattering
TB, triblock copolymer
TD, tetradecane
W/O, water-in-oil

■ REFERENCES

(1) Larsson, K. On the structure of isotropic phases in lipid-water systems. *Chem. Phys. Lipids* **1972**, *9*, 181−195.

(2) Larsson, K. Two cubic phases in monoolein-water system. *Nature* **1983**, *304*, 664.

(3) Larsson, K. Cubic lipid-water phases: structures and biomembrane aspects. *J. Phys. Chem.* **1989**, *93*, 7304−7314.

(4) Seddon, J. M.; Templer, R. H. Polymorphism of Lipid-Water Systems. In *Handbook of Biological Lipids*; Lipowski, R., Sackmann, E., Eds; Elsevier Science B.V.: Amsterdam, 1995; Vol. 1, pp 97−159.

(5) Qiu, H.; Caffrey, M. The phase diagram of the monoolein/water system: metastability and equilibrium aspects. *Biomaterials* **2000**, *21*, 223−234.

(6) Mezzenga, R.; Meyer, C.; Servais, C.; Romoscanu, A. I.; Sagalowicz, L.; Hayward, R. C. Shear Rheology of Lyotropic Liquid Crystals: A Case Study. *Langmuir* **2005**, *21*, 3322−3333.

(7) Barauskas, J.; Landh, T. Phase behavior of the phytantriol/water system. *Langmuir* **2003**, *19*, 9562−9565.

(8) Dong, Y.-D.; Larson, I.; Hanley, T.; Boyd, B. J. Bulk and Dispersed Aqueous Phase Behavior of Phytantriol: Effect of Vitamin E Acetate and F127 Polymer on Liquid Crystal Nanostructure. *Langmuir* **2006**, *22*, 9512−9518.

(9) Boyd, B. J.; Rizwan, S. B.; Dong, Y.-D.; Hook, S.; Rades, T. Self-Assembled Geometric Liquid-Crystalline Nanoparticles Imaged in Three Dimensions: Hexosomes Are Not Necessarily Flat Hexagonal Prisms. *Langmuir* **2007**, *23*, 12461−12464.

(10) Rizwan, S. B.; Dong, Y.-D.; Boyd, B. J.; Rades, T.; Hook, S. Characterisation of bicontinuous cubic liquid crystalline systems of phytantriol and water using cryo field emission scanning electron microscopy (cryo FESEM). *Micron* **2007**, *38*, 478−485.

(11) Gustafsson, J.; Ljusberg-Wahren, H.; Almgren, M.; Larsson, K. Cubic Lipid−Water Phase Dispersed into Submicron Particles. *Langmuir* **1996**, *12*, 4611−4613.

(12) Gustafsson, J.; Ljusberg-Wahren, H.; Almgren, M.; Larsson, K. Submicron Particles of Reversed Lipid Phases in Water Stabilized by a Nonionic Amphiphilic Polymer. *Langmuir* **1997**, *13*, 6964−6971.

(13) Larsson, K. Aqueous dispersions of cubic lipid-water phases. *Curr. Opin. Colloid Interface Sci.* **2000**, *5*, 64−69.

(14) Spicer, P. T.; Hayden, K. L.; Lynch, M. L.; Ofori-Boateng, A.; Burns, J. L. Novel Process for Producing Cubic Liquid Crystalline Nanoparticles (Cubosomes). *Langmuir* **2001**, *17*, 5748−5756.

(15) Mele, S.; Murgia, S.; Monduzzi, M. Monoolein based liquid crystals to form long-term stable emulsions. *Colloids Surf., A* **2003**, *228*, 57−63.

(16) Angelova, A.; Ollivon, M.; Campitelli, A.; Bourgaux, C. Lipid Cubic Phases as Stable Nanochannel Network Structures for Protein Biochip Development: X-ray Diffraction Study. *Langmuir* **2003**, *19*, 6928−6935.

(17) Angelova, A.; Angelov, B.; Garamus, V. M.; Couvreur, P.; Lesieur, S. Small-Angle X-ray Scattering Investigations of Biomolecular Confinement, Loading, and Release from Liquid-Crystalline Nanochannel Assemblies. *J. Phys. Chem. Lett.* **2012**, *3*, 445−457.

(18) Abraham, T.; Hato, M.; Hirai, M. Glycolipid based cubic nanoparticles: preparation and structural aspects. *Colloids Surf., B* **2004**, *35*, 107−118.

(19) Spicer, P. T. Progress in liquid crystalline dispersions: Cubosomes. *Curr. Opin. Colloid Interface Sci.* **2005**, *10*, 274−279.

(20) Barauskas, J.; Johnsson, M.; Joabsson, F.; Tiberg, F. Cubic Phase Nanoparticles (Cubosome†): Principles for Controlling Size, Structure, and Stability. *Langmuir* **2005**, *21*, 2569−2577.

(21) Boyd, B. J.; Dong, Y.-D.; Rades, T. Nonlamellar liquid crystalline nanostructured particles: advances in materials and structure determination. *J. Liposome Res.* **2009**, *19*, 12−28.

(22) Monduzzi, M.; Ljusberg-Wahren, H.; Larsson, K. A ¹³C NMR Study of Aqueous Dispersions of Reversed Lipid Phases. *Langmuir* **2000**, *16*, 7355−7358.

(23) Yaghmur, A.; de Campo, L.; Salentinig, S.; Sagalowicz, L.; Leser, M. E.; Glatter, O. Oil-loaded monolinolein-based particles with confined inverse discontinuous cubic structure (Fd3m). *Langmuir* **2006**, *22*, 517−521.

(24) Yaghmur, A.; de Campo, L.; Sagalowicz, L.; Leser, M. E.; Glatter, O. Emulsified microemulsions and oil-containing liquid crystalline phases. *Langmuir* **2005**, *21*, 569−577.

(25) Yaghmur, A.; de Campo, L.; Sagalowicz, L.; Leser, M. E.; Glatter, O. Control of the internal structure of MLO-based isasomes by the addition of diglycerol monooleate and soybean phosphatidylcholine. *Langmuir* **2006**, *22*, 9919−9927.

(26) Almgren, M.; Edwards, K.; Gustafsson, J. Cryotransmission electron microscopy of thin vitrified samples. *Curr. Opin. Colloid Interface Sci.* **1996**, *1*, 270−278.

(27) Sagalowicz, L.; Michel, M.; Adrian, M.; Frossard, P.; Rouvet, M.; Watzke, H. J.; Yaghmur, A.; De Campo, L.; Glatter, O.; Leser, M. E. Crystallography of dispersed liquid crystalline phases studied by cryo-transmission electron microscopy. *J. Microsc.* **2006**, *221*, 110−121.

(28) Guillot, S.; Salentinig, S.; Chemelli, A.; Sagalowicz, L.; Leser, M. E.; Glatter, O. Influence of the Stabilizer Concentration on the Internal Liquid Crystalline Order and the Size of Oil-Loaded Monolinolein-Based Dispersions. *Langmuir* **2010**, *26*, 6222−6229.

(29) Chong, J. Y. T.; Mulet, X.; Waddington, L. J.; Boyd, B. J.; Drummond, C. J. Steric stabilisation of self-assembled cubic lyotropic liquid crystalline nanoparticles: high throughput evaluation of triblock polyethylene oxide-polypropylene oxide-polyethylene oxide copolymers. *Soft Matter* **2011**, *7*, 4768−4777.

(30) Chong, J. Y. T.; Mulet, X.; Waddington, L. J.; Boyd, B. J.; Drummond, C. J. High-Throughput Discovery of Novel Steric Stabilizers for Cubic Lyotropic Liquid Crystal Nanoparticle Dispersions. *Langmuir* **2012**, *28*, 9223−9232.

(31) Tilley, A. J.; Drummond, C. J.; Boyd, B. J. Disposition and association of the steric stabilizer Pluronic F127 in lyotropic liquid crystalline nanostructured particle dispersions. *J. Colloid Interface Sci.* **2013**, *392*, 288.

(32) Rodriguez, A. M. B.; Binks, B. P.; Sekine, T. Emulsion stabilisation by complexes of oppositely charged synthetic polyelectrolytes. *Soft Matter* **2018**, *14*, 239−254.

(33) Pickering, S. U. CXCVI.-Emulsions. *J. Chem. Soc. Trans.* **1907**, *91*, 2001−2021.

(34) Ramsden, W. Separation of Solids in the Surface-Layers of Solutions and "Suspensions" (Observations on Surface-Membranes, Bubbles, Emulsions, and Mechanical Coagulation). – Preliminary Account. *Proc. R. Soc. London* **1903**, *72*, 156−164.

(35) Ashby, N. P.; Binks, B. P. Pickering Emulsions Stabilised by Laponite Clay Particles. *Phys. Chem. Chem. Phys.* **2000**, *2*, 5640−5646.

(36) Aveyard, R.; Binks, B. P.; Clint, J. H. Emulsions Stabilised Solely by Colloidal Particles. *Adv. Colloid Interface Sci.* **2003**, *100−102*, 503−546.

(37) Binks, B. P.; Lumsdon, S. O. Stability of Oil-in-Water Emulsions Stabilised by Silica Particles. *Phys. Chem. Chem. Phys.* **1999**, *1*, 3007−3016.

(38) Binks, B. P. Particles as surfactants-similarities and differences. *Curr. Opin. Colloid Interface Sci.* **2002**, *7*, 21−41.

(39) Binks, B. P.; Lumsdon, S. O. Pickering Emulsions Stabilized by Monodisperse Latex Particles: Effects of Particle Size. *Langmuir* **2001**, *17*, 4540−4547.

(40) Frelichowska, J.; Bolzinger, M.-A.; Chevalier, Y. Effects of solid particle content on properties of o/w Pickering emulsions. *J. Colloid Interface Sci.* **2010**, *351*, 348−356.

(41) Larson-Smith, K.; Jackson, A.; Pozzo, D. C. SANS and SAXS Analysis of Charged Nanoparticle Adsorption at Oil-Water Interfaces. *Langmuir* **2012**, *28*, 2493−2501.

(42) Sadeghpour, A.; Pirolt, F.; Glatter, O. Submicrometer-Sized Pickering Emulsions Stabilized by Silica Nanoparticles with Adsorbed Oleic Acid. *Langmuir* **2013**, *29*, 6004−6012.

(43) Muller, F.; Salonen, A.; Glatter, O. Monoglyceride-based cubosomes stabilized by Laponite: Separating the effects of stabilizer, pH and temperature. *Colloids Surf., A* **2010**, *358*, 50−56.

(44) Muller, F.; Salonen, A.; Glatter, O. Phase behavior of Phytantriol/water bicontinuous cubic Pn3m cubosomes stabilized by Laponite disc-like particles. *J. Colloid Interface Sci.* **2010**, *342*, 392−398.

(45) Santini, E.; Guzmán, E.; Ravera, F.; Ciajolo, A.; Alfè, M.; Liggieri, L.; Ferrari, M. Soot Particles at the Aqueous Interface and Effects on Foams Stability. *Colloids Surf., A* **2012**, *413*, 216−223.

(46) Zhai, J.; Waddington, L.; Wooster, T. J.; Aguilar, M.-I.; Boyd, B. J. Revisiting β-Casein as a Stabilizer for Lipid Liquid Crystalline Nanostructured Particles. *Langmuir* **2011**, *27*, 14757−14766.

(47) Destribats, M.; Rouvet, M.; Gehin-Delval, C.; Schmitt, C.; Binks, B. P. Emulsions stabilised by whey protein microgel particles: towards food-grade Pickering emulsions. *Soft Matter* **2014**, *10*, 6941−6954.

(48) Sjöblom, J. *Encyclopedic Handbook of Emulsion Technology*; Marcel Dekker: New York, 2001.

(49) Tadros, T. F. *Emulsion Formation and Stability*; Wiley-VCH, 2013.

(50) Ushikubo, F. Y.; Cunha, R. L. Stability mechanisms of liquid water-in-oil emulsions. *Food Hydrocolloids* **2014**, *34*, 145−153.

(51) Fingas, M.; Fieldhouse, B. Studies of the formation process of water-in-oil emulsions. *Mar. Pollut. Bull.* **2003**, *47*, 369−396.

(52) Fingas, M. F. Water-in-Oil Emulsions: Formation and Prediction. *J. Pet. Sci. Res.* **2014**, *3*, 38.

(53) Yarranton, H. W.; Hussein, H.; Masliyah, J. H. Water-in-Hydrocarbon Emulsions Stabilized by Asphaltenes at Low Concentrations. *J. Colloid Interface Sci.* **2000**, *228*, 52−63.

(54) Jiao, J.; Burgess, D. J. Ostwald ripening of water-in-hydrocarbon emulsions. *J. Colloid Interface Sci.* **2003**, *264*, 509−516.

(55) Morales, C. J.; Riebel, U.; Guzmán, N. M.; Guerra, M. Formulation of water in paraffin emulsions. *Lat. Am. Appl. Res.* **2011**, *41*, 105−112.

(56) Kulkarni, C. V.; Mezzenga, R.; Glatter, O. Water-in-oil nanostructured emulsions: towards the structural hierarchy of liquid crystalline materials. *Soft Matter* **2010**, *6*, 5615−5624.

(57) Binks, B. P.; Lumsdon, S. O. Effects of oil type and aqueous phase composition on oil-water mixtures containing particles of intermediate hydrophobicity. *Phys. Chem. Chem. Phys.* **2000**, *2*, 2959−2967.

(58) Guillot, S.; Moitzi, C.; Salentinig, S.; Sagalowicz, L.; Leser, M. E.; Glatter, O. Direct and indirect thermal transitions from hexosomes to emulsified micro-emulsions in oil-loaded monoglyceride-based particles. *Colloids Surf., A* **2006**, *291*, 78−84.

(59) Alam, M. M.; Aramaki, K. Hexagonal Phase Based Gel-Emulsion (O/H1Gel-Emulsion): Formation and Rheology. *Langmuir* **2008**, *24*, 12253−12259.

(60) Alexandridis, P.; Hatton, T. A. Poly(ethylene oxide)poly-(propylene oxide)poly(ethylene oxide) block copolymer surfactants in aqueous solutions and at interfaces: thermodynamics, structure, dynamics, and modeling. *Colloids Surf., A* **1995**, *96*, 1−46.

(61) Alexandridis, P.; Olsson, U.; Lindman, B. Self-Assembly of Amphiphilic Block Copolymers: The (EO)13(PO)30(EO)13-Water-p-Xylene System. *Macromolecules* **1995**, *28*, 7700−7710.

(62) Leitgeb, A.; Wappel, J.; Slugovc, C. The ROMP toolbox upgraded. *Polymer* **2010**, *51*, 2927−2946.

(63) Burtscher, D.; Lexer, C.; Mereiter, K.; Winde, R.; Karch, R.; Slugovc, C. Controlled living ring-opening metathesis polymerization with a ruthenium indenylidene initiator. *J. Polym. Sci., Part A: Polym. Chem.* **2008**, *46*, 4630−4635.

(64) Hollauf, M.; Zach, P. W.; Borisov, S. M.; Müller, B. J.; Beichel, D.; Tscherner, M.; Köstler, S.; Hartmann, P.; Knall, A.-C.; Trimmel, G. Dye functionalized-ROMP based terpolymers for the use as a light up-converting material via triplet-triplet annihilation. *J. Mater. Chem. C* **2017**, *5*, 7535−7545.

(65) Sandholzer, M.; Fritz-Popovski, G.; Slugovc, C. Synthesis and self assembly of eosin functionalized amphiphilic block-random copolymers prepared by ring opening metathesis polymerization. *J. Polym. Sci., Part A: Polym. Chem.* **2008**, *46*, 401−413.

(66) Koppel, D. E. Analysis of macromolecular polydispersity in intensity correlation spectroscopy: the method of cumulants. *J. Chem. Phys.* **1972**, *57*, 4814−4820.

(67) Freiberger, N.; Glatter, O. Small-angle scattering from hexagonal liquid crystals. *J. Phys. Chem. B* **2006**, *110*, 14719−14727.

(68) Griffin, W. C. Classification of surface-active agents by HLB. *J. Cosmet. Sci.* **1949**, *1*, 97.

(69) Griffin, W. C. Calculation of HLB values of non-ionic surfactants. *J. Cosmet. Sci.* **1954**, *5*, 249−256.

(70) Tadros, T. F.; Dederen, C.; Taelman, M. C. A new polymeric emulsifier. *Cosmet. Toiletries* **1997**, *112*, 75−87.

(71) Hassan, T. H.; Metz, H.; Mäder, K. Novel semisolid SNEDDS based on PEG-30-dipolyhydroxystearate: Development and characterization. *Int. J. Pharm.* **2014**, *477*, 506−518.

(72) Yan, N.; Gray, M. R.; Masliyah, J. H. On water-in-oil emulsions stabilized by fine solids. *Colloids Surf., A* **2001**, *193*, 97−107.

(73) Drelich, A.; Gomez, F.; Clausse, D.; Pezron, I. Evolution of water-in-oil emulsions stabilized with solid particles. *Colloids Surf., A* **2010**, *365*, 171−177.

Supporting Information

Reverse Hexosome Dispersions in Alkane – The Challenge of Inverting Structures

Franz Pirolt†, Otto Glatter‡, Gregor Trimmel†*

† Institute for Chemistry and Technology of Materials, Graz University of Technology,

Stremayrgasse 9, 8010 Graz, Austria

‡ Institute for Inorganic Chemistry, Graz University of Technology,

Stremayrgasse 9, 8010 Graz, Austria

Number of pages: 13

Number of figures: 8

Number of tables: 1

Screening of Bulk Phases from E4–E9. Two-component systems of primary surfactant and water (δ value) were prepared in a number of different ratios. The samples were heated to 80°C to allow homogeneous mixing. Characterization was done by SAXS and polarization microscopy after cooling with an airgun during vortexing. Figure S1 and S2 show the results for the Genapol® samples E4–E9 with ethylene oxide unit numbers between 4 and 9.

E4 to E6 showed primarily the formation of a lamellar phase recognizable by the Maltese crosses in the polarization microscope pictures, and equidistant reflexes in the SAXS curve.
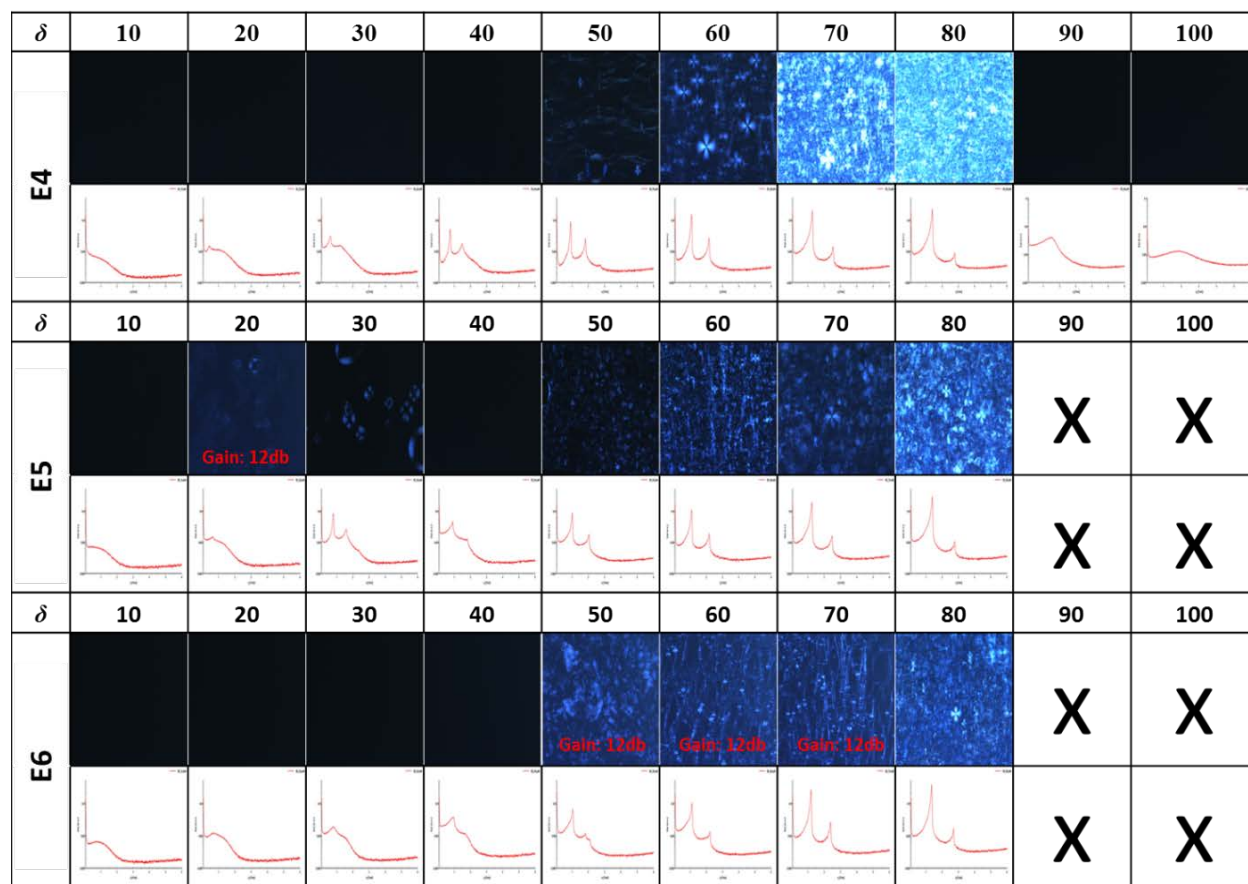
Figure S1: 1) Screening of bulk phases, results for E4–E6. **X**: insufficient sample for measurement. Upper rows: polarization-microscope pictures; lower rows: SAXS curves (log(intensity) vs. q)

E7–E9 exhibit different behavior from that shown by E4–E6: A hexagonal phase appears when δ lies between 40 and 60. The lattice parameter of E7–E9 is estimated to be between 7.20 nm at δ = 40 and 6.17 nm at δ = 60.
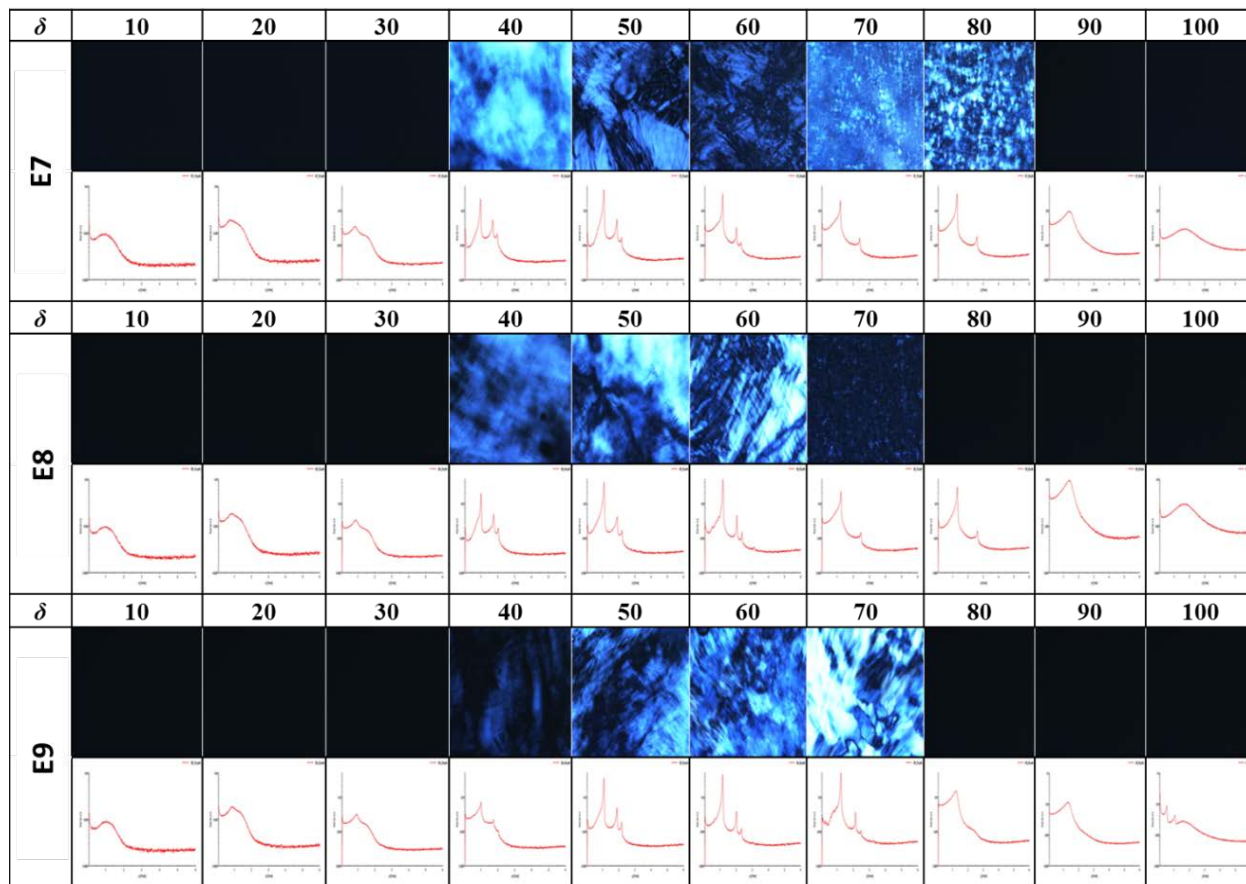
Figure S2: Screening of bulk phases for E7–E9. Upper rows: polarization-microscope pictures; lower rows: SAXS curves (log(intensity) vs. q)

L64 showed a H_I hexagonal phase at δ 55. Starting at δ 65 a weak lamellar phase ($L\alpha$) was formed and vanished above δ 80 .
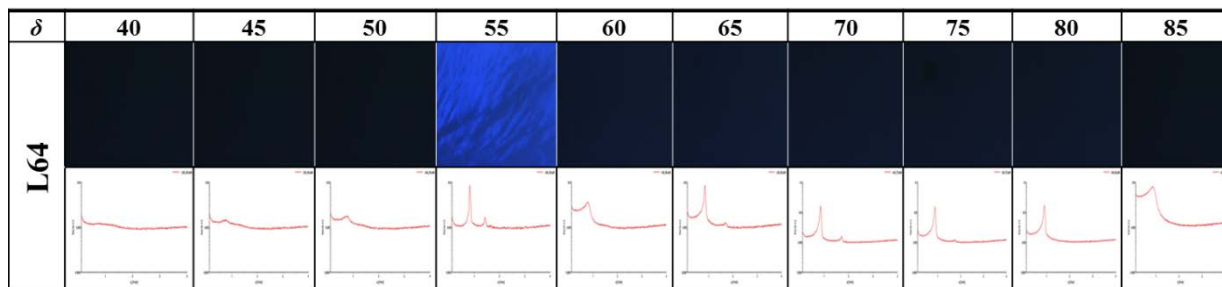
Figure S3: Screening of bulk phases for L64. Upper rows: Polarization-microscope pictures; lower rows: SAXS curves (log(Intensity) vs. q)
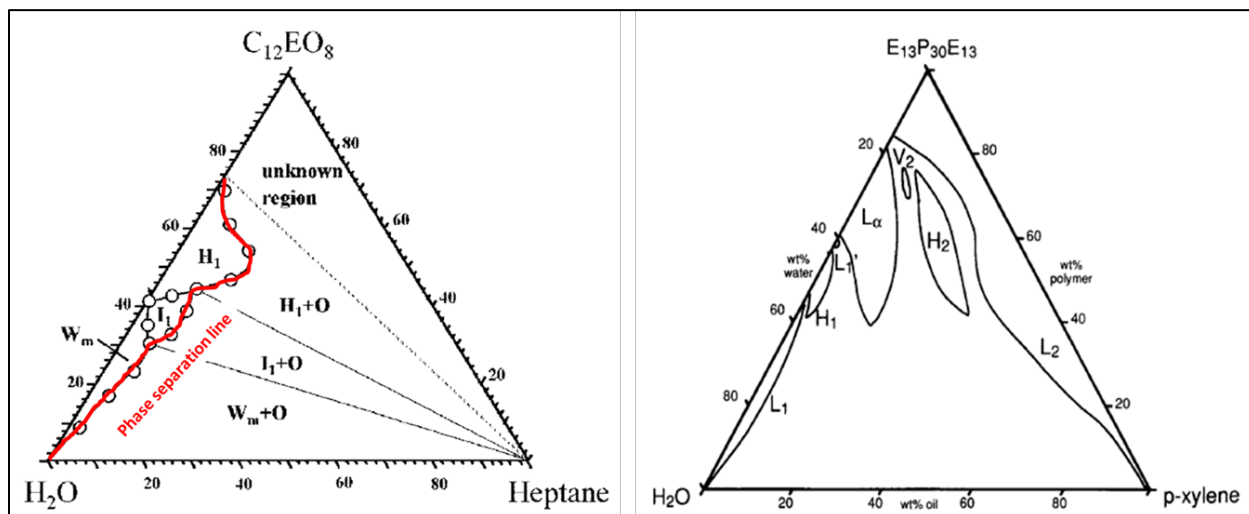
Figure S4: Phase diagrams. Left side: Brij $C_{12}EO_8$ (8 ethylene oxide units) adapted from Aramaki et al.[1] Right side: L64 from Alexandridis et al.[2]

1) Oil Loading
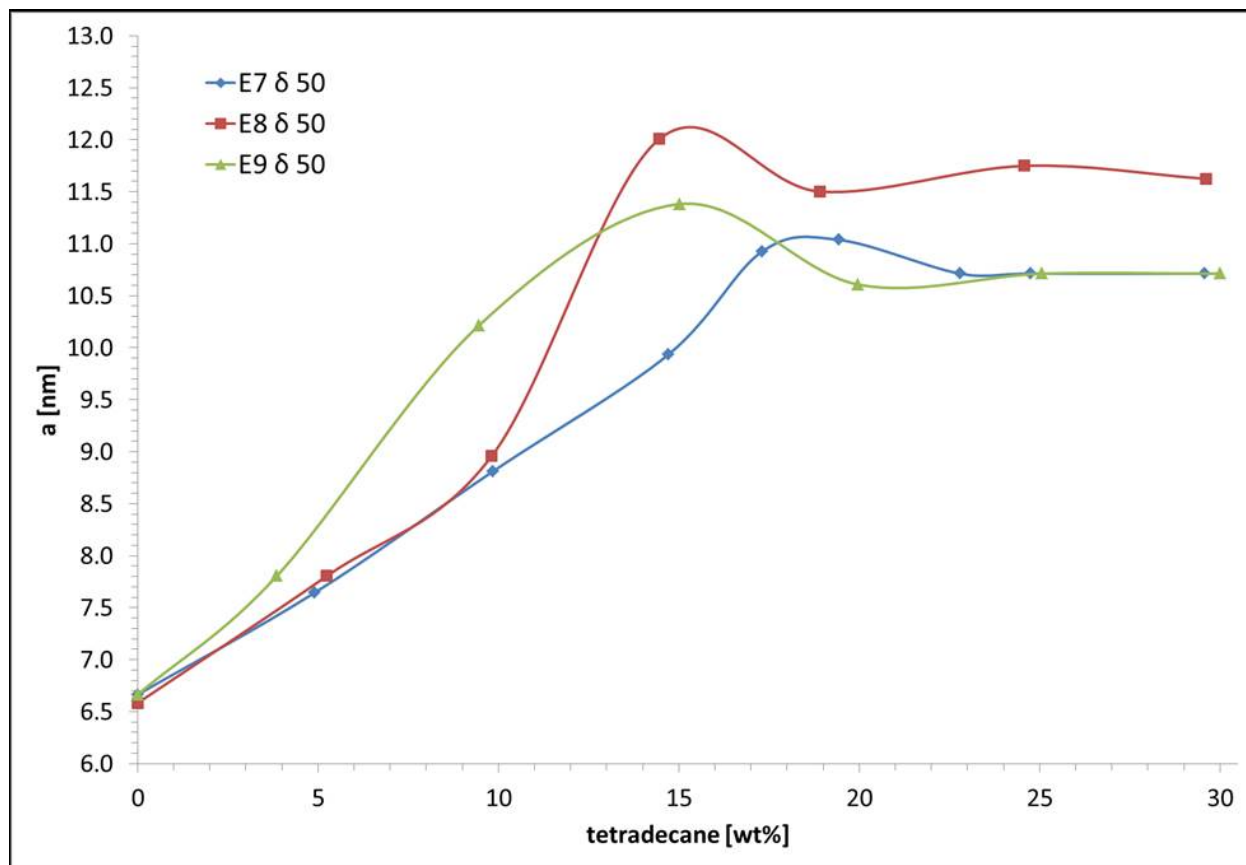
Figure S5: Oil-loading capacity of E7–E9: swelling of the lattice constant *a*.

Tetradecane was added successively to the bulk samples consisting of primary surfactant and water. At each step, the samples were heated to 80°C to melt the liquid crystal and to allow the oil to be incorporated. After accelerated cooling with an airgun during vortexing to ensure homogeneity, the samples were characterized with SAXS, and the lattice parameter *a* was estimated from the SAXS curves.

2) Monomer Synthesis
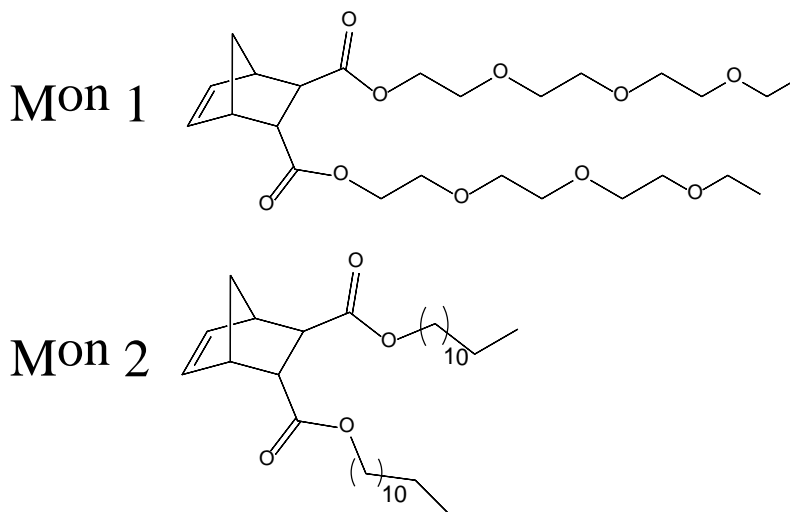
Figure S6: Monomeric units.

Mon1: Norbornene-2,3-di-carboxylic acid-di-2-(2-(2-ethoxyethoxy)ethoxy)ethylester, hydrophilic unit.

Mon2: Norbornene-2,3-di-carboxylic acid-di-dodecylester, lipophilic unit

Synthesis procedures and characterization

The reaction apparatuses were dried by heating, repeated evacuation and purging with N_2 gas. All reagents and solvents were purchased from commercial sources like Sigma Aldrich (Switzerland) or ABCR (Germany) and were used as received.

Complex M31 [1,3-bis (2,4,6-trimethylphenyl)-2-imidazolidinylidene]dichloro-(3-phenyl-1H-inden-1-ylidene) (pyridyl) ruthenium(II) was obtained from UMICORE AG Co.

^{1}H NMR spectroscopy was performed on a Bruker Avance 300 MHz spectrometer. Deuterated solvents (chloroform-d, DMSO-d[6], D_2O) were obtained from Cambridge Isotope Laboratories Inc. Remaining solvent peaks were referenced according to the literature[3]. Peak shapes are specified as follows: s (singlet), bs (broad singlet), d (doublet), dd (doublet of doublets),

t (triplet), q (quadruplet) and m (multiplet). Silica gel 60 F254 was used for thin layer chromatography (TLC), purchased from Merck. Bands were visualised under UV light or by dipping into an aqueous solution of $KMnO_4$ (0.1 wt%).

Synthesis of Norbornene-2,3-di-carboxylic acid-di-2-(2-ethoxyethoxy)ethoxyethylester (Mon1)

The synthesis was adapted from Sandholzer et al.[4] A 150 mL round bottom flask was filled with norbornene-2,3-di-carbonyl chloride (0.50 g, 2.30 mmol) and dichloromethane (10 mL; dry). To the mixture were added 2-(2-(2-ethoxyethoxy)ethoxy)ethanol (0.65 g, 4.82 mmol; predried by lyophilisation) and 4-(dimethylamino)-pyridine (0.01 g, 0.11 mmol) before the mixture was cooled in an ice bath. Pyridine (0.38 g, 4.82 mmol) was dissolved in dichloromethane (10 mL; dry) and added dropwise to the cooled mixture, after which the mixture was stirred for 24 h at room temperature. The reaction was monitored by TLC. Water (2 mL) was added to quench the remaining carbonyl chloride. The resulting white precipitate was filtered, and the reaction mixture was extracted with hydrochloric acid (3 x 10 mL; 2M) to remove the pyridine. The organic layer was dried with Na_2SO_4 and filtered. The solvent was removed *in vacuo*. The product was purified by column chromatography (SiO_2 / dichloromethane : acetone, 10 : 1) to afford a colorless oil in 46% yield. ^{1}H-NMR (δ, 20°C, $CDCl_3$, 300 MHz): 1.41–1.46 (d, $^3J_{HH}$ = 9.0 Hz, 1H, H_{nb7a}), 1.58–1.64 (d, $^3J_{HH}$ = 9.0 Hz, 1H, H_{nb7b}), 2.72–2.74 (m, 1H, H_{nb3}), 3.14 (bs, 1H, H_{nb4}), 3.28 (bs, 1H, H_{nb1}), 3.41–3.44 (t, $^3J_{HH}$ = 3.81 Hz ,1H, H_{nb2}), 3.48–3.73 (m, 12H, 2x -O-CH_2-CH_2-O-), 4.12–4.31 (m, 4H, 2x -OOC-CH_2-), 6. 04–6.09 (m, 1H, H_{nb6}), 6. 25–6.28 (m, 1H, H_{nb5}).

Synthesis of Norbornene-2,3-di-carboxylic acid-di-dodecylester (Mon2)

The procedure was analogous to the synthesis of monomer 1, but using norbornene-2,3-di-carbonylchloride (0.5 g, 2.30 mmol), and dodecan-1-ol (0.90 g, 4.82 mmol). The product was purified by column chromatography (SiO_2 / dichloromethane) to afford a colorless oil in 36% yield. ^{1}H-NMR (δ, 20°C, $CDCl_3$, 300 MHz): 6.27–6.06 (m, 2H, $H_{nb5,6}$), 4.09–4.02 (m, 4H, 2*[COO-CH_2-CH_2]), 3.37, 3.25, 3.11, 2.67 (t,s,s,d, 4H, H_{nb1-4}), 1.61 (m, 5H, 2*[COO-CH_2-CH_2],H_{nb7b}), 1.44 (m, 1H, H_{nb7a}), 1.26 (m, 36H, 2*[-CH_2-(CH_2)$_9$-CH_3]), 0.88 (m, 6H, 2*[-CH_2-CH_3])

ROM Polymerization

Diblock copolymer (DB)

Mon2 (0.20 g, 0.39 mmol) was dissolved in THF (5 mL; dry) in a 50 mL round bottom flask. A solution of M31 catalyst ($3.21*10^{-3}$ M) in THF (2 mL; dry) was prepared and added all at once. The reaction mixture was stirred at room temperature until TLC showed complete conversion. **Mon1** (0.05 g, 0.13 mmol) was dissolved in THF (2 mL; dry) and added to the reaction mixture, which was stirred until TLC showed full conversion. The reaction was quenched by addition of ethyl-vinylether (50 µL). After 30 min, the solvent was partially removed *in vacuo* and the product was precipitated three times in cold MeOH. The product was dried *in vacuo* to afford a highly viscose, slightly brown resin in ca. 90% yield, and was used without further purification. The slight coloration of the product was due to residual catalyst. ^{1}H-NMR (δ, 20°C, $CDCl_3$, 300 MHz): 5.59–5.15 (m, 2H, CH_2), 4.25–3.88 (m, 1H, H_{Cp4}, 4H, -COOCH_2-), 3.71–3.45 (m, 3H, -O-CH_2-CH_2-O), 3.29–2.84 (2x bs, 3H, H_{Cp1-3}), 1.95 (bs, 1H,

H_{Cp5a}), 1.66–1.39 (m, 1H, H_{Cp5b}, 4H, –COO-CH$_2$-CH$_2$), 1.36–1.00 (m,19H, -CH$_2$-), 1.21–1.13 (m, 1H, -CH$_3$), 0.90–0.84 (t, 3H, –CH$_3$)

Gel permeation chromatography showed a molecular weight of 37,315 g/mol (PDI: 1.18), which is in good agreement with the theoretic value of 39,418 g/mol. Differential scanning calorimetry showed no glass temperature T_g, but an apparent melting temperature T_m at 0°C[4].

Triblock copolymer (TB)

Mon2 (0.50 g, 0.96 mmol) was dissolved in dichloromethane (5 mL; dry) in a 50 mL round bottom flask. A solution of M31 catalyst (0.01 M) in dichloromethane (2 mL; dry) was prepared and added all at once. The reaction mixture was stirred at room temperature until TLC showed complete conversion. To the mixture was added a solution of **Mon1** (0.13 g, 0.32 mmol) in dichloromethane (2 mL; dry). The reaction mixture was stirred until TLC showed full conversion. This step was repeated with **Mon2** (0.50 g, 0.96 mmol). The reaction was quenched by addition of ethyl-vinylether (50 µL). After 30 min, the solvent was partially removed *in vacuo* and the product was precipitated three times in cold MeOH. The product was dried *in vacuo* to afford a highly viscose, slightly brown resin in ca. 80% yield, and was used without further purification. The slight coloration of the product was due to residual catalyst. ^{1}H-NMR (δ, 20°C, CDCl$_3$, 300 MHz): 5.59–5.15 (m, 2H, CH$_2$), 4.25–3.88 (m, 1H, H_{Cp4}, 4H, -COOCH$_2$-), 3.71–3.45 (m, 3H, -O-CH$_2$-CH$_2$-O-), 3.29–2.84 (2x bs, 3H, H_{Cp1-3}), 1.95 (bs, 1H, H_{Cp5a}), 1.66-1.39 (m, 1H, H_{Cp5b}, 4H, –COO-CH$_2$-CH$_2$-), 1.36–1.00 (m,29H, -CH$_2$-), 1.21–1.13 (m, 1H, -CH$_3$), 0.90–0.84 (t, 3H, –CH$_3$)

Gel permeation chromatography showed a molecular weight of 59,470 g/mol (PDI: 1.23). Differential scanning calorimetry showed no T_g, but an apparent melting temperature at -1.5 °C.

E7–Stabilizer Influence

The influence of stabilizers on the formation of the liquid crystal is shown for samples with a δ value of 50 (hexagonal crystal).
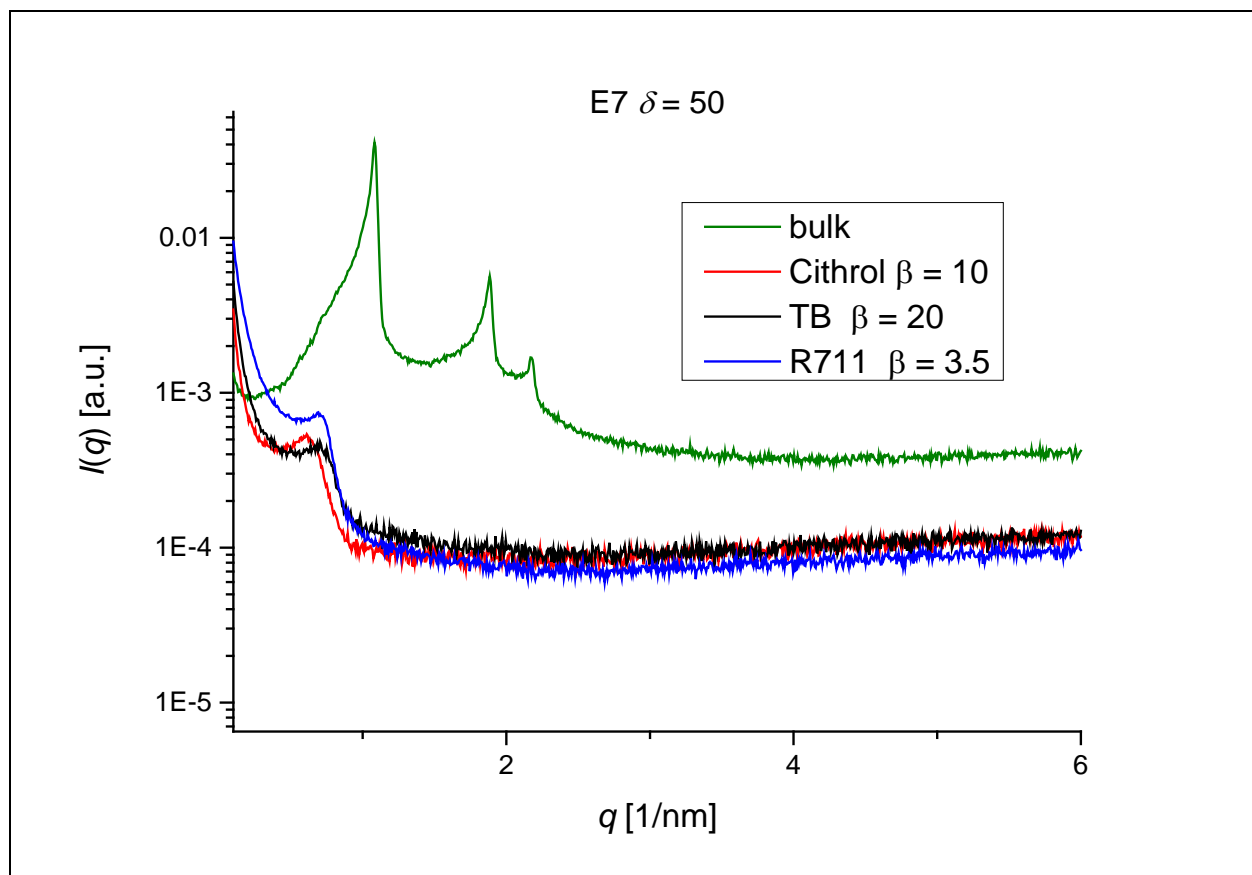
Figure S7: SAXS results for dispersions from E7 at $\delta = 50$, with different stabilizers

The bulk sample clearly shows the presence of the hexagonal crystal. The formation of a microemulsion in the dispersion instead of the expected hexagonal phase indicates an interaction between the primary surfactant and the stabilizers.
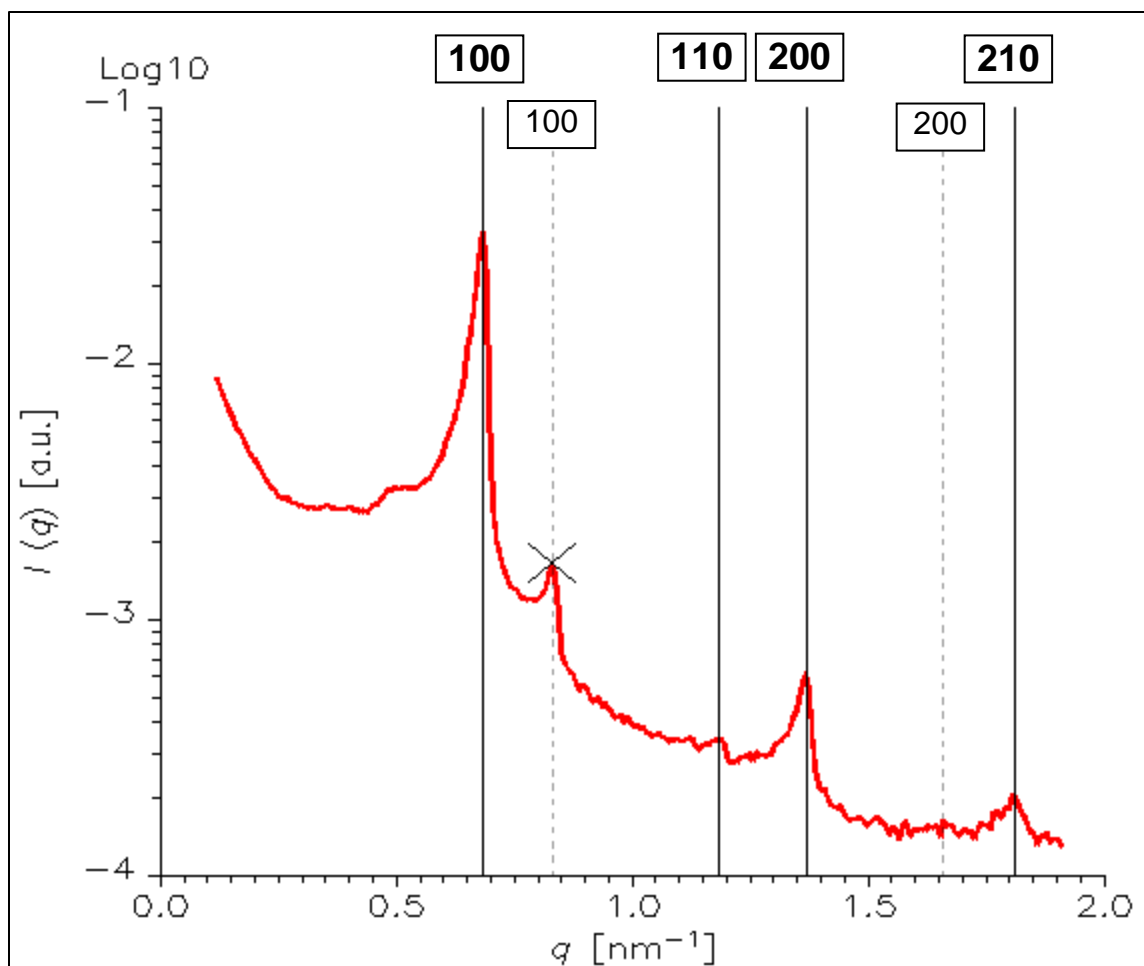
Figure S8: E7 δ = 60 stabilized with Aerosil R711 β = 2. The space group indexing shows the coexistence of the dominating H_I phase (full lines) with a weak lamellar phase ($L_α$, dotted line) See also Fig. S2, δ = 70.

Long-Term Stability Test of Water Stabilized in Tetradecane. The samples were prepared by dissolving the corresponding stabilizer in tetradecane, and adding water to this solution. The samples were ultrasonicated for 10 min. (0.2 ON / 2 OFF, 120 W). The samples were measured by using dynamic light scattering directly after preparation, and again after 1, 5, 10 and 20 days. Before the measurement, the otherwise turbid samples were diluted with tetradecane and hand-

shaken (no further ultrasonication was used). The R_H value was determined using the cumulant method.

Table S1: long-term stability test of water stabilized in tetradecane. Stabilizer concentration is 1 wt% for all samples. DB = diblock; TB = triblock; DPHS = (PEG-30) Dipolyhydroxystearate; X: large agglomerates

Stabilizer	R_H [nm]					Water Content
	0 days	1 day	5 days	10 days	20 days	
DB	122 ± 2	559 ± 10	155 ± 1	178 ± 1	239 ± 2	
TB	176 ± 1	176 ± 4	111 ± 1	132 ± 2	103 ± 3	**1 $^v/_v$ %**
DPHS	82 ± 0.2	121 ± 1	125 ± 3	129 ± 1	116 ± 1	
DB	422 ± 4	503 ± 4	1182 ± 14	1150 ± 13	X	
TB	384 ± 8	1324 ± 8	695 ± 7	397 ± 8	201 ± 6	**5 $^v/_v$ %**
DPHS	158 ± 1	222 ± 1	128 ± 1	227 ± 8	134 ± 2	
DB	508 ± 3	1632 ± 22	1583 ± 32	X	X	
TB	962 ± 5	1653 ± 37	628 ± 13	1568 ± 91	188 ± 4	**10 $^v/_v$ %**
DPHS	169 ± 1	159 ± 1	127 ± 1	145 ± 1	162 ± 4	

References

1.   Alam, M. M.; Aramaki, K., Hexagonal Phase Based Gel-Emulsion (O/H1 Gel-Emulsion): Formation and Rheology. Langmuir 2008, 24 (21), 12253–12259.

2.   Alexandridis, P.; Olsson, U.; Lindman, B., Self-Assembly of Amphiphilic Block Copolymers: The (EO)13(PO)30(EO)13-Water-p-Xylene System. Macromolecules 1995, 28, 7700-7710.

3.   Fulmer, G. R.; Miller, A. J. M.; Sherden, N. H.; Gottlieb, H. E.; Nudelman, A.; Stoltz, B. M.; Bercaw, J. E.; Goldberg, K. I., NMR chemical shifts of trace impurities: Common laboratory solvents, organics, and gases in deuterated solvents relevant to the organometallic chemist. Organometallics 2010, 29 (9), 2176-2179.

4.   Sandholzer, M.; Fritz-Popovski, G.; Slugovc, C., Synthesis and self assembly of eosin functionalized amphiphilic block-random copolymers prepared by ring opening metathesis polymerization. J. Polym. Sci. A 2008, 46, 401-413.

Chapter IV

Lipid Transfer in Oil-in-Water Isasome Emulsions: Influence of Arrested Dynamics of the Emulsion Droplets Entrapped in a Hydrogel

Iglesias, G. R., Pirolt, F., Sadeghpour, A., Tomšič, M. & Glatter, O., Langmuir 29, 15496–15502 (2013).

Lipid Transfer in Oil-in-Water Isasome Emulsions: Influence of Arrested Dynamics of the Emulsion Droplets Entrapped in a Hydrogel

Guillermo Ramón Iglesias,[‡] Franz Pirolt,[†] Amin Sadeghpour,[†] Matija Tomšič,[§] and Otto Glatter*,[†]

[†]Department of Chemistry, Karl-Franzens-University Graz, Heinrichstraße 28, 8010 Graz, Austria
[‡]Department of Applied Physics, School of Science University of Granada, 18071 Granada, Spain
[§]Faculty of Chemistry and Chemical Technology, University of Ljubljana, Aškerčeva cesta 5, 1000 Ljubljana, Slovenia

ABSTRACT: The transfer kinetics of lipids between internally self-assembled droplets of O/W emulsions is studied. The droplets (isasomes) consist of various liquid-crystalline phases or W/O microemulsions stabilized by a polymeric stabilizer F127. The various internal phases were identified by the relative peak positions in the small-angle X-ray scattering (SAXS) curves. An arrested system composed of isasomes embedded in a gel matrix actually provides an additional possibility to control these systems in terms of the release of various host molecules. These experiments have been applied to examine the kinetics of the internal phase reorganization imposed by the lipids' release and uptake by the droplets embedded in a κ-carrageenan (KC) hydrogel network. Increasing the concentration of the gelling agent slows down the transfer from one droplet to the other through the aqueous phase. We examined the region where the free diffusion is stopped. i.e., the point where the system changes from the ergodic to the nonergodic state and the kinetics is essentially slowed down. This effect can be balanced by the addition of small amounts of free polymeric stabilizer, which speeds up the kinetics. This is even possible in the case of highly arrested dynamics of the emulsion droplets, as found for the highest KC hydrogel concentrations forming nonergodic systems.
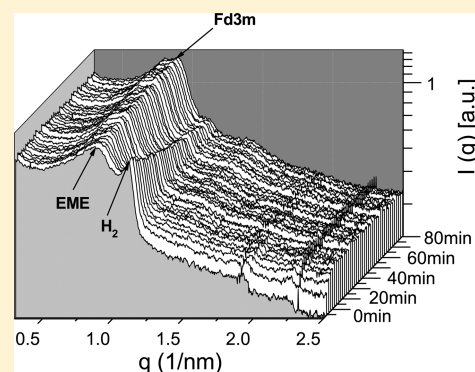
■ INTRODUCTION

Oil-in-water type emulsions with internally self-assembled lipid particles (mainly cubosomes and hexosomes),[1−5] also referred to as isasomes,[6] have aroused great interest in biotechnology, especially in the pharmaceutical, medical, cosmetics, food, and agricultural industries.[7−11] In particular, they have been studied as unique microenvironments for controlled release, for example, in drug delivery[12−17] to biological targets[4,18−31] and as nanocarriers.[32−35] Isasomes, like cubosomes, were developed in order to take advantage of the special features of liquid-crystalline phases but allowing for low-viscosity fluids.[36,37]

Isasomes are hierarchically organized colloidal systems, i.e., submicrometer-sized droplets, which are dispersed and kinetically stabilized as aqueous emulsions with self-assembled internal structures. These structures are either fluid isotropic water-in-oil (W/O) microemulsions (L_2 phase), or liquid-crystalline mesophases, including bicontinuous cubic, hexagonal, and discontinuous micellar cubic.[36−40]

Binary monoglyceride/water systems have rich phase diagrams, depending on their concentration and temperature,[41−45] including fluid isotropic (L_2), lamellar (L_α), inverted hexagonal (H_2), and reversed bicontinuous cubic phases (V_2). Larsson and co-workers have shown[36,37,46] that monoglycerides can be dispersed in water by using various dispersing agents, whereby submicrometer-sized droplets are formed.

We recently established that the internal structure of monolinolein-based droplets in aqueous dispersions stabilized with the triblock copolymer Pluronic F127 corresponds to the nondispersed bulk phase saturated with water.[38] This means that the internal structures formed are in thermodynamic equilibrium.

By adding increasing amounts of an oil, such as tetradecane, the internal structure changes at room temperature from bicontinuous cubic $Pn3m$ (cubosomes) to inverted hexagonal H_2 (hexosomes), and then to discontinuous micellar cubic $Fd3m$ (micellar cubosomes). Finally, as we have demonstrated, a W/O microemulsion phase (emulsified microemulsion, EME) can also be formed at room temperature. In these EME droplets, a W/O microemulsion phase is dispersed in a continuous water phase. Kinetically stabilized isasomes are stable against coalescence for months.[39]

However, when two isasome emulsions with different compositions (different amounts of oil) are mixed, they equilibrate due to the exchange of oil and monolinolein, as shown by Moitzi et al.[47] The transfer kinetics depend strongly on the length of the oil molecule (alkane) and only slightly on

the volume fraction of oil. Utilizing small-angle X-ray scattering (SAXS) and dynamic light scattering, we showed that isasomes can be entrapped in the aqueous κ-carrageenan (KC) system, which is a gel up to room temperature and a sol at higher temperature.[48] The viscosity of the gel, and therefore the strength of entrapment of the isasomes, can be controlled by changing the amount of gelling agent. This idea has also been extended to high-temperature gels formed by methylcellulose and mixed gels (KC + methylcellulose), which are stable in a wide temperature regime.[8] It has also been shown that the isasomes are not destroyed by this entrapment, even when the gels are dried to films.[49] In a recent study based on dynamic light scattering, we showed that the diffusion dynamics of the isasomes can be arrested as a function of the concentration of the gelling agent KC.[50]

The working hypothesis of this work was the following: if the process of compositional ripening is controlled only by the water solubility of the lipid components, the transfer kinetics should not depend on the diffusivity of the isasome droplets. Otherwise, a slowdown with arrested motion would give evidence for the importance of close approach of the isasomes during the diffusion process. Second, if free surfactant micelles promote the exchange of lipids, the effect of the arrested motion of the isasomes might, at least partially, be balanced by the effect of micellar transport.

■ MATERIALS AND METHODS

Sample Preparation. Isasomes were prepared by using mono-linolein Dimodan-U/J (DU) as the structure-forming lipid component, tetradecane as the oil component, and Pluronic F127 as an emulsion stabilizer. DU was a gift from Danisco (Brabrand, Denmark). This material is a distilled monoglyceride mixture (mostly C_{18} chains) comprising 96% monoglycerides with 62% linoleate and 25% oleate; the rest are diglycerides and free fatty acids. Tetradecane (n-$C_{14}H_{30}$) and octadecane (n-$C_{18}H_{38}$) were purchased from Sigma-Aldrich (Germany). κ-Carrageenan (KC) was purchased from Fluka.

By changing the mass ratio of DU in the oil phase of the system, which is quantified by the mass fraction of the structure-forming lipid (δ), it was possible to tune the internal structure of the droplets.

$$\delta = \frac{m_{\text{DU}}}{m_{\text{DU}} + m_{\text{TC}}} \times 100 \tag{1}$$

Here m_{DU} and m_{TC} are the masses of lipid (dimodan-U/J, DU) and oil (tetradecane, TC), respectively.

The value of δ (eq 1) can be varied from 100% down to 50% to obtain nanostructures of bicontinuous-cubic ($Pn3m$),[51] hexagonal (H_2),[51] micellar-cubic ($Fd3m$),[40] and fluid-isotropic (L_2).

The triblock copolymer PEO$_{99}$−PPO$_{67}$−PEO$_{99}$ (F127) was a gift from BASF SE (Florham Park, NJ). All chemicals were used without further purification. Water was purified by using a Millipore system (Millipore).

Isasome samples (monoglyceride, water, oil, and stabilizer) were mixed together and subjected to ultrasonication with a Vibra-Cell sonicator (SY-LAB GmbH, Pukersdorf, Austria) for 10 min (0.5 s pulses with 1.5 s delays) at 30% of the maximum power.

The mass ratio of the emulsion stabilizer and amphiphilic/hydrophobic components, β, was kept constant at 9% for all samples and is given by

$$\beta = \frac{m_{\text{F127}}}{m_{\text{DU}} + m_{\text{TC}}} \times 100 \tag{2}$$

The mass fraction of the dispersed phase Φ is

$$\Phi = \frac{m_{\text{F127}} + m_{\text{DU}} + m_{\text{TC}}}{m_{\text{F127}} + m_{\text{DU}} + m_{\text{TC}} + m_{\text{water}}} \times 100 \tag{3}$$

The preparation of isasomes with a specific internal nanostructure was based on the published phase diagram of isasomes in water prepared from DU, tetradecane, and F127.[52] All isasomes discussed in this paper were made from the DU−tetradecane system.

The isasome samples contained 10% of the dispersed phase (Φ = 10) and were prepared with three values of δ corresponding to three types of internal structure at room temperature: isasomes with reverse hexagonal H_2 phase at δ = 84% (hexosomes), isasomes with discontinuous cubic structure $Fd3m$ at δ = 70.5% (micellar cubosomes), and isasomes with emulsified liquid isotropic L_2 microemulsion phase at δ = 57% (emulsified microemulsions).

The medium used for entrapping the emulsion droplets was the gelling polymer KC dissolved in water at high temperature (>60 °C). Aqueous solutions of KC are known to undergo reversible sol/gel transitions with decreasing temperature at around 30 °C.[8] The isasome solutions were mixed at a volume ratio of 1:1 at 60 °C with varying KC concentration so that the final sample measured had a constant mass fraction of 5% isasomes and a KC concentration between 0 and 1%.

To study the influence of adding F127 to the emulsion after the isasomes are formed and entrapped by the gel, we also prepared samples with additional F127 in the KC solution in order to obtain a final concentration of free F127 between 0.1 and 1% dissolved in the aqueous phase.

The transfer was started by mixing the isasome (H_2 and EME)/gel samples at 55 °C. Immediately after mixing, the sample was transferred to the X-ray capillary of 1 mm diameter, which was then rapidly cooled in an ice−water bath for 5 min to initiate gelation, then equilibrated for 1 min in a water bath (25 °C), and finally transferred to the X-ray camera, with the sample holder thermostated at 25 °C. The delay between mixing (start of the transfer) and the start of the measurements was 600 s (10 min). Typical exposure times were 2 min.

Sample preparation sequence can be summarized as follows: for the production of isasomes all components (DU and tetradecane, F 127, and 90% water) are simply mixed in arbitrary sequence before sonication. The hydrogel is prepared from KC dissolved in water at temperatures above 60 °C, in special cases with extra F 127 added. Then the isasome emulsions were mixed 1:1 with the hydrogel at 55 °C, and this mixture was filled immediately into the SAXS capillary.

Small-Angle X-ray Scattering (SAXS). The internal structures of the sols and gels were studied by using SAXS. The SAXS equipment comprises a SAXSess camera with high flux and low background (Anton-Paar, Graz, Austria) connected to an X-ray generator (Philips, PW 3830/40) operated at 40 kV and 50 mA with a sealed-tube Cu anode. A Göbel mirror is used to convert the divergent polychromatic X-ray beam into a focused line-shaped beam of Cu Kα radiation (wavelength λ = 0.154 nm). The 2D scattering pattern is recorded by a PI-SCX fused fiber-optic taper CCD camera (Princeton Instruments) and integrated into the one-dimensional scattering function $I(q)$, where q is the magnitude of the scattering vector defined as $q = (4\pi/\lambda)\sin(\theta/2)$, with θ being the scattering angle. The CCD detector featured a 2084 × 2084 array with a 24 × 24 μm^2 pixel size (chip size: 50 × 50 mm^2). The temperature of the capillary and the metallic sample holder are controlled by a Peltier element.

Hexagonal and cubic structures were fully determined by the relative positions of the scattering peaks displayed in the intensity spectra. These Bragg peaks correspond to the reflections from a family of planes {hkl} (Miller indices). The distance between two parallel planes of the same family is given by $d_{hkl} = 2\pi/q_{hkl}$, which allows the determination of the mean lattice parameter a of the ordered structure. The L_2 phase, and especially its emulsified state EME, is described by a characteristic distance $d = 2\pi/q_0$ deduced from the maximum intensity of the broad correlation peak at the position q_0.[39]

■ RESULTS AND DISCUSSION

In order to verify whether the internal structure of isasomes is preserved when entrapped in a KC polymer network, we have performed SAXS experiments of the mixed gels isasomes/κ-carrageenan. Figure 1 shows the experimental SAXS results for samples containing only one type of isasome: δ = 84,
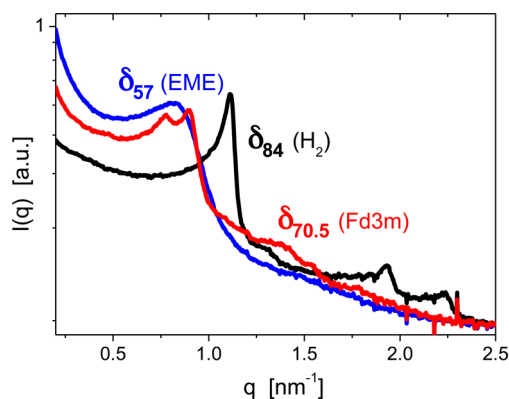
Figure 1. SAXS measurements of $\delta = 84$, hexosomes; $\delta = 70.5$, discontinuous micellar cubosomes; and $\delta = 57$, EME embedded in a 1% w/w KC hydrogel. The peak indices of the different structures can be found in Figure 1 of ref 40. The data acquisition time for these experiments was 900 s.

hexosomes; $\delta = 57$, EME; and $\delta = 70.5$ (mixed composition), discontinuous micellar cubosomes. These results show clearly that the internal structure of the isasomes is not influenced by embedding them in the hydrogel.

We will now focus on the question how the kinetics of the transfer process between the isasomes is influenced by the hydrogel. The time-resolved SAXS experiment of the sample with the mixture ($\delta_{84} + \delta_{57}$) without KC is shown as a reference in Figure 2. The theoretical end point of the transfer is in the
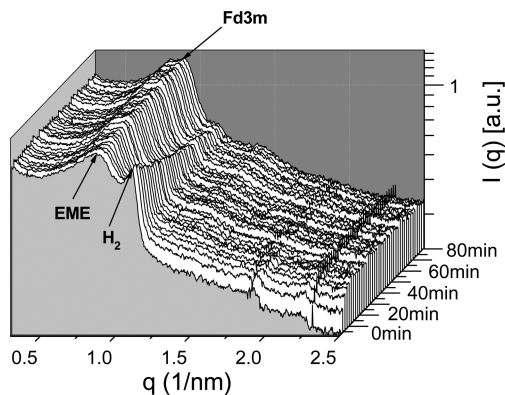
Figure 2. Transfer kinetics by time-resolved SAXS of a mixture of hexosomes (δ_{84}) with an emulsified microemulsion (δ_{57}) in water. Spectra were recorded for a duration of 2 min each. The hexagonal main peak (H_2) decreases in height, and the broad *EME* peak begins to split into two as the micellar cubosomes (*Fd3m*) are formed.

regime of discontinuous micellar cubosomes ($\delta_{70.5}$). We can clearly see that shortly after mixing, two types of droplet are present (broad correlation peak of the EME and the first peak of the hexagonal phase H_2 at $q \approx 1.2$ nm^{-1}). The first measurement of the mixture is nearly the same as the average of the two dispersions measured separately before mixing; just the noise level is higher due to the shorter measurement time. With time, the hexagonal peak decreases in height and the broad peak of the EME starts to split into two as the micellar cubosomes are formed. At the end of the experiment, the scattering of the mixture is nearly the same as that of the sample that was prepared with $\delta_{70.5}$. Only the absolute value of the scattering intensity is slightly lower, which is caused by partial creaming of the droplets.[47] In this study, data evaluation

was conducted by means of pattern recognition of the different phases. For the sample without KC, the hexagonal peak disappears after about 2 h (data in Figure 2 only shown up to 80 min), while the typical double peak for the micellar cubic phase constantly builds up during this time (transformation from hexosomes and EME to discontinuous micellar cubosomes). For a numerical analysis, see the second part of this section.

In Figure 3, the time-resolved scattering experiments of the mixture of two samples ($\delta_{84} + \delta_{57}$) embedded in the hydrogel
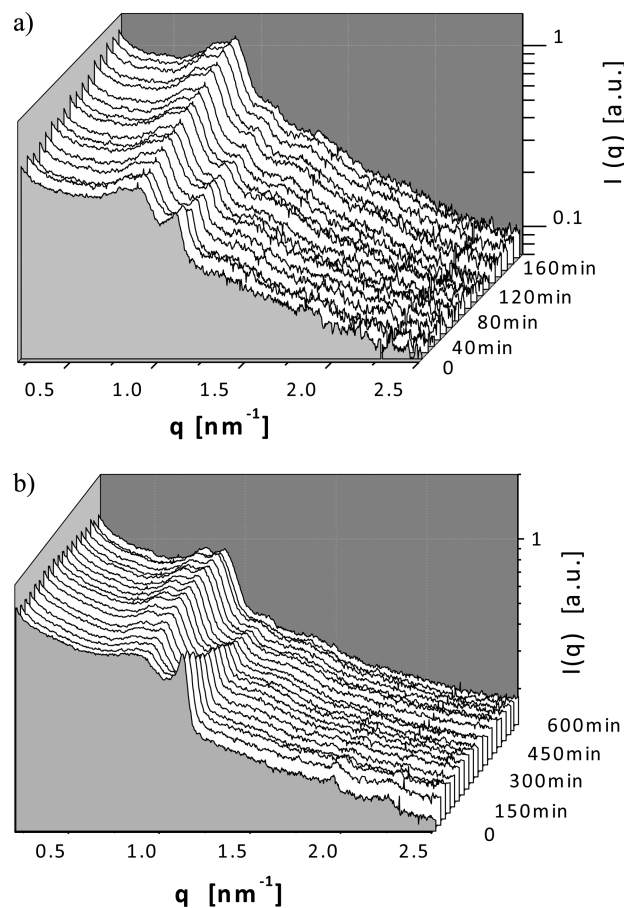
Figure 3. Transfer kinetics by time-resolved SAXS of a mixture of hexosomes (δ_{84}) with an emulsified microemulsion (δ_{57}) embedded in a KC hydrogel: (a) 0.80% KC; (b) 1% KC. As for Figure 2, spectra were recorded for 2 min each, but for clarity only every 5th curve (a) or every 15th curve (b) is shown in the graph.

are shown for two different concentrations of KC, i.e., 0.80% w/w KC and 1% w/w KC. In the case of a hydrogel with 0.80% w/w KC, the transfer is finished after about 3 h, and this increases to approximately 6 h for the 1% w/w KC gel; i.e., transfer time increases strongly with KC concentration. This difference in transfer rate is also visible from the first curves in Figure 3a,b, Figure 3a showing that the *EME* signal is already mixed with the *Fd*3m signature and the H_2 peak is much lower than in Figure 3b, where the *EME* and H_2 signals are clearly seen.

Let us now look at the kinetics of the transfer process in the 1% KC sample but now influenced by the addition of extra F127 (not used for the formation of the emulsions!). Figure 4 shows only two examples of the time-resolved SAXS measurements for 1% KC with 0.1% w/w and 0.25% w/w F127 added

a)

b)
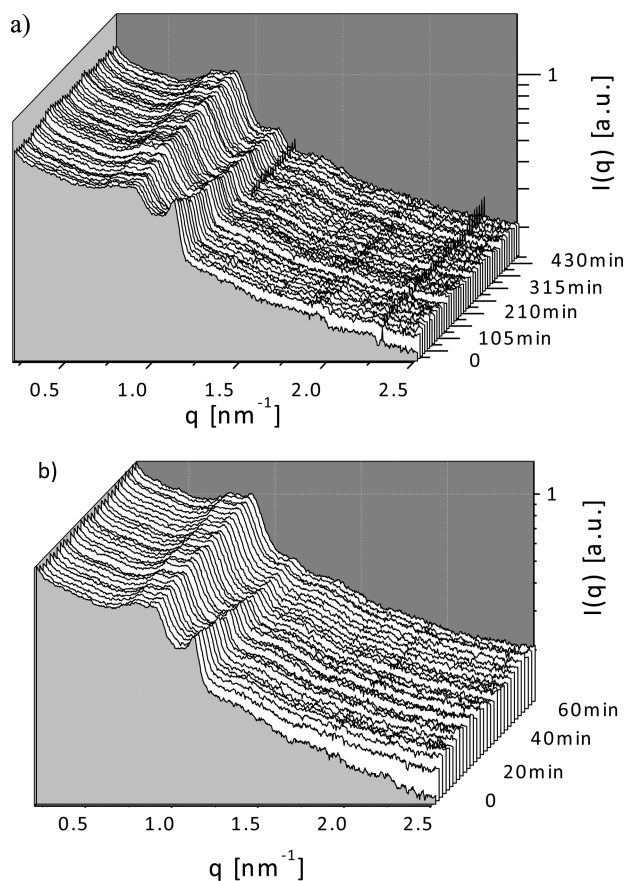
Figure 4. Transfer kinetics by time-resolved SAXS measurements of a mixture of hexosomes (δ_{84}) with an emulsified microemulsion (δ_{57}) embedded in a 1% KC solution with extra F127 added: (a) 0.1% F127 and (b) 0.25% F127. As for Figure 3, spectra were recorded every 2 min, but for clarity only every fifth curve in (a) is shown in the graph.

a)

b)

Figure 5. (a) Fraction X of the hexagonal phase (H_2) for different KC content as a function of time after mixing of $\delta_{84} + \delta_{57}$. The decay of the hexagonal phase was fitted with a single-exponential decay. (b) Decay time $T = 3\tau = 3/k$ as a function of KC concentration.

Table 1. Decay Rates k and Decay Times T, As Determined from the Data Shown in Figure 5

KC [%]	k [1/s]	T [h]
0.00	5.42 ± 0.24	1.54
0.50	4.61 ± 0.10	1.81
0.60	4.01 ± 0.08	2.08
0.70	3.39 ± 0.03	2.46
0.80	2.42 ± 0.05	3.45
1.00	1.25 ± 0.02	6.67

(data for 0.15% and 0.20% not shown). The decay of the hexagonal structure δ_{84} becomes faster with increasing F127 concentration.

For 0.5% F127 or more, the transfer is too fast to be detectable under our experimental conditions (data not shown). With these experimental data sets, we have examined the various phases following the same analysis of the transfer kinetics as performed by Moitzi et al.[47] This procedure enables one to determine the concentration of the different phases from the time-resolved SAXS measurements by using a function that decays exponentially with time e^{-kt}, where k [s^{-1}] is the decay rate. In this analysis, we focus only on the hexagonal δ_{84} phase, which starts at a fraction of approximately 50%, as the sample at mixing time ($t = 0$) is a mixture of both droplet types ($\delta_{84} + \delta_{57}$).

Figure 5a shows the fractions of the hexagonal phase [X] as a function of time after mixing. The decay was fitted for all concentrations with a single-exponential decay. The whole relaxation process is well described by these single-exponential fits. The decay rates determined from Figure 5 are shown in Table 1. One can also calculate the time needed for the signal to drop below 5% of its maximum amplitude ($t_{0.05}$), which is simply triple the value of the decay time $\tau = 1/k$ ($T = 3\tau$). These values are given in the third column of Table 1.

We did the same analysis for the data shown in Figure 4 with extra F127 added. The kinetic results are plotted in Figure 6a for a complete series of 0.1, 0.15, 0.2, and 0.25% extra F127 and

without extra F127 for comparison. The corresponding decay rates and times are shown in Table 2.

Clearly, the addition of 0.25% F127 is enough to accelerate the transfer by a factor of 3. The decay times are plotted in Figure 6b.

Effect of the Gelling Agent. The decay times increase nearly linearly and only moderately with concentration up to about 0.7% KC. At higher concentrations, we find a much stronger increase; i.e., the decay time only doubles between 0 and 0.7%, while it triples in the short interval from 0.7 to 1.0%. This rapid rise can be explained by the dramatic change in the diffusion behavior in this regime.[50] Up to 0.65% KC, the system is still ergodic; i.e., the droplets diffuse more slowly but do not show an arrested state. Such an arrested state was found at KC concentrations $\geq 0.7\%$. Even after an experimental time of several hours, the correlation function is still close to one and
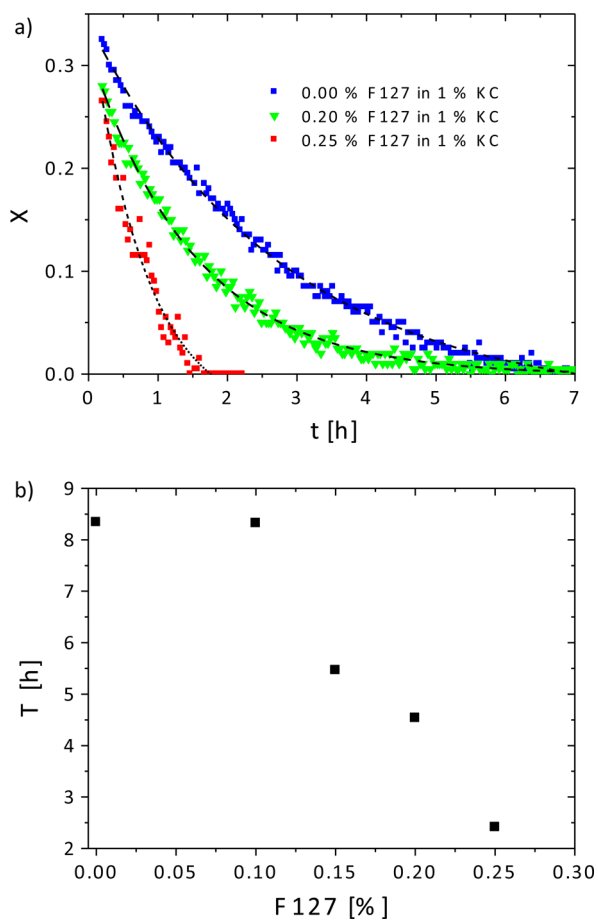
Figure 6. (a) Fraction X of the hexagonal phase H_2 at a fixed concentration of KC (1%) and increasing additional amounts of F127 as a function of time after mixing of $\delta_{84} + \delta_{57}$. The decay of the hexagonal phase was fitted to a single-exponential decay. The amount of additional F127 was 0.1%, 0.15%, 0.20%, 0.25%, and 0%. (b) The decay time $T = 3\tau = 3/k$ as a function of concentration of extra added F127.

Table 2. Decay Rates k and Decay Times T Determined from the Data Shown in Figure 6

F127 [%]	k [1/s]	T [h]
0.00	0.999 ± 0.01	8.34
0.10	1.001 ± 0.01	8.32
0.15	1.52 ± 0.01	5.46
0.20	1.84 ± 0.02	4.53
0.25	3.45 ± 0.34	2.42

has not started to relax to zero. This means that at least over several hours the system is "frozen" or, in other words, the emulsion droplets cannot diffuse through the KC network. The corresponding strong increase in decay times of the transfer experiments shown here can therefore be understood in the way that free diffusion and temporary contact of droplets is an important parameter controlling the transfer kinetics.

Effect of Additional F127. We have previously shown that the transfer rate is accelerated linearly by the addition of extra F127 to the KC-free system.[47] Here, we studied the influence of extra F127 on the system containing 1% KC, i.e., to the more or less arrested droplet system. Above 0.1% additional F127, the decay or transfer time decreases linearly with added polymeric surfactant. With 0.25% additional F127, the slowing down

effect of the hydrogel is completely balanced. Note that the total concentration of free F127 in the aqueous phase is not known because, on the one hand, not all the F127 molecules may be used up in the emulsification process and, on the other hand, some F127 may be adsorbed to the KC network. In this context it would also be interesting to know the interaction of added free surfactant with the KC network. However, such an interaction and/or aggregation cannot be easily detected in such mixed systems. From DLS experiments (data not shown here) we know that even at high KC concentrations (2%) one can still see the micellar diffusion decay, even though somewhat slowed down. The existence of free micelles is also detectable from the strong influence on the transfer rates as shown in Figure 6 for rather low added F127 concentrations. Higher amounts of F127 might necessitate the use of synchrotron radiation, but also there the detection limit for the first experiment was in the order of 30 s.[53]

CONCLUSION

In this study, we used nanostructured emulsions of various compositions to follow the transfer of lipophilic molecules between the emulsion droplets. This process can be followed by time-resolved SAXS experiments as the changing composition leads to structural changes on the nanoscale. Previous results[5,47] promoted the picture that the lipophilic molecules are transferred from one droplet to the other through the aqueous phase. Because of the low concentration dependence, it was not clear whether droplet collisions were important for the transfer process.

From the results in this contribution, we can now conclude that the hindered diffusion of the droplets due to the hydrogel, as deduced from dynamic light scattering experiments,[50] slows down the transfer with increasing concentration of the gelling agent. This effect can be balanced by the addition of relatively small amounts of free surfactant. Clearly, these free micelles act as a shuttle, promoting the transfer even in the case of highly arrested dynamics of the emulsion droplets as found at KC concentrations of about 1%.

It would be extremely interesting to complement these results with surfactant-free Pickering emulsions. Such a system would not have any free micelles that could promote the transfer, so slower transfer rates could be expected. Such studies are currently underway in our research team.

AUTHOR INFORMATION

Corresponding Author
*E-mail otto.glatter@uni-graz.at.

Notes
The authors declare no competing financial interest.

REFERENCES

(1) Hyde, S. T. Bicontinuous structures in lyotropic liquid crystals and crystalline hyperbolic surfaces. *Curr. Opin. Solid State Mater. Sci.* **1996**, *1*, 653−662.

(2) Seddon, J. M. Surfactant liquid crystals. *Curr. Opin. Colloid Interface Sci.* **2001**, *6*, 242−243.

(3) Squires, A. M.; Templer, R. H.; Seddon, J. M.; Woenckhaus, J.; Winter, R.; Finet, S.; Theyencheri, N. Kinetics and mechanism of the lamellar to gyroid inverse bicontinuous cubic phase transition. *Langmuir* **2002**, *18*, 7384–7392.

(4) Larsson, K. Cubic lipid-water phases: structures and biomembrane aspects. *J. Phys. Chem.* **1989**, *93*, 7304–7314.

(5) Luzzati, V.; Vargas, R.; Mariani, P.; Gulik, A.; Delacroix, H. Cubic phases of lipid-containing systems: Elements of a theory and biological connotations. *J. Mol. Biol.* **1993**, *229*, 540–551.

(6) Salonen, A.; Moitzi, C.; Salentinig, S.; Glatter, O. Material transfer in cubosome-emulsion mixtures: Effect of alkane chain length. *Langmuir* **2010**, *26*, 10670–10676.

(7) Mezzenga, R.; Schurtenberger, P.; Burbidge, A.; Michel, M. Understanding foods as soft materials. *Nat. Mater.* **2005**, *4*, 729–740.

(8) Tomsic, M.; Guillot, S.; Sagalowicz, L.; Leser, M. E.; Glatter, O. Internally self-assembled thermoreversible gelling emulsions: Isasomes in methylcellulose, kappa-carrageenan, and mixed hydrogels. *Langmuir* **2009**, *25*, 9525–9534.

(9) Salentinig, S.; Sagalowicz, L.; Glatter, O. Self-assembled structures and pK$_a$ value of oleic acid in systems of biological relevance. *Langmuir* **2010**, *26*, 11670–11679.

(10) Ubbink, J.; Burbidge, A.; Mezzenga, R. Food structure and functionality: a soft matter perspective. *Soft Matter* **2008**, *4*, 1569–1581.

(11) Sagalowicz, L.; Mezzenga, R.; Leser, M. E. Investigating reversed liquid crystalline mesophases. *Curr. Opin. Colloid Interface Sci.* **2006**, *11*, 224–229.

(12) Sagalowicz, L.; Leser, M. E.; Watzke, H. J.; Michel, M. Monoglyceride self-assembly structures as delivery vehicles. *Trends Food Sci. Technol.* **2006**, *17*, 204–214.

(13) Yaghmur, A.; Glatter, O. Characterization and potential applications of nanostructured aqueous dispersions. *Adv. Colloid Interface Sci.* **2009**, *147–48*, 333–342.

(14) Hirlekar, R.; Jain, S.; Patel, M.; Garse, H.; Kadam, V. Hexosomes: A novel drug delivery system. *Curr. Drug Delivery* **2010**, *7*, 28–35.

(15) Nguyen, T.-H.; Hanley, T.; Porter, C. J. H.; Larson, I.; Boyd, B. J. Phytantriol and glyceryl monooleate cubic liquid crystalline phases as sustained-release oral drug delivery systems for poorly water soluble drugs I. Phase behaviour in physiologically-relevant media. *J. Pharm. Pharmacol.* **2010**, *62*, 844–855.

(16) Seyfoddin, A.; Shaw, J.; Al-Kassas, R. Solid lipid nanoparticles for ocular drug delivery. *Drug Delivery* **2010**, *17*, 467–489.

(17) Garg, G.; Saraf, S.; Saraf, S. Cubosomes: An overview. *Biol. Pharm. Bull.* **2007**, *30*, 350–353.

(18) Pouton, C. W. Formulation of self-emulsifying drug delivery systems. *Adv. Drug Delivery Rev.* **1997**, *25*, 47–58.

(19) Boyd, B. J. Characterisation of drug release from cubosomes using the pressure ultrafiltration method. *Int. J. Pharm.* **2003**, *260*, 239–247.

(20) Engstrom, S.; Norden, T. P.; Nyquist, H. Cubic phases for studies of drug partition into lipid bilayers. *Eur. J. Pharm. Sci.* **1999**, *8*, 243–254.

(21) Drummond, C. J.; Fong, C. Surfactant self-assembly objects as novel drug delivery vehicles. *Curr. Opin. Colloid Interface Sci.* **1999**, *4*, 449–456.

(22) Leslie, S. B.; Puvvada, S.; Ratna, B. R.; Rudolph, A. S. Encapsulation of hemoglobin in a bicontinuous cubic phase lipid. *Biochim. Biophys. Acta, Biomembr.* **1996**, *1285*, 246–254.

(23) Clogston, J.; Caffrey, M. Controlling release from the lipidic cubic phase. Amino acids, peptides, proteins and nucleic acids. *J. Controlled Release* **2005**, *107*, 97–111.

(24) Shah, J. C.; Sadhale, Y.; Chilukuri, D. M. Cubic phase gels as drug delivery systems. *Adv. Drug Delivery Rev.* **2001**, *47*, 229–250.

(25) Boyd, B. J.; Whittaker, D. V.; Khoo, S. M.; Davey, G. Lyotropic liquid crystalline phases formed from glycerate surfactants as sustained release drug delivery systems. *Int. J. Pharm.* **2006**, *309*, 218–226.

(26) Boyd, B. J.; Whittaker, D. V.; Khoo, S.-M.; Davey, G. Hexosomes formed from glycerate surfactants - Formulation as a colloidal carrier for irinotecan. *Int. J. Pharm.* **2006**, *318*, 154–162.

(27) Baciu, M.; Sebai, S. C.; Ces, O.; Mulet, X.; Clarke, J. A.; Shearman, G. C.; Law, R. V.; Templer, R. H.; Plisson, C.; Parker, C. A.; Gee, A. Degradative transport of cationic amphiphilic drugs across phospholipid bilayers. *Philos. Trans. R. Soc., A* **2006**, *364*, 2597–2614.

(28) Angelova, A.; Angelov, B.; Mutafchieva, R.; Lesieur, S.; Couvreur, P. Self-assembled multicompartment liquid crystalline lipid carriers for protein, peptide, and nucleic acid drug delivery. *Acc. Chem. Res.* **2011**, *44*, 147–156.

(29) Han, S.; Shen, J.-q.; Gan, Y.; Geng, H.-m.; Zhang, X.-x.; Zhu, C.-l.; Gan, L. Novel vehicle based on cubosomes for ophthalmic delivery of flurbiprofen with low irritancy and high bioavailability. *Acta Pharmacol. Sin.* **2010**, *31*, 990–998.

(30) Malmsten, M. Phase transformations in self-assembly systems for drug delivery applications. *J. Dispersion Sci. Technol.* **2007**, *28*, 63–72.

(31) Zhao, X. Y.; Zhang, J.; Zheng, L. Q.; Li, D. H. Studies of cubosomes as a sustained drug delivery system. *J. Dispersion Sci. Technol.* **2004**, *25*, 795–799.

(32) Angelov, B.; Angelova, A.; Mutafchieva, R.; Lesieur, S.; Vainio, U.; Garamus, V. M.; Jensen, G. V.; Pedersen, J. S. SAXS investigation of a cubic to a sponge (L-3) phase transition in self-assembled lipid nanocarriers. *Phys. Chem. Chem. Phys.* **2011**, *13*, 3073–3081.

(33) Angelov, B.; Angeova, A.; Papahadjopoulos-Sternberg, B.; Hoffmann, S. V.; Nicolas, V.; Lesieur, S. Protein-containing PEGylated cubosomic particles: Freeze-fracture electron microscopy and synchrotron radiation circular dichroism study. *J. Phys. Chem. B* **2012**, *116*, 7676–7686.

(34) Angelova, A.; Angelov, B.; Garamus, V. M.; Couvreur, P.; Lesieur, S. Small-angle X-ray scattering investigations of biomolecular confinement, loading, and release from liquid-crystalline nanochannel assemblies. *J. Phys. Chem. Lett.* **2012**, *3*, 445–457.

(35) Angelova, A.; Angelov, B.; Drechsler, M.; Garamus, V. M.; Lesieur, S. Protein entrapment in PEGylated lipid nanoparticles. *Int. J. Pharm.* **2013**, *454*, 625–632.

(36) Gustafsson, J.; LjusbergWahren, H.; Almgren, M.; Larsson, K. Cubic lipid-water phase dispersed into submicron particles. *Langmuir* **1996**, *12*, 4611–4613.

(37) Gustafsson, J.; Ljusberg-Wahren, H.; Almgren, M.; Larsson, K. Submicron particles of reversed lipid phases in water stabilized by a nonionic amphiphilic polymer. *Langmuir* **1997**, *13*, 6964–6971.

(38) de Campo, L.; Yaghmur, A.; Sagalowicz, L.; Leser, M. E.; Watzke, H.; Glatter, O. Reversible phase transitions in emulsified nanostructured lipid systems. *Langmuir* **2004**, *20*, 5254–5261.

(39) Yaghmur, A.; de Campo, L.; Sagalowicz, L.; Leser, M. E.; Glatter, O. Emulsified microemulsions and oil-containing liquid crystalline phases. *Langmuir* **2005**, *21*, 569–577.

(40) Yaghmur, A.; de Campo, L.; Salentinig, S.; Sagalowicz, L.; Leser, M. E.; Glatter, O. Oil-loaded monolinolein-based particles with confined inverse discontinuous cubic structure (Fd3m). *Langmuir* **2006**, *22*, 517–521.

(41) Briggs, J.; Chung, H.; Caffrey, M. The temperature-composition phase diagram and mesophase structure characterization of the monoolein/water system. *J. Phys. II* **1996**, *6*, 723–751.

(42) Qiu, H.; Caffrey, M. Lyotropic and thermotropic phase behavior of hydrated monoacylglycerols: Structure characterization of monovaccenin. *J. Phys. Chem. B* **1998**, *102*, 4819–4829.

(43) Qiu, H.; Caffrey, M. Phase behavior of the monoerucin/water system. *Chem. Phys. Lipids* **1999**, *100*, 55–79.

(44) Qiu, H.; Caffrey, M. The phase diagram of the monoolein/water system: metastability and equilibrium aspects. *Biomaterials* **2000**, *21*, 223–234.

(45) Salonen, A.; Guillot, S.; Glatter, O. Determination of water content in internally self-assembled monoglyceride-based dispersions from the bulk phase. *Langmuir* **2007**, *23*, 9151–9154.

(46) Larsson, K. Colloidal dispersions of ordered lipid-water phases. *J. Dispersion Sci. Technol.* **1999**, *20*, 27–34.

(47) Moitzi, C.; Guillot, S.; Fritz, G.; Salentinig, S.; Glatter, O. Phase reorganization in self-assembled systems through interparticle material transfer. *Adv. Mater.* **2007**, *19*, 1352−1358.

(48) Guillot, S.; Tomsic, M.; Sagalowicz, L.; Leser, M. E.; Glatter, O. Internally self-assembled particles entrapped in thermoreversible hydrogels. *J. Colloid Interface Sci.* **2009**, *330*, 175−179.

(49) Kulkarni, C. V.; Tomsic, M.; Glatter, O. Immobilization of nanostructured lipid particles in polysaccharide films. *Langmuir* **2011**, *27*, 9541−9550.

(50) Iglesias, G. R.; Pirolt, F.; Glatter, O. Arrested Dynamics of Liquid Crystalline Emulsion Droplets in Hydrogels: A DLS Study Combining a Multispeckle CCD Instrument with a Single Mode Fiber − Brute Force Set-up with a Thin Flat Sample Cell. In preparation, 2013.

(51) Spicer, P. T.; Hayden, K. L.; Lynch, M. L.; Ofori-Boateng, A.; Burns, J. L. Novel process for producing cubic liquid crystalline nanoparticles (cubosomes). *Langmuir* **2001**, *17*, 5748−5756.

(52) Guillot, S.; Moitzi, C.; Salentinig, S.; Sagalowicz, L.; Leser, M. E.; Glatter, O. Direct and indirect thermal transitions from hexosomes to emulsified micro-emulsions in oil-loaded monoglyceride-based particles. *Colloids Surf., A* **2006**, *291*, 78−84.

(53) Tilley, A.; Dong, Y.-D.; Amenitsch, H.; Rappolt, M.; Boyd, B. J. Transfer of lipid and phase reorganisation in self-assembled liquid crystal nanostructured particles based on phytantriol. *Phys. Chem. Chem. Phys.* **2011**, *13*, 3026−3032.

Chapter V

Submicrometer-Sized Pickering Emulsions Stabilized by Silica Nanoparticles with Adsorbed Oleic Acid

Sadeghpour, A., Pirolt, F. & Glatter, O., Langmuir 29, 6004–6012 (2013).

Submicrometer-Sized Pickering Emulsions Stabilized by Silica Nanoparticles with Adsorbed Oleic Acid

Amin Sadeghpour, Franz Pirolt, and Otto Glatter*

Department of Chemistry, Karl-Franzens-University Graz, Heinrichstrasse 28, 8010 Graz, Austria

ABSTRACT: Oil−water Pickering emulsions of about 200 nm were stabilized by nanosized hydrophilic silica after a simple surface treatment method. We have modified the aqueous silica nanoparticle dispersions by simple adsorption of oleic acid to their surfaces, improving the hydrophobicity of the particles while maintaining their charge and stability. The adsorption was monitored by small-angle X-ray scattering and electrophoretic measurements to estimate the interparticle interactions and surface charges. The effect of various parameters, such as nanoparticle concentration, amount of oleic acid, ionic strength, and pH, on the droplets' size and stability was investigated by dynamic light scattering. Furthermore, the ability of these modified silica nanoparticles to stabilize long-chain alkanes, liquid paraffin, and liquid-crystalline phases was examined.
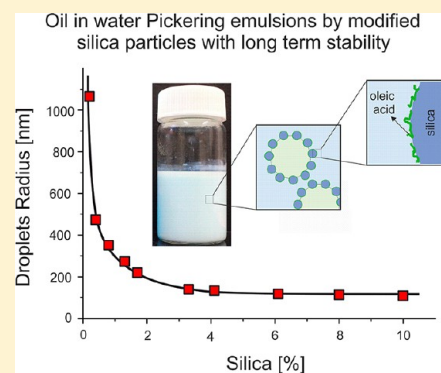
■ INTRODUCTION

Pickering emulsions are stabilized by the adsorption of solid particles at the interface between two immiscible liquids. If one of the liquids wets the solid particle more than the other, the poorly wetting liquid will be dispersed.[1−10] The main advantage of Pickering emulsions over other more traditional stabilization methods is its surfactant-free preparation, which is highly relevant for medical and skincare applications.[11−15] Furthermore, the high adsorption energy of the particles at the interface leads to a higher stability of the droplets. The energy necessary to detach a particle from the oil−water interface depends on the particle's size, contact angle, and the interfacial tension between water and oil.[16] For particles of about 10 nm radius, the attachment energy can be estimated at around 4000 kT according to the following equation:

$$\Delta E = -\pi R^2 \gamma_{ow}(1 - |\cos \theta_c|)^2$$

Nontreated aqueous silica particle dispersions are cheap, readily available spherical particles; these properties make them potentially good candidates for the preparation of Pickering emulsions. However, such particles are also rather hydrophilic under basic conditions due to their surface charge, which reduces their usability for these emulsions. Reducing the pH can be achieved by surface-charge neutralization, which would also, however, destabilize the dispersion because the particles would quickly aggregate. On the other hand, the use of hydrophobic fumed silica particles has been reported for stabilizing Pickering emulsions. In one case, particles with a mean diameter of about 20 nm (available as dispersed aggregates of 100 nm mean diameter after sonication), industrially named Aerosil, were used to create Pickering emulsions with a droplet size of about 5 μm in water with rather hydrophilic oil phases, such as diisopropyl adipate and diisobutyl adipate.[17] Other reports are available on using the hydrophobic silica particles to prepare the w/o emulsions of about 2 or 70 μm using 5−30 or 280 nm sized particles, respectively.[18,19]

As a simple surface hydrophobization method, a number of surfactants have been examined regarding their potential to create Pickering emulsions.[20,21] For example, adsorption of cetyltrimethylammonium bromide onto silica particles is accompanied by surface-charge neutralization, while further adsorption leads to surface-charge reversal.[22] The nonionic surfactant, pentaethylene glycol monododecyl ether, leads to surface hydrophobization when adsorbed onto silica particles, as confirmed by small-angle neutron scattering,[23] but also to destabilization of the system, due to the loss of electrostatic repulsive interactions.[24] Sodium dodecyl sulfate, on the other hand, despite its negatively charged headgroup, can be, at least partially, adsorbed onto the negatively charged silica surface, increasing the latter's effective charge and hence preserving the stability of the particles while increasing the surface hydrophobicity, as shown by small-angle scattering experiments, dynamic light scattering, and zeta-potential measurements.[25]

It has been reported that oleic acid can be used to modify particles by using a chloroform/oleic acid mixture, followed by precipitation from solution with methanol and finally drying the nanoparticles at 120 °C. This method was used to stabilize several hundred micrometer sized high internal phase emulsions (HIPEs).[26,27] However, it is a well established fact that nanoparticles are difficult to redisperse in aqueous phase once they are dried. Even at high sonication energy these particles often form raspberry-like larger aggregates which are prohibitive for the formation of small Pickering droplets. So

there is a need for an easy and, most importantly, surfactant-free (in the sense of micelle formation) way of hydrophobizing silica particles while maintaining their stability in aqueous solutions. Such a method would be especially attractive if the materials used were more compatible for biological media and body-care applications. We report herein the simple adsorption of oleic acid, which is a fatty acid and mostly dissociated at basic conditions, onto the surface of dispersed silica nanoparticles to create submicrometer sized o/w Pickering emulsions. In this contribution, we examined the interparticle interactions and the electrophoretic behavior of the silica particles as the amount of oleic acid was increased. The effectiveness of the oleic acid-modified silica particles for the stabilization of hydrophobic oils and self-assembled liquid-crystalline phases in water is discussed. Finally, droplet size and stability against coalescence at various ionic strengths and pHs were investigated.

■ EXPERIMENTAL SECTION

Materials. A colloidal dispersion of silica nanoparticles (18.3% nanoparticles, by volume; specific surface area 300 m^2/g; density 2.1 g/cm^3; pH 10.5), industrially named Levasil 300 (Le300), was supplied by H.C. Starck (Bavaria, Germany). Oleic acid (>90%), octadecene (>90%), liquid paraffin (Paraffin oil, viscosity 110−230 mPa·s), erioglaucine sodium salt, and sodium chloride were purchased from Sigma-Aldrich. Internally self-assembled liquid-crystalline structures were composed of Milli-Q water (Millipore), tetradecane (Sigma-Aldrich), and Dimodan U/J (DU) (DANISCO A/S, Braband, Denmark). DU contains monoglycerides (96%, distilled), linoleate (62%), and oleate (25%). All chemicals were used as received without further purification, and all solutions and dispersions were prepared using Milli-Q water.

Emulsion Preparation. The Le300 silica particles were ultrasonicated (Vibra-Cell, Sonics & Materials, Newtown, CT) for 10 min at 30% power prior to use to avoid aggregation. The particle dispersion had a transparent and slightly bluish appearance. The oleic acid−water mixture was also ultrasonicated for 10 min at 30% power to effectively disperse oleic acid in water as micrometer-sized droplets. Afterward, the proper amounts of this mixture were added to the silica particles suspension. The resulting sample was either mechanically stirred at 2500 rpm for 2 min and about 75 °C or ultrasonicated at 30% power in pulse mode (2.5 s pulses with 0.5 s pauses) for 10 min to provide further energy for mixing and adsorption.

To prepare the emulsions, the modified silica particle dispersions were transferred to a vial, to which water, and then the lipophilic phase, were added. For pure oil dispersions, 30% of the total volume was oil (octadecene in liquid form with melting point of 14−16 °C or liquid paraffin), whereas the liquid-crystalline phases were dispersed at 10% of the total mass of the sample. In the latter case, the lyotropic phases are comprised of tetradecane and Dimodan U/J at the wanted mass ratio. The resulting mixture was either heated to 75 °C with mechanical stirring at 2500 rpm for 2 min or ultrasonicated to disperse the oil phase for 10 min, which led to a milky suspension. All measurements were performed at 25 °C.

Small-Angle X-ray Scattering (SAXS). The SAXS experiments were performed on a laboratory equipment like described in a previous publication.[25]

The structures of internally self-assembled structures (isasomes) were determined by the relative positions of the peaks in the scattering patterns. The interactions between the pure and coated silica particles were evaluated by analyzing the scattering profiles with the generalized indirect Fourier transformation (GIFT) method.[28,29] According to this method, the scattered intensity can be expressed as

$$I(q) = nP(q)S(q)$$

where n is the number density of the particles, $P(q)$ is the particle form factor, and $S(q)$ is their structure factor. It is the generalized form of IFT calculation which transforms the measured scattering curve into the pair distance distribution function (PDDF), $p(r)$. The PDDF is the convolution square of the electron density fluctuation and represents a histogram of the distances inside the particle weighted with the electron-density differences relative to the solvent. This transformation considers the maximum dimension of the particles when the PDDF function becomes zero. We applied the charged and monodisperse spherical particles model with the Yukawa potential and hypernetted chain theory (HNC) for the structure factor in our GIFT calculations. The particles' form factor, $P(q)$, was obtained from a moderately concentrated pure silica dispersion of 5% (v/v) and thereafter was introduced as an input file in the calculation of the structure factors of extensively coated silica particles at the same concentration.

Dynamic Light Scattering. A goniometer with a green diode pumped laser (Verdi 5W, Coherent) of wavelength 532 nm and single-mode fiber detection optics (OZ from GMP, Zurich, Switzerland) was used for the dynamic light scattering measurements. The device was equipped with a photomultiplier detector, which was combined with pseudo-cross-correlation and an ALV5000/E correlator with fast expansion (ALV, Langen, Germany). The emulsions were diluted prior to measurement so that the final lipophilic droplet concentration was about 0.004%. The correlation functions were collected 10 times with 30 s running time each. The functions were averaged while correlation functions showing the intermediate plateau due to dust particles passing through the beam were ignored. For the time-resolved measurements, every run was considered. The scattered intensity was evaluated at a scattering angle of 90°, while a second-order cumulant fit was applied to the correlation function for the calculation of the mean hydrodynamic radius.

Electrophoretic Measurements. The charge properties of the silica particles coated with oleic acid were investigated by electrophoresis with a Brookhaven instrument ZetaPALS (Holtsville, NY), using the phase-analysis light-scattering method. The measurements were performed with 2−3 h of equilibrium time after preparation, for 5 times, each 12 runs, and averaged. The silica content in all samples was set to 5% (v/v).

■ RESULTS AND DISCUSSION

Oleic Acid Adsorption on Silica Particles. Oleic acid is a fatty acid with a 17-carbon alkene chain and a carboxylic acid headgroup. It has very low solubility in water (1×10^{-5} mol/L) as measured by total organic carbon analysis.[30] Like other fatty acids, its solubility depends on the pH. Its pK_a was reported by Kanicky et al. to be 9.85, as measured by potentiometric titration.[31] Those authors reported that, by decreasing pH and hence increasing the protonation of the carboxyl groups, the oleic acid is expelled from water to minimize the energy of the system which leads to aggregation of the oleic acid and finally to larger droplets. Kamogawa et al. reported that the droplet size ranges from the order of 100 nm to several micrometers.[30] In another study by Salentinig et al. the apparent pK_a of oleic acid was reported to be between 6 and 7.[32]

Because of the low solubility of oleic acid, we started with ultrasonication of the oleic acid/water mixture which leads to creation of submicrometer-sized droplets. Then, we investigated how the oleic acid droplet size changes after adsorption onto the silica surface by dynamic light scattering (DLS) at a scattering angle of 90°. For this purpose, the sonicated oleic acid−water mixture was added to the silica dispersion to give a mixture with pH 9.7, 0.8% v/v silica, and 2 mM oleic acid. For comparison with the individual components, the oleic acid solution and the silica dispersion were adjusted to pH 9.7. All samples were sonicated just before the DLS measurement to avoid any aging effect on the oleic acid droplet size.[30]

The size distributions were calculated by inverse Laplace transformation from the correlation functions. Figure 1 shows
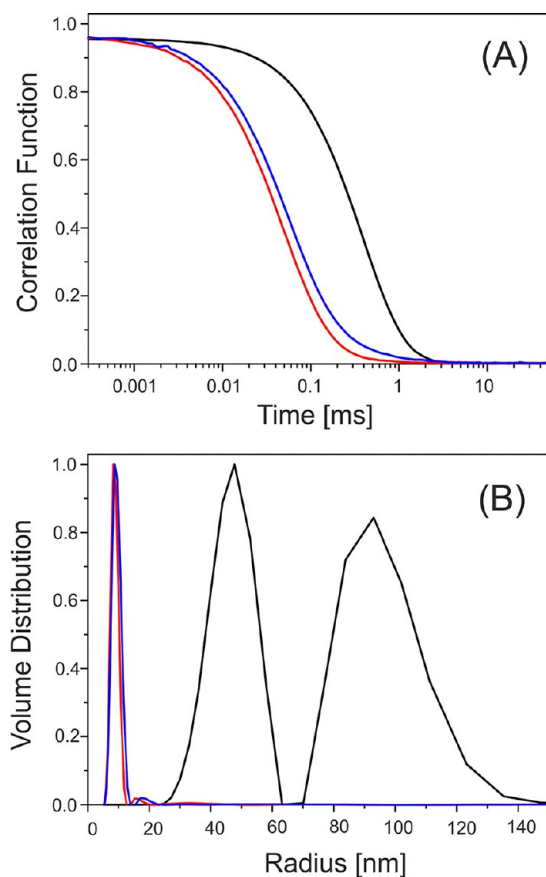
Figure 1. DLS correlation functions (A) and corresponding size distributions obtained by inverse Laplace transformation (B) of pure oleic acid at 2 mM (black), pure silica at 0.8% v/v (red), and a mixture of the two (blue). The pH of the first two samples was set to 9.7, which is also the pH of the mixture.

Figure 2. SAXS profiles of 5% silica particles in the presence of oleic acid. Scattering functions at varying concentrations of oleic acid: 0.79, 2.37, 3.96, 5.94, 7.92, 11.88, 15.84, 19.80, and 23.76 mM. The arrow in the inset shows how the concentration of oleic acid increases (A). The PDDF function of the particles; determined from the 5% untreated silica dispersion (B).

that silica particles have a similar size distribution with and without oleic acid, whereas the oleic acid droplets at the same concentration are clearly larger. Furthermore, the scattering intensity from pure oleic acid was about 5 times greater than that of the untreated silica particles due to the stronger scattering from the larger particles. However, the scattering intensity of the silica/oleic acid mixture is very similar to that of the untreated silica. This also confirms that the oleic acid droplets dissolve due to the adsorption of oleic acid molecules onto the silica surfaces. The adsorption of oleic acid onto the silica particles was also investigated by SAXS and electrophoretic mobility measurements, as discussed below.

Surface-Charge Variation by Adsorption of Oleic Acid. SAXS and electrophoretic mobility measurements were carried out to determine the surface charge variation as the amount of oleic acid added to the silica dispersions increased. The SAXS profiles, shown in Figure 2A, were analyzed within the reliable q range. The q_{min} was estimated from the Guinier plot, where the first experimental point appears on the linear fit.

For pure and moderately concentrated silica dispersions (5% v/v), a radius of gyration of 8.1 nm and an effective charge of about 12.2 were found. The pair-distance distribution function (PDDF) reveals a maximum at about 9 nm. As can be seen in Figure 2B, the curve has a slightly asymmetric distribution, which originates from the polydispersity of the sample. The form factor obtained from this calculation was used as the input file to analyze the data from silica particles with various

amounts of oleic acid added. In fact, we assumed that the adsorption of oleic acid does not effectively change the particles' form factor. On the other hand, the GIFT calculation is very sensitive to slight variations in the ion concentration due to the shielding of surface charge and the resulting effect on particle–particle interactions. As a result, when varying the oleic acid concentration, the variation in the free ion concentration must be taken into account.

The amount of adsorbed oleic acid on the surface could be estimated from the adsorption isotherm. However, two extreme conditions can be considered. The first condition is that all of the oleic acid is adsorbed onto the silica surface; we term this the *full adsorption assumption*. Under this assumption, when varying the total amount of oleic acid, the free-ion concentration is assumed to be constant. The second condition is that all of the oleic acid stays in solution: the so-called *no adsorption assumption*. In this situation, the free-ion concentration will be dependent on the oleic acid content. The structure factors corresponding to the above conditions are represented in the Figure 3 at various oleic acid concentrations. The related effective charge as a function of oleic acid concentration is summarized in Figure 4A. At *full adsorption*
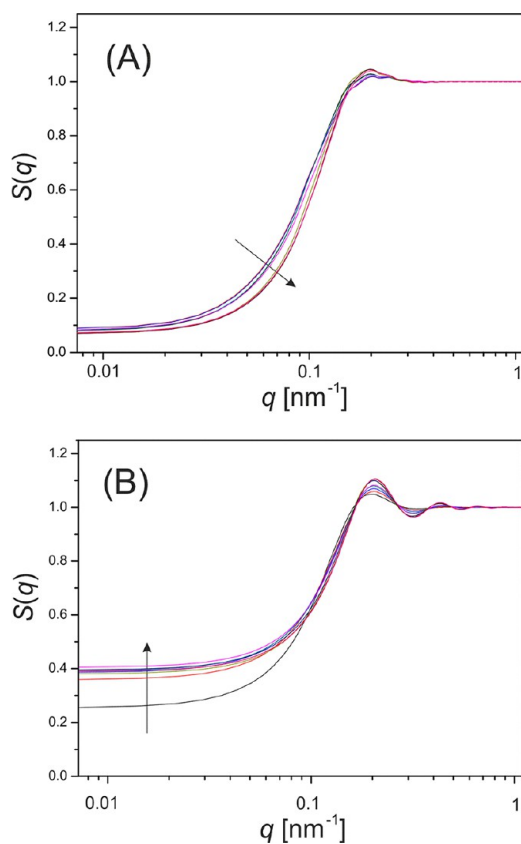
Figure 3. Structure factors of the silica samples in the presence of various amounts of oleic acid calculated by using the *full adsorption assumption* (A) or the *no adsorption assumption* (B). The arrows show the direction of increasing oleic acid concentration.

Figure 4. Effective charge of silica particles versus the oleic acid concentration calculated from SAXS data; the squares within the shaded region were obtained by assuming 50% adsorption of the oleic acid on the particles (A). The electrophoretic mobility of silica particles as a function of oleic acid concentration is shown in (B).

assumption, the effective charge shows very little increase with increasing oleic acid concentration, whereas a sharp rise can be seen under the *no adsorption assumption*.

In a real situation, the oleic acid will be adsorbed partially on the surface, as shown as the shaded area in Figure 4A. If hypothetical conditions are assumed, in which 50% of oleic acid is adsorbed on the surface, the curve of effective charge appears almost in the middle of the shaded field, showing a significant increase in effective charge relative to oleic acid concentration.

Further investigations by electrophoretic mobility of the same samples are shown in Figure 4B. The mobility of the particles increases with increasing oleic acid concentration, with a maximum mobility of about 9×10^{-8} m^2/(V s) being reached at an oleic acid concentration of around 12.5 mM. The increase in mobility arises from the higher surface charge accumulated by the head groups of the oleic acid molecules. The resulting supercharging of the silica particles enhances the stability of the colloid because of the stronger electrostatic repulsive forces between the particles. The long alkene chain of oleic acid also renders the surface more hydrophobic, which is desired in making Pickering emulsions. The optimum ratio of silica particles to oleic acid for silica modification is taken to be 5% (v/v) silica to 12.5 mM oleic acid.

Stabilization of Oil Droplets with Colloids by Mechanical Stirring. To investigate the efficiency of the particle modification procedure, oil-droplet stabilization by pure silica particles was compared with that of the modified particles. Figure 5 shows the macroscopic view of the effect of the two different particles on octadecene stabilization a day after the
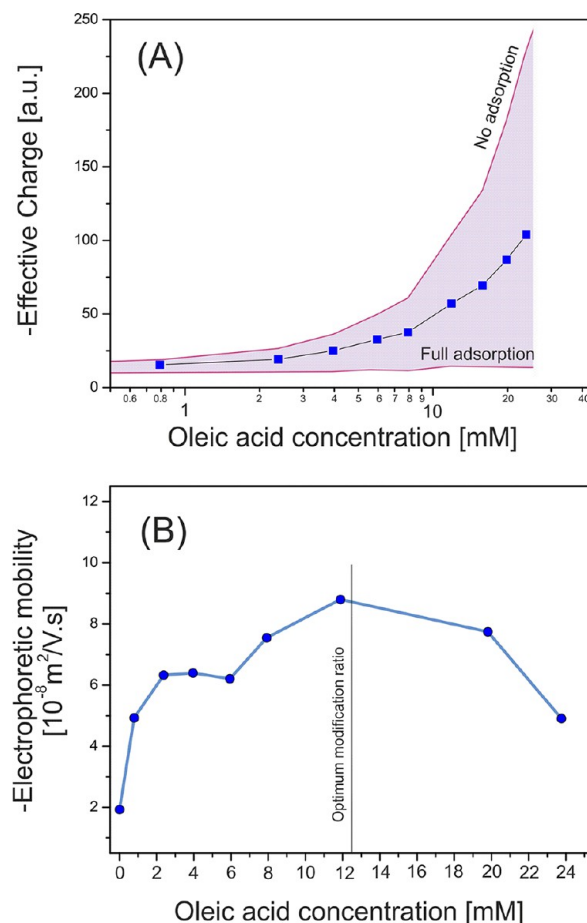
Figure 5. Oil stabilized by untreated silica particles (A), untreated oleic acid (B), and silica particles modified with oleic acid (C). A thin white layer of emulsion can be seen at the interface between the two phases in (B). The clear white upper part in (C) is showing the creamed, but stable, oil emulsion droplets.

preparation of the dispersions. The 30% (v/v) oil phase was used to be stabilized by mechanical stirring with untreated silica particles (Figure 5A) or silica particles modified with oleic acid (Figure 5C). To confirm the effect of the modified particles, the stabilization of the octadecene with pure oleic acid is also

shown (Figure 5B). Three drops of 0.1% (w/w) solution of erioglaucine sodium salt as an inorganic hydrophilic dye was added to the water phase for better visual representation. Within a few minutes after mixing of the sample with pure silica particles, macroscopic phase separation into water and oil phases was observed. After complete phase separation, the hydrodynamic radius of the aqueous phase was measured to be about 12 nm, which corresponds to the radius of untreated silica particles.

Pure oleic acid shows a very low stabilizing effect due to its very low hydrophilic−lipophilic balance value.[30] This explains the formation of a very thin white emulsion layer at the interface of oil−water phase in Figure 5B. This shows that very little amount of oil is stabilized by pure oleic acid and that the remaining part is phase separated. In contrast, the oil droplets stabilized by the modified silica particles remain stable for at least 3 months. The modified silica particles can easily be adsorbed at the oil/water interface by mixing, which leads to a milky dispersion. These droplets are very stable due to the high energy requirement for detachment of the particles from the interface. As is shown in Figure 5C, the droplets do undergo creaming to the top because the droplets are large. The DLS measurements of these samples were performed with the laser beam passing through the middle of the vial, 15 s after gentle shaking. Consideration of the times is crucial due to the fast creaming of the droplets. The size cannot be finely evaluated; however, a poor quality cumulant fit gives an estimate for the mean hydrodynamic radius of about 2 μm and a polydispersity of 60%. An optical microscopy image of the prepared o/w emulsions is shown in Figure 6. The preparation of much smaller droplets with finer polydispersity will be shown in the next section where also the effect of ultrasonication will be discussed.
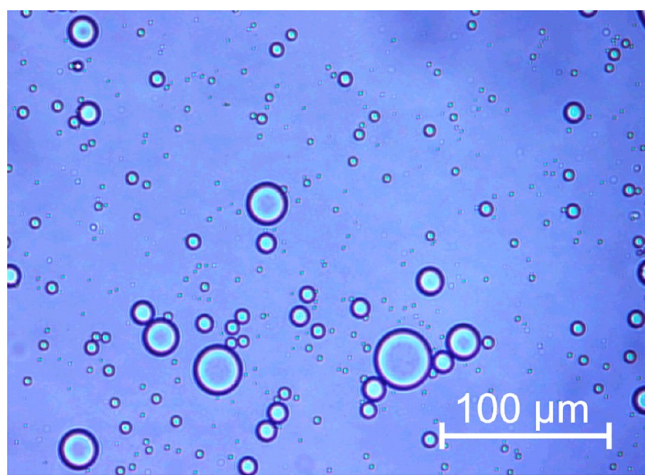
Figure 6. Optical microscopy image of droplets of 30% (v/v) octadecene stabilized by silica particles modified with oleic acid (0.8% v/v); prepared by mechanical stirring.

Stabilization of Oil Droplets with Colloids by Ultrasonication.
Conventional mechanical stirring to disperse oil droplets in the aqueous phase leads in most cases like ours to polydisperse large particles. However, it is a useful method for comparing the efficiency of various materials on the oil stabilization. The higher dispersing energy provided by ultrasonication leads to finer dispersions and therefore greater interface area between the oil and water phases. The stabilizing

particles can thus be adsorbed at the interface more easily, which normally leads to smaller and more homogeneous droplets. We examined this increased efficiency by using scattering measurements from the Pickering emulsions prepared with varying ultrasonication times. The hydrodynamic radius and light scattering intensity at 90° were recorded and averaged over 10 runs. As summarized in Figure 7, the droplets
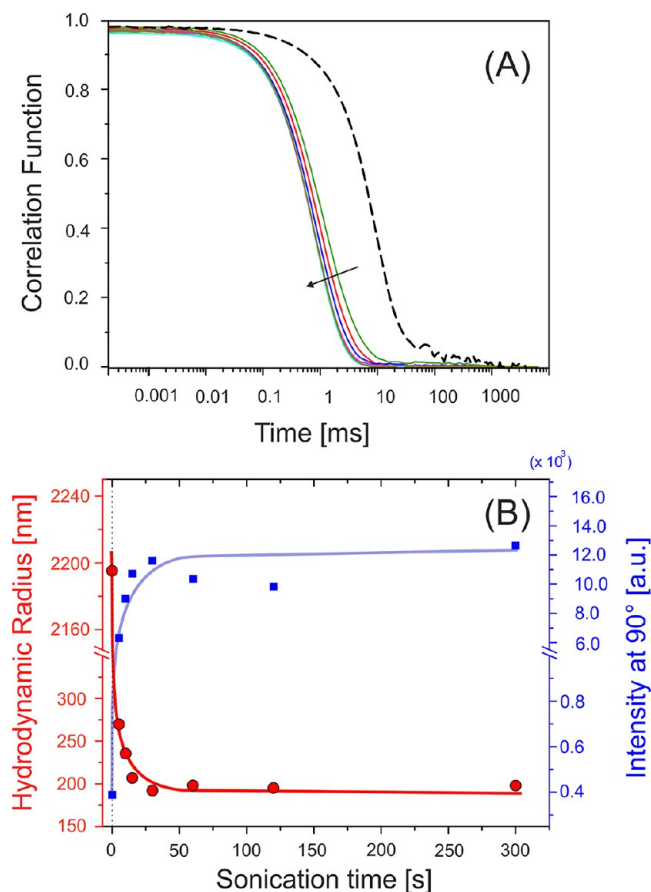
Figure 7. Effect of ultrasonication on the stabilization and homogeneity of the oil droplets stabilized by modified silica particles. DLS correlation functions from the emulsions before (dashed line) and after (solid lines) ultrasonication. The arrow shows how the curves shift to smaller correlation time with increasing ultrasonication time (A). The variation in mean size of the droplets (●) and the scattering intensity (■) as a function of ultrasonication time (B). The sample includes 30% (v/v) octadecene added to the aqueous phase, which contains 0.8% (v/v) silica particles modified with 2 mM oleic acid.

formed from 30% octadecene without ultrasonication have a mean hydrodynamic radius of about 2 μm with very poor cumulant fit quality due to the high polydispersity in droplet size. One minute of ultrasonication is sufficient to reduce the radius to about 200 nm with a much more homogeneous size distribution, as can be seen in Figure 7A by comparing the correlation functions on nonsonicated samples with sonicated ones. These changes are accompanied by an increase in the scattered intensity. In Figure 8, the macroscopic view of the emulsions prepared by ultrasonication, made of untreated silica as well as oleic acid modified silica particles, is represented. In all of the following experiments, the preparation of the emulsions was performed using ultrasonication.
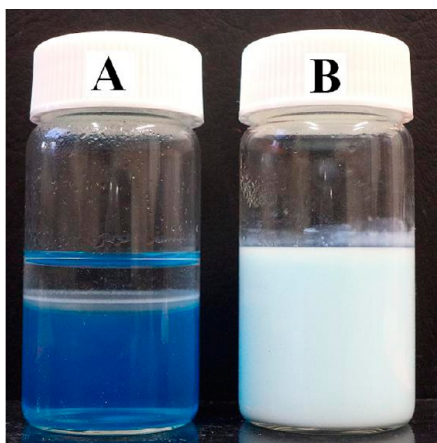
Figure 8. Clear phase separation in the emulsion stabilized by untreated silica particles (A) and stable oil droplets emulsified by modified silica particles (B) using ultrasonication. The photo is taken a week after the preparation.

Effect of Stabilizer Concentration. The effect of stabilizer concentration was investigated by varying the amount of modified silica particles while keeping the volume of the oil phase constant at 30%. The silica particles were modified at the optimum ratio (5% silica: 12.5 mM oleic acid). Octadecene and liquid paraffin were the oil phases. The scattered intensity and hydrodynamic radius were plotted against stabilizer concentration β in Figure 9. β is defined as the mass ratio between particles and oil:

$$\beta = \frac{\text{mass of modified silica particles}}{\text{mass of lipophilic phase}} \times 100$$

The experiments reveal that increasing the stabilizer leads to smaller droplets, as shown by an increase in the scattered intensity. This is due to the fact that particles of a few hundred nanometers contribute more strongly to the intensity at a scattering angle of 90° than those of several micrometers (effect of form factor). At β values around 20, the size distributions obtained from inverse Laplace transformation of correlation functions show the main population at a hydrodynamic radius of about 100 nm for both octadecene and liquid paraffin. Very small volumes of droplets around 200 nm in radius can also be detected. To confirm these findings and to exclude the existence of essential amounts of much larger droplets, DLS experiments were also performed at the scattering angle of 30°. Under this condition, the peak at 200 nm radius becomes more pronounced; however, the main population was still obtained around 100 nm. Overall, no contribution of droplets with the radii bigger than 300 nm can be detected from the size distribution. Further addition of particles has no effect on the size due to saturation of the interface between the lipophilic phase and water. The surface coverage can be roughly estimated to around 0.9 at a β value of 20 assuming a droplet radius of about 100 nm.

Stability of the Droplets. The stability of dispersed phase was monitored over time by light scattering. Evolution of ripening or phase separation can be observed by the scattered intensity or by the hydrodynamic radius of the droplets. The emulsions were maintained at 25 °C and, prior to each DLS experiment, were stirred to eliminate any creaming. Then, they were diluted about 6000 times, and the scattering intensities were recorded at a scattering angle of 90°. The emulsions were
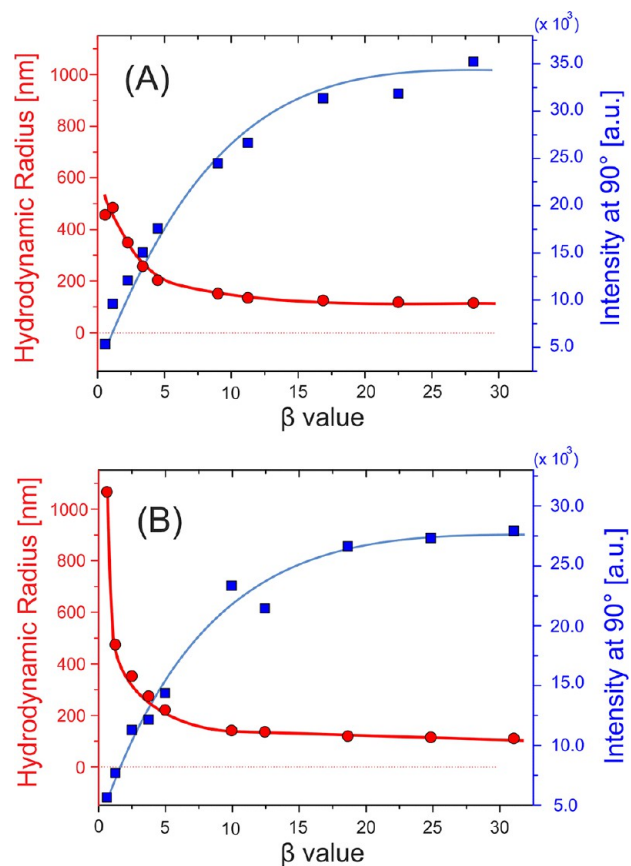
Figure 9. 30% (v/v) of liquid paraffin (A) and octadecene (B) stabilized by various amounts of modified silica particles, as represented by variation in hydrodynamic radius (●) and scattering intensity (■).

relatively stable over a long period, the particle size only increasing about 8% over two months, as shown in Figure 10 for octadecene droplets. Accordingly, the scattering intensity decreases slightly over the same period.

Our experiments revealed that the prepared emulsions are quite stable against the variation of pH. The size of the droplets stabilized by treated silica particles at β value of 18.6 were examined at the pH range of 4.2 to 10.0, and no significant
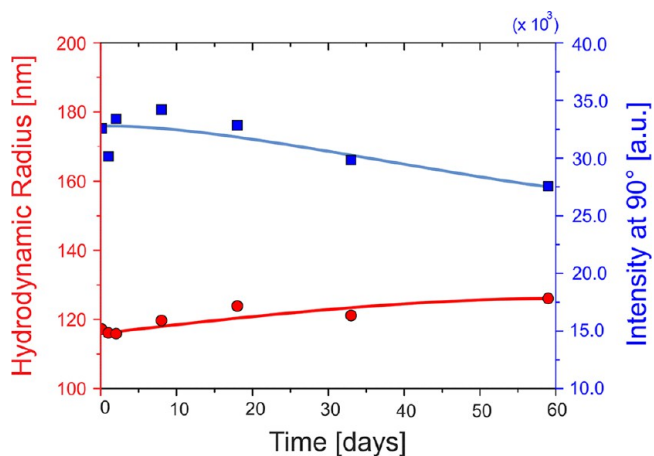
Figure 10. Hydrodynamic radius (●) and scattered intensity (■) evolution with time from the droplets of octadecene (30% v/v) stabilized by silica particles at a β value of 18.6.

change in size was observed within a day. Furthermore, the stability of the particles in the presence of salt is also relevant because a certain amount of salt is always present in natural media and biological systems. Our emulsions are expected to undergo ripening or coalescence more easily in the presence of salt. The ripening is normally seen as an initial increase in the hydrodynamic radius due to the high Laplace pressure inside the droplets and then a plateau. In contrast, once coalescence starts, it continues until phase separation occurs, so that a clear oil phase will appear at the top of the mixture and will not scatter light passing through the middle of the vial. These effects can be explored by using time-resolved light scattering. Figure 11A reveals the evolution of hydrodynamic radius with
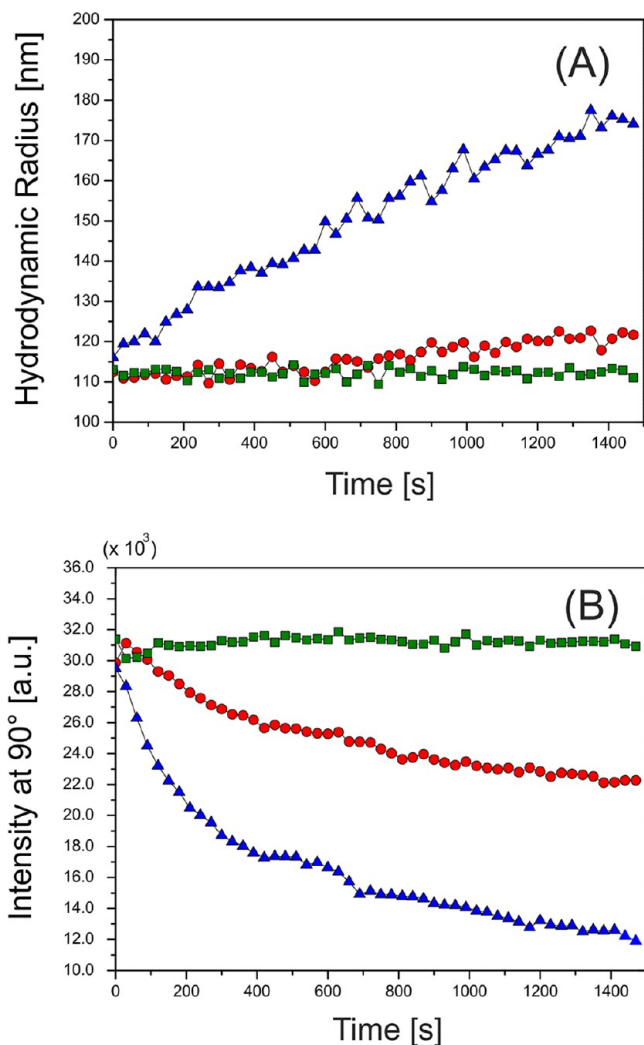
Figure 11. Increase in droplet size (A) and decay in the scattered intensity (B) of the droplets of Pickering emulsion from octadecene in the presence of NaCl added after emulsification. The NaCl concentrations are 0.30 (▲), 0.15 (●), and 0.05 M (■). The β value was fixed at 18.6.

time. The droplet size remains almost constant at low salt concentrations; the droplets then start to grow as the salt increases. Furthermore, the rate of increase in size of the droplets is faster at higher salt concentrations. As shown in Figure 11B, the scattering intensity of unstable samples decays at various rates, depending on the salt concentration. At concentrations below 50 mM, the dispersion is stable, at least

over several hours. At a moderate salt level (around 150 mM, which is close to the ionic strength at biological media), the emulsions show an intermediate stability. Very fast decay is observed at 300 mM NaCl concentration, leading to coalescence of the droplets and phase separation. Such phase separation has also been observed macroscopically for samples of higher droplet concentrations at elevated salt contents.

Pickering Emulsions from Self-Assembled Liquid-Crystalline Phases. Monoglyceride-based internally self-assembled particles (isasomes) dispersed in aqueous phase have received many attentions in recent years.[33−38] These particle structures are comprised of monoglycerides, an oil, and water in the internal phase and a stabilizer (in our case modified silica particles) at the interface. The internal structures can be tuned by temperature or oil content. The phase diagrams of such structures are normally presented according to the mass ratio between the monoglyceride (e.g., Dimodan U/J) and the total lyotropic phase, termed δ.[39]

$$\delta = \frac{\text{mass of Dimodan U/J}}{\text{mass of Dimodan U/J} + \text{mass of tetradecane}} \times 100$$

We used tetradecane as the oil, with δ values selected to give various self-assembled structures at room temperature. The lyotropic phase content in these samples was 10% (w/w), prepared at a β value of 12.4. The final milky dispersion with narrow size distribution was obtained after 20 min of ultrasonication. Emulsified microemulsions (EME, $\delta = 57$), micellar cubosomes (Fd3m, $\delta = 70.5$), and hexosomes (H$_2$, $\delta = 84$) were successfully stabilized using modified silica particles.

SAXS measurements were performed to determine the internal structures of these particles, and the resulting scattering profiles are shown in Figure 12. The characteristic scattering
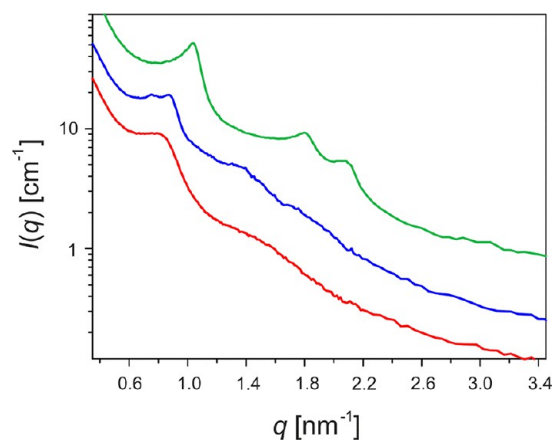
Figure 12. SAXS curves from internally self-assembled structures: hexosomes (green), micellar cubosomes (blue), and emulsified microemulsions (red) stabilized by modified silica nanoparticles using a β value of 12.4. Curves are vertically shifted for better visibility.

peaks for hexagonal and micellar cubic phases appeared at the expected q values. The broad microemulsion correlation peak indicates EME formation. The upturn in all these curves at small q values originates from the silica particles. All the above structures were well stabilized by silica particles. The droplet size was determined by DLS, and the results are summarized in Table 1. All of them show a mean hydrodynamic radius around 100 nm, which is extremely small. These particles show long-term stability like the emulsions prepared with simple oils, as discussed above. The cubic Pn3m phase, which is formed at a δ

Table 1. Characteristics of Pickering Emulsions from Self-Assembled Nanostructures[a]

δ	structure formed	hydrodynamic radius [nm]	comment
0	emulsion	107	completely stabilized
57	emulsified microemulsion	90	completely stabilized
70.5	micellar cubosomes	89	completely stabilized
84	hexosomes	80	completely stabilized
100	bicontinuous cubosomes	92	partially stabilized

[a]The lyotropic phase was 10% (w/w), and the β value was 12.4.

value of 100, can only be partially stabilized, as previously reported in related studies.[40]

CONCLUSIONS

Hydrophobic, well-charged, nonaggregated silica particle dispersions were produced by adsorption of oleic acid onto the particles surface. Very hydrophobic oils were stabilized, and Pickering emulsions with extremely small droplets were obtained. The droplets remain unchanged by variation of pH; however, stability was reduced by increasing salt concentration. SAXS experiments confirmed that the modified silica particles were not aggregated and stabilized liquid-crystalline phases. These results show that adsorption of oleic acid onto the surface of silica particles can be a valuable method for biological and body-care applications especially in the case of Pickering emulsions of self-assembled liquid crystalline materials. The high stability and small droplet size of the emulsions produced, the simplicity of the procedure, and the more biocompatible materials used here are the main advantages of our method over others.

AUTHOR INFORMATION

Corresponding Author

*E-mail otto.glatter@uni-graz.at (O.G.).

Notes

The authors declare no competing financial interest.

REFERENCES

(1) Ashby, N. P.; Binks, B. P. Pickering Emulsions Stabilised by Laponite Clay Particles. *Phys. Chem. Chem. Phys.* **2000**, 2 (24), 5640−5646.

(2) Aveyard, R.; Binks, B. P.; Clint, J. H. Emulsions Stabilised Solely by Colloidal Particles. *Adv. Colloid Interface Sci.* **2003**, 100, 503−546.

(3) Binks, B. P.; Lumsdon, S. O. Stability of Oil-in-Water Emulsions Stabilised by Silica Particles. *Phys. Chem. Chem. Phys.* **1999**, 1 (12), 3007−3016.

(4) Binks, B. P. Particles as Surfactants - Similarities and Differences. *Curr. Opin. Colloid Interface Sci.* **2002**, 7 (1−2), 21−41.

(5) Binks, B. P.; Duncumb, B.; Murakami, R. Effect of Ph and Salt Concentration on the Phase Inversion of Particle-Stabilized Foams. *Langmuir* **2007**, 23 (18), 9143−9146.

(6) Binks, B. P.; Fletcher, P. D. I. Particles Adsorbed at the Oil-Water Interface: A Theoretical Comparison between Spheres of Uniform Wettability and "Janus" Particles. *Langmuir* **2001**, 17, 4708−4710.

(7) Binks, B. P.; Lumsdon, S. O. Pickering Emulsions Stabilized by Monodisperse Latex Particles: Effects of Particle Size. *Langmuir* **2001**, 17, 4534−4539.

(8) Binks, B. P.; Lumsdon, S. O. Catastrophic Phase Inversion of Water-in-Oil Emulsions Stabilized by Hydrophobic Silica. *Langmuir* **2000**, 16, 2539−2547.

(9) Santini, E.; Guzman, E.; Ravera, F.; Ciajolo, A.; Alfe, M.; Liggieri, L.; Ferrari, M. Soot Particles at the Aqueous Interface and Effects on Foams Stability. *Colloids Surf., A* **2012**, 413, 216−223.

(10) Frelichowska, J.; Bolzinger, M. A.; Chevalier, Y. Effects of Solid Particle Content on Properties of O/W Pickering Emulsions. *J. Colloid Interface Sci.* **2010**, 351 (2), 348−356.

(11) Arditty, S.; Whitby, C. P.; Binks, B. P.; Schmitt, V.; Leal-Calderon, F. Some General Features of Limited Coalescence in Solid-Stabilized Emulsions. *Eur. Phys. J. E* **2003**, 11 (3), 273−281.

(12) Leal-Calderon, F.; Schmitt, V. Solid-Stabilized Emulsions. *Curr. Opin. Colloid Interface Sci.* **2008**, 13 (4), 217−227.

(13) Frelichowska, J.; Bolzinger, M. A.; Pelletier, J.; Valour, J. P.; Chevalier, Y. Topical Delivery of Lipophilic Drugs from O/W Pickering Emulsions. *Int. J. Pharm.* **2009**, 371 (1−2), 56−63.

(14) Laredj-Bourezg, F.; Chevalier, Y.; Bolzinger, M. A. Skin Delivery of Hydrophobic Drugs Using Biocompatible and Biodegradable Carriers: Pickering Emulsions and Block Copolymer Nanoparticles. Correlation to Drug Localization within the Skin Layers as Determined by Confocal Fluorescence Microscopy. *Exp. Dermatol.* **2012**, 21 (9), E2−E2.

(15) Wei, Z. J.; Wang, C. Y.; Liu, H.; Zou, S. W.; Tong, Z. Facile Fabrication of Biocompatible Plga Drug-Carrying Microspheres by O/W Pickering Emulsions. *Colloids Surf., B* **2012**, 91.

(16) Larson-Smith, K.; Jackson, A.; Pozzo, D. C. SANS and SAXS Analysis of Charged Nanoparticle Adsorption at Oil-Water Interfaces. *Langmuir* **2012**, 28 (5), 2493−2501.

(17) Frelichowska, J.; Bolzinger, M.; Chevalier, Y. Pickering Emulsions with Bare Silica. *Colloids Surf., A* **2009**, 343, 70−74.

(18) Gao, Q. X.; Wang, C. Y.; Liu, H. X.; Wang, C. H.; Liu, X. X.; Tong, Z. Suspension Polymerization Based on Inverse Pickering Emulsion Droplets for Thermo-Sensitive Hybrid Microcapsules with Tunable Supracolloidal Structures. *Polymer* **2009**, 50 (12), 2587−2594.

(19) Gao, Q. X.; Wang, C. Y.; Liu, H. X.; Chen, Y. H.; Tong, Z. Dual Nanocomposite Multihollow Polymer Microspheres Prepared by Suspension Polymerization Based on a Multiple Pickering Emulsion. *Polym. Chem.* **2010**, 1 (1), 75−77.

(20) Aveyard, R.; Binks, B. P.; Esquena, J.; Fletcher, P. D. I.; Buscall, R.; Davies, S. Flocculation of Weakly Charged Oil-Water Emulsions. *Langmuir* **1999**, 15 (4), 970−980.

(21) Liggieri, L.; Santini, E.; Guzman, E.; Maestro, A.; Ravera, F. Wide-Frequency Dilational Rheology Investigation of Mixed Silica Nanoparticle-Ctab Interfacial Layers. *Soft Matter* **2011**, 7 (17), 7699−7709.

(22) Ravera, F.; Santini, E.; Loglio, G.; Ferrari, M.; Liggieri, L. Effect of Nanoparticles on the Interfacial Properties of Liquid/Liquid and Liquid/Air Surface Layers. *J. Phys. Chem. B* **2006**, 110, 19543−19551.

(23) Lugo, D.; Oberdisse, J.; Karg, M.; Schweins, R.; Findenegg, G. H. Surface Aggregate Structure of Nonionic Surfactants on Silica Nanoparticles. *Soft Matter* **2009**, 5 (15), 2928−2936.

(24) Iglesias, G.; Wachter, W.; Ahualli, S.; Glatter, O. Interactions between Large Colloids and Surfactants. *Soft Matter* **2011**, 7 (10), 4619−4622.

(25) Ahualli, S.; Iglesias, G. R.; Wachter, W.; Dulle, M.; Minami, D.; Glatter, O. Adsorption of Anionic and Cationic Surfactants on Anionic Colloids: Supercharging and Destabilization. *Langmuir* **2011**, 27 (15), 9182−9192.

(26) Ikem, V. O.; Menner, A.; Bismarck, A. Tailoring the Mechanical Performance of Highly Permeable Macroporous Polymers Synthesized Via Pickering Emulsion Templating. *Soft Matter* **2011**, 7 (14), 6571−6577.

(27) Ikem, V. O.; Menner, A.; Bismarck, A. High Internal Phase Emulsions Stabilized Solely by Functionalized Silica Particles. *Angew. Chem., Int. Ed.* **2008**, *47* (43), 8277−8279.

(28) Fritz, G.; Bergmann, A.; Glatter, O. Evaluation of Small-Angle Scattering Data of Charged Particles Using the Generalized Indirect Fourier Transformation Technique. *J. Chem. Phys.* **2000**, *113* (21), 9733−9740.

(29) Bergmann, A.; Fritz, G.; Glatter, O. Solving the Generalized Indirect Fourier Transformation (Gift) by Boltzmann Simplex Simulated Annealing (BSSA). *J. Appl. Crystallogr.* **2000**, *33*, 1212−1216.

(30) Kamogawa, K.; Akatsukac, H.; Matsumotoc, M.; Yokoyamad, S.; Sakaic, T.; Sakaib, H.; Abe, M. Surfactant-Free O/W Emulsion Formation of Oleic Acid and Its Esters with Ultrasonic Dispersion. *Colloids Surf., A* **2001**, *180*, 41−53.

(31) Kanicky, J.; Shah, D. O. Effect of Degree, Type, and Position of Unsaturation on the pK_a of Long-Chain Fatty Acids. *J. Colloid Interface Sci.* **2002**, *256*, 201−207.

(32) Salentinig, S.; Sagalowicz, L.; Glatter, O. Self-Assembled Structures and pK_a Value of Oleic Acid in Systems of Biological Relevance. *Langmuir* **2010**, *26* (14), 11670−11679.

(33) Chang, C.; Bodmeier, R. Swelling of and Drug Release from Monoglyceride-Based Drug Delivery Systems. *J. Pharm. Sci.* **1997**, *86*, 747−752.

(34) Mezzenga, R.; Schurtenberger, P.; Burbidge, A.; Michel, M. Understanding Foods as Soft Materials. *Nat. Mater.* **2005**, *4* (10), 729−740.

(35) Mezzenga, R.; Grigorov, M.; Zhang, Z. D.; Servais, C.; Sagalowicz, L.; Romoscanu, A. I.; Khanna, V.; Meyer, C. Polysaccharide-Induced Order-to-Order Transitions in Lyotropic Liquid Crystals. *Langmuir* **2005**, *21* (14), 6165−6169.

(36) Alam, M. M.; Mezzenga, R. Particle Tracking Microrheology of Lyotropic Liquid Crystals. *Langmuir* **2011**, *27* (10), 6171−6178.

(37) Mezzenga, R.; Meyer, C.; Servais, C.; Romoscanu, A. I.; Sagalowicz, L.; Hayward, R. C. Shear Rheology of Lyotropic Liquid Crystals: A Case Study. *Langmuir* **2005**, *21* (8), 3322−3333.

(38) Dulle, M.; Glatter, O. Internally Self-Assembled Submicrometer Emulsions Stabilized with a Charged Polymer or with Silica Particles. *Langmuir* **2012**, *28* (2), 1136−1141.

(39) Guillot, S.; Moitzi, C.; Salentinig, S.; Sagalowicz, L.; Leser, M.; Glatter, O. Direct and Indirect Thermal Transitions from Hexosomes to Emulsified Micro-Emulsions in Oil-Loaded Monoglyceride-Based Particles. *Colloids Surf., A* **2006**, *291*, 78−84.

(40) Salonen, A.; Muller, M.; Glatter, O. Internally Self-Assembled Submicrometer Emulsions Stabilized by Spherical Nanocolloids: Finding the Free Nanoparticles in the Aqueous Continuous Phase. *Langmuir* **2010**, *26*, 7981−7987.